



TECHNISCHE UNIVERSITÄT
CHEMNITZ

Padan 95 SP treatment by electrochemical process and its combination with other techniques

von der Fakultät für Naturwissenschaften der Technischen Universität Chemnitz

genehmigte Dissertation zur Erlangung des akademischen Grades

doctor rerum naturalium

(Dr. rer. nat.)

vorgelegt von Msc. Hoang Nguyen Tien

geboren am 12.03.1987 in Vietnam

eingereicht am: 29.07.2019

Gutachter:	Prof. Dr. Rudolf Holze
	Prof. Dr. Werner Goedel
Vorsitzender:	Prof. Dr. Wolfgang Einhäuser-Treyer
Beisitzer:	Prof. Dr. Michael Sommer

Tag der Verteidigung: 28.10.2019

Bibliographische Beschreibung und Referat

Nguyen Tien Hoang

“Padan 95 SP Behandlung durch einen elektrochemischen Prozess und die Kombination mit anderen Techniken”

Diese Dissertation befasst sich mit der Reduktion des gesamten organischen Kohlenstoffs (TOC) aus wässrige Lösung, die Padan 95 SP enthält. Als Methoden zur Minimierung von TOC wurde die elektrochemische Oxidation von Padan 95 SP auf Bor-dotierter Diamant (BDD) Elektroden durch $\bullet\text{OH}$ Radikale, Elektro-Fenton und die Kombination mit Adsorptionstechnologien verwendet. Die $\bullet\text{OH}$ Radikale wurden dabei durch indirekte Methoden, z. B. die Bildung von 2-HTA gemessen. Zur Quantifizierung der Hydroxylradikalbildung wurde in dieser Studie die Bildung von 2-Hydroxylterephthalsäure (2-HTA) an BDD-Elektroden über die Reaktion zwischen Terephthalsäure (TA) und $\bullet\text{OH}$ untersucht. Weiterhin befasst sich die Arbeit mit dem Abbau von Cartap in Padan 95SP (95% Cartap) auf BDD über die Reaktion zwischen Cartap und Hydroxylradikalen. Betriebsparameter wie die angewandte Stromdichte, die Elektrolytarten und die Anfangskonzentration von Padan 95SP wurden variiert, um ihre Wirkung auf die Abbaueffizienz von Cartap zu bestimmen. Die Konzentration von Cartap wurde mittels UV-Vis-Spektroskopie mit dem 5,5-Dithiobis-(2-Nitrobenzoesäure) (DTNB) Verfahren bestimmt. Hochleistungs-Flüssigkeitschromatographie (HPLC) und Gaschromatographie/Massenspektrometrie (GC-MS) wurden verwendet, um das kommerziell erhältliche Padan 95SP und die Bildung von Nebenprodukten beim Abbau von Cartap zu charakterisieren. Die optimalen Bedingungen für die Cartap-Degradation durch den elektrochemischen Prozess wurden festgelegt: Konzentration des Elektrolyten: 0.05 M Na_2SO_4 , Padan 95SP Anfangskonzentration: $300 \text{ mg}\cdot\text{L}^{-1}$, pH = 3, Stromdichte: $j = 20 \text{ mA}\cdot\text{cm}^{-2}$. Unter diesen Bedingungen sinkt Cartap auf 41% und der TOC erreicht 8 % des jeweiligen Ausgangswertes. Um den TOC-Zerfall bei höher Padan 95 SP Konzentration in Wasser zu erhöhen, wurde die Kombination des elektrochemischen Prozesses mit anderen Techniken vorgeschlagen, z.B.: Elektro-Fenton-Technik, Oxidation mit NaOCl , oder die Kombination des elektrochemischen Prozesses mit einem Adsorptionsprozess.

Bei der Elektro-Fenton-Technik wurde der Einfluss von Faktoren wieder Anwesenheit von NaOCl in der Prozessvorbehandlung, Auswirkungen der H_2O_2 -Konzentration, Fe^{2+} -Dosierung, Metallionen als Cokatalysatoren und der pH-Wert der Lösung untersucht, um

die Wirkung auf die Abbau-Effizienz für Cartap zu bestimmen. Es konnten mit dieser Methode rund 80 % TOC, ausgehend von $700 \text{ mg} \cdot \text{L}^{-1}$ Padan 95SP, entfernt werden.

Die Kombination des elektrochemischen Prozesses mit einer Adsorptionsmethode ermöglicht eine effiziente Entfernung von TOC und Padan 95SP (95% Cartap). Dies basiert auf der Oxidation und anschließender Adsorption auf granularer Aktivkohle (GAC). Der Einfluss von Faktoren wie Leitelektrolyten, Flussrate, Betthöhe, Recyclingzahl sowie die Anfangskonzentration von Padan 95 SP wurde untersucht, um deren Auswirkungen auf die TOC Entfernung zu bestimmen. Durch die Kombination konnten so 75% des TOC und mehr als 90% Cartap bei $700 \text{ mg} \cdot \text{L}^{-1}$ Padan 95 SP entfernt werden. Fourier-Transformations-Infrarot (FT-IR) und BET-Oberflächenanalyse wurden angewendet, um GAC vor und nach der Verwendung zu untersuchen. Die Ergebnisse haben gezeigt, dass die Kombination des elektrochemischen Prozesses mit anderen Methoden eine potentielle Option für die Behandlung von Abwasser, das Padan 95 SP enthält, sein kann.

Schlüsselwörter: BDD-Elektrode, $\bullet\text{OH}$ -Radikal, Cartap, körnige Aktivkohle, gesamter organischer Kohlenstoff, chemischer Oxidationsprozess, Fenton-Methode, Adsorptionsmethode.

Abstract

Nguyen Tien Hoang

“Padan 95 SP treatment by electrochemical process and its combination with other techniques”

This dissertation describes electrochemical oxidation of Padan 95 SP on Boron-doped diamond (BDD) electrode mainly by $\bullet\text{OH}$ radicals (which was measured by indirect method, i.e: the formation of 2-Hydroxyterephthalic acid (2-HTA)), Electro-Fenton and the combination with adsorption technology for increasing total organic carbon (TOC) removal efficiency. In this study, the formation of 2-HTA on BDD electrode via the reaction between terephthalic acid (TA) and $\bullet\text{OH}$ as a method to quantify hydroxyl radical formation was investigated. The degradation of Cartap in Padan 95SP (95 % Cartap) on BDD was investigated. Operating parameters such as applied current density, types of electrolyte and initial concentration of Padan 95SP were varied in order to determine their effect on the degradation efficiency of Cartap. The concentration of Cartap was determined by UV-Vis spectroscopy according to 5,5-Dithiobis-(2-nitrobenzoic acid) (DTNB) procedure. High Performance Liquid Chromatography (HPLC) and Gas Chromatography/Mass Spectrometry (GC-MS) were used to characterize the commercial Padan 95SP and the formation of by-products. The optimal conditions for Cartap degradation by electrochemical process have been established: concentration of electrolyte: 0.05 M Na_2SO_4 , initial concentration of Padan 95SP: $300 \text{ mg}\cdot\text{L}^{-1}$, pH = 3, current density: $j = 20 \text{ mA}\cdot\text{cm}^{-2}$. At this condition, Cartap decreases to 41 %, TOC decay reaches 8 %. To increase TOC decay at higher Padan 95 SP concentration in aqueous solution, the combination technique of electrochemical process with other techniques was proposed, e.g.: Electro-Fenton technique, pre-oxidizing by NaOCl or the Electro-Adsorption combination.

In the Electro-Fenton technique, we investigated the influence of factors such as the presence of NaOCl in pretreatment of process, affects of H_2O_2 concentration, Fe^{2+} dosage, co-catalysts metals ion and pH. The efficiency shows approximately 80 % of TOC removed at $700 \text{ mg}\cdot\text{L}^{-1}$ Padan 95 SP.

The combination of electrochemical with adsorption method shows the efficient removals of TOC and Padan 95SP (95 % Cartap) based on reagents oxidation in electrochemical process and adsorption of granular activated carbon (GAC), respectively. The influence of factors

such as supporting electrolytes, flow rate, bed height, recycling number as well as initial concentration were investigated in order to determine their effects on TOC removal. The efficiency of this combination shows approximately 75 % of TOC and more than 90 % of Cartap removed at $700 \text{ mg}\cdot\text{L}^{-1}$ Padan 95 SP. Fourier Transform Infrared (FT-IR) and (Brunauer–Emmett–Teller) BET surface analysis were applied to investigate GAC before and after usage. The results have shown that the application of electrochemical technique with other methods can be the potential option for treatment of wastewater containing Padan 95 SP.

Keywords: BDD electrode, $\bullet\text{OH}$ radical, Cartap, granular activated carbon, Total Organic Carbon, chemical oxidation process, Fenton method, adsorption method.

Die vorliegende Arbeit wurde in der Zeit von August 2015 bis February 2019 unter Leitung von Prof. Dr. Rudolf Holze am Lehrstuhl für Elektrochemie der Technische Universität Chemnitz durchgeführt.

Dedication

To my Parents
To my wife
And
Lovely Daughter

Nguyen Tien Hoang

Table of contents

Bibliographische Beschreibung und Referat	2
Abstract.....	4
Dedication	7
Acknowledgements	11
List of abbreviations	12
CHAPTER 1 INTRODUCTION.....	14
1.1 Global water usage	14
1.2 Causes of water pollution	14
1.2.1 Industrial wastewater	15
1.2.2 Sewage	16
1.2.3 Agricultural activity: Fertilizers and pesticides	17
1.3 The application of Cartap and its current experimental treatment scale	17
1.4 Wastewater treatment technology	18
1.4.1 Biological method.....	18
1.4.2 Physical method	19
1.4.3 Chemical method	21
1.5 The treatment methods in thesis	23
1.5.1 Chemical method (advanced oxidation processes).....	23
1.5.1.1 Electrochemical oxidation	23
1.5.1.2 Electro-Fenton process	25
1.5.2 Physical method (adsorption process by GAC).....	27
1.6 Aims of the study (objectives).....	28
CHAPTER 2 MATERIALS AND METHODS	30
2.1 Materials	30
2.2 Experimental methods	30
2.2.1 Electrochemical experiment	30

2.2.3 Electro-Fenton experiment and pretreatment by sodium hypochlorite	31
2.2.4 The combination of electrochemical and adsorption processes.....	32
2.3 Analytical methods	32
2.3.1 Determination of Cartap content according to the 5,5-Dithiobis-(2-nitrobenzoic acid) (DTNB) procedure	32
2.3.2 Fluorescence spectrometer.....	33
2.3.3 UV-Vis spectrometer, TOC analyzer and calculation of efficiency	33
2.3.4 HPLC	35
2.3.5 GC-MS.....	35
2.3.6 Anions concentration measurement.....	36
2.3.7 Characterization of activated carbon	36
CHAPTER 3 RESULTS AND DISCUSSION	37
3.1 Effect of operating conditions on trapping the •OH radicals via TA in the electrochemical process - the efficiency of this method	37
3.1.1 Calibration curve for 2-HTA	37
3.1.2 Effect of applied current density.....	38
3.1.3 Effect of different electrolyte anions	40
3.1.4 Effect of different concentrations of Na ₂ SO ₄	41
3.1.5 Effect of initial terephthalic acid concentration.....	43
3.1.6 Effect of NaOH concentration	44
3.1.7 By-products and the reliability of •OH determination technique	45
3.1.8 Conclusions.....	49
3.2 Electrochemical process for Padan 95SP degradation	50
3.2.1 Analysis of ingredients in pesticide Padan 95SP	50
3.2.2 Effect of pH on hydrolysis rate of Cartap in Padan 95SP	51
3.2.3 Effect of applied current density.....	52
3.2.4 Effect of different electrolyte anions	54

3.2.5 Effect of Na ₂ SO ₄ concentration	57
3.2.6 Effect of initial Padan 95SP concentration	58
3.2.7 By-products and their release	59
3.2.8 Time-dependent concentrations of oxidizing ions and the influence of inorganic anions as supporting electrolytes.....	62
3.2.9 Conclusion	64
3.3 Electro-Fenton process and effect of NaOCl on this process.....	65
3.3.1 Padan 95SP degradation with NaOCl.....	65
3.3.2 Effect of H ₂ O ₂ addition.....	66
3.3.3 Effect of metal ion catalysts.....	70
3.3.4 Effect of Fe ²⁺ concentration.....	71
3.3.5 Effect of pH	72
3.3.6 Identification of intermediates and proposed degradation pathway	74
3.4 The combination of electrochemical and adsorption techniques.....	79
3.4.1 Effect of flow rate on TOC removal.....	79
3.4.2 Effect of bed height.....	80
3.4.3 Effect of electrolyte anions from EC process on the adsorption process	81
3.4.4 Effect of treated volume	82
3.4.5 Effect of initial Padan 95 SP concentration	83
3.4.6 FT-IR analysis of GAC.....	85
3.4.7 Adsorption mechanism of Cartap	86
3.4.8 Conclusions.....	88
CHAPTER 4 CONCLUSION AND RECOMMENDATIONS FOR FUTURE WORKS .	89
4.1 Conclusion.....	89
4.2 Recommendation for future works	90
CHAPTER 5 SUPPORTING INFORMATION	92
REFERENCES	98

Acknowledgements

The work was funded by Vietnam International Education Development and supported from Chemnitz University of Technology regarding to the material as well as instrumental devices.

I am sincerely grateful to my supervisor, Prof. Rudolf Holze for his support, guidance and encouragement, thankful to Prof. Michael Mehring, Dr. Enrico Dietzsch for his experimental support, for sharing his experience and constructive comments.

I would like to thank Mr. Max Hofmann as well as my colleagues for their experimental supports and insightful comments which helped me improve this thesis.

I would also like to express my thanks for all the support I have received from the many staffs of Chemnitz University of Technology. Special thanks to Mr Frank Diener from Institut für chemie's mechanical workshop for the fabrication of experimental reactor.

Finally, I would thank to my parents for their unconditional love that encouraged and supported me throughout my study; my wife who encouraged me and supported me to get over the hard times in the past four years; my friends for their encouragements, reminding me of the colorful world beyond PhD.

List of abbreviations

AC	Activated carbon
AOPs	Advanced oxidation processes
BDD	Boron-doped diamond
BET	Brunauer-Emmett-Teller
BOD	Biochemical Oxygen Demand ($\text{mg}\cdot\text{L}^{-1}$)
COD	Chemical oxygen demand ($\text{mg}\cdot\text{L}^{-1}$)
DTNB	5,5 -Dithiobis-(2-nitrobenzoic acid)
EOPs	Electrochemical oxidation processes
EC	Electrochemical
FID	Flame ionization detector
FT-IR	Fourier transform infrared
GAC	Granular activated carbon
GC-FID	Gas chromatography- Flame ionization detector
GC-MS	Gas Chromatography/Mass Spectrometry
HPLC	High Performance Liquid Chromatography
HPs	Hydroxylation products
4-HBA	4-hydroxybenzoic acid
2-HTA	2-Hydroxyl-terephthalic acid
MCE	Mineralization current efficiency
•OH	Hydroxyl radical
PAC	Powdered activated carbon
RAR	Relative area ratio
SEC	Specific energy consumption
SFAC	Silkworm feces activated carbon
SS	Suspended solids

TA	Terephthalic acid
TOC	Total organic carbon
UV-Vis	Ultraviolet-visible

CHAPTER 1 INTRODUCTION

1.1 Global water usage

Water is an essential natural resource for the development of life and for human activities. Globally, 74 % of water source is used for agriculture and irrigation, 18 % for industrial uses and only 8 % on domestic uses, the detailed report can be seen in Fig. 1. By 2050, feeding a planet of about 9 billion people will require an estimated 50 percent increase in agricultural production and a 15 % increase in water withdrawals [1].

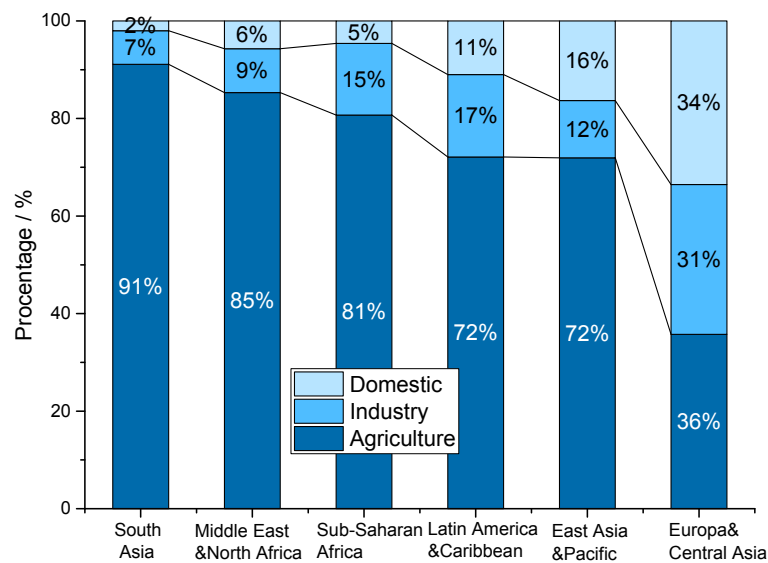


Figure 1 Global water consumption in 2014 [1].

Currently, its scarcity is one problem that causes great concern in our society. 84 % of population who don't have access to improved water, also live in rural areas, where they live principally through subsistence agriculture [2]. According to Population Action International, based on the UN Medium Population Projections of 1998, more than 2.8 billion people in 48 countries will face water stress, in term of water scarcity and quality deterioration [3], by 2025.

Nowadays, water issue is common and it is an area of high alert. We need to take an action to preserve water for us to live a tomorrow.

1.2 Causes of water pollution

1.2.1 Industrial wastewater

Industries produce huge amount of wastewater which contains toxic chemicals and pollutants discharged into rivers, lakes and coastal areas leading to serious pollution problems in the water environment and affecting the eco-system as well as human's life. Based on different industries, the sources of industrial wastewater can be listed out below:

Battery manufacturing: Battery manufacturers specialize in fabricating small devices for electronics and portable equipment (e.g., power tools), or larger, high-powered units for cars, trucks and other motorized vehicles. Pollutants generated at manufacturing plants includes cadmium, chromium, cobalt, copper, cyanide, iron, lead, manganese, mercury, nickel, oil and grease, silver and zinc [4].

Organic chemicals manufacturing: The specific pollutants discharged by organic chemical manufacturers vary widely from plant to plant, depending on the types of products manufactured, such as bulk organic chemicals, resins, pesticides, plastics, or synthetic fibers. Some of the organic compounds that may be discharged are benzene, chloroform, naphthalene, phenols, toluene and vinyl chloride. Metal pollutant discharges may include chromium, copper, lead, nickel and zinc [5].

Electric power plants: Fossil-fuel power stations, particularly coal-fired plants, are a major source of industrial wastewater. Many of these plants discharge wastewater with significant levels of metals such as lead, mercury, cadmium and chromium, as well as arsenic, selenium and nitrogen compounds. Wastewater streams include flue-gas desulfurization, fly ash, bottom ash and flue gas mercury control [6].

Food industry: Wastewater from food industry has distinctive characteristics. It is biodegradable and non-toxic, but has high concentrations of biological oxygen demand (BOD) and suspended solids (SS). The components of food and agriculture wastewater are complicated to predict, due to the fluctuation in BOD and pH in effluents from vegetable, fruit, and meat products and due to the seasonal nature of food processing and post-harvesting.

Iron and steel industry: Water as a lubricant and coolant is applied in the conversion of iron or steel into sheet, wire or rods requires hot and cold mechanical transformation stages. Cooling waters are inevitably contaminated with products especially ammonia and cyanide. Contamination of waste streams includes gasification products such as benzene, naphthalene, anthracene, cyanide, ammonia, phenols, cresols together with a range of more complex organic compounds known collectively as polycyclic aromatic hydrocarbons (PAH) [7].

Nuclear industry: The waste production from the nuclear and radio-chemicals industry is dealt with as radioactive waste.

Petroleum refining and petrochemicals: Pollutants discharged from petroleum refineries and petrochemical plants consist of conventional pollutants (i.e: BOD, oil and grease, suspended solids), ammonia, chromium, phenols and sulfides [8].

Textile Dyeing: Textile dyeing plants generate wastewater which contains synthetic and natural dyestuff, gum thickener (guar) and various wetting agents, pH buffers and dye retardants or accelerators.

1.2.2 Sewage

Sewage (or domestic wastewater or municipal wastewater) is a type of wastewater that is produced by a community of people. It consists mostly of grey-water (from sinks, tubs, showers, dishwashers, and clothes washers), black-water (the water used to flush toilets, combined with the human waste that it flushes away); soaps and detergents [9].

However, the fact is that most wastewater produced globally remains untreated causing widespread water pollution, especially in poor countries. In many developing countries a huge of domestic and industrial wastewater is discharged without any treatment or only after primary treatment [9].

Sewage is a complex mixture of chemicals, with many distinctive chemical characteristics. For example, the high concentrations of ammonium, nitrate, nitrogen, phosphorus, high conductivity (due to high dissolved solids), high alkalinity, with pH typically ranging between 7 and 8. The organic matter of sewage is measured by determining its BOD or the chemical oxygen demand (COD).

1.2.3 Agricultural activity: Fertilizers and pesticides

The nitrogen content in chemical fertilizers may vary depending on the cropping system used. Nutrients are more immediately available for plant uptake in chemical fertilizers than in manure; however, they may be more easily leached into groundwater if used in excess. Chemical pesticides are used to protect crops from insects and bacteria. Both are necessary for the plants growth. Pesticide runoff can result in devastating effects on non-target organisms as well. Runoff can carry pesticides into aquatic environments meanwhile wind can carry them to other fields, grazing areas, human settlements and undeveloped areas, potentially affecting other species living in those areas. Also, the chemicals mixes up with rainwater and flow down into rivers and canals which pose serious damages for aquatic animals.

1.3 The application of Cartap and its current experimental treatment scale

The chemical Cartap (which is also named 1,3-di(carbamoylthio)-2-dimethylaminopropan) based on its chemical structure) is a derivative of Nereistoxin, a naturally occurring insecticidal substance isolated from the marine segmented worms, Lumbrineris. Cartap hydrochloride insecticides have been registered in Japan since 1967, and are widely used in Asia, Europe and South America. Cartap hydrochloride is used against a relatively broad spectrum of insects but particularly against the rice stem borer, Lepidopterous pests of vegetables and Colorado potato beetle. Commercial formulations include water soluble powders, dusts and granules. Approximately 70 % of the world production is applied to rice. It is generally used at the rate of $0.5\text{--}1.5\text{ kg}\cdot\text{ha}^{-1}$ with a pre-harvest interval of 7 to 21 days [10].

Several methods have been developed for the determination of Cartap residues and a gas-chromatographic (GC) method appears suitable for regulatory analysis. The method is based on the conversion of the parent compound and metabolites to Nereistoxin which can be measured by means of a flame photometric detector equipped with a sulphur mode filter. The limit of determination is $0.005\text{ mg}\cdot\text{kg}^{-1}$ [10].

With the content of 95% in Padan 95SP, Cartap is the main compound to cause the pollution of water due to its runoff into canals or rivers. To deal this urgent problem, many advanced oxidation processes (AOPs) have been proposed for Cartap degradation in laboratory scale,

e.g.: photo-catalytic degradation of Cartap on TiO_2 [11], Fenton degradation of Cartap hydrochloride [12]. In AOPs $\bullet\text{OH}$ radicals are considered as the main oxidizing agent for Cartap degradation leading the formation of smaller molecules or the end products (e.g. CO_2 , H_2O and inorganic ions).

1.4 Wastewater treatment technology

The wastewater treatment technology is basically divided into 3 methods: biological, physical and chemical methods.

1.4.1 Biological method

Biological treatment is an important and integral part of any wastewater treatment plant that treats wastewater from either municipality or industry having soluble organic impurities or a mix of the two types of wastewater sources [13]. It can be divided into two categories:

Aerobic processes: take place in the presence of air and utilize those microorganisms (also called aerobes), which use molecular/free oxygen to convert organic impurities into carbon dioxide, water and biomass [13].

Anaerobic processes: take place in the absence of air by those microorganisms (also called anaerobes) which do not require air (molecular/free oxygen) to assimilate organic impurities. The final products of organic assimilation in anaerobic treatment are methane and carbon dioxide gas and biomass [13]. Fig. 2 and 3 depict simplified principles of two processes.

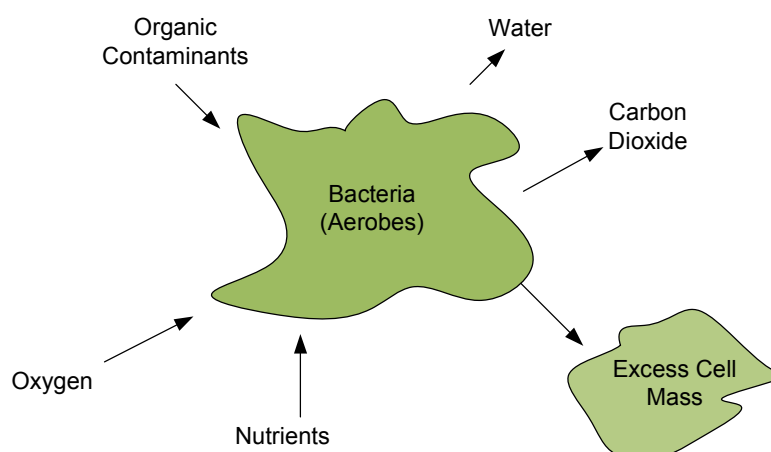


Figure 2 Aerobic treatment principle [13].

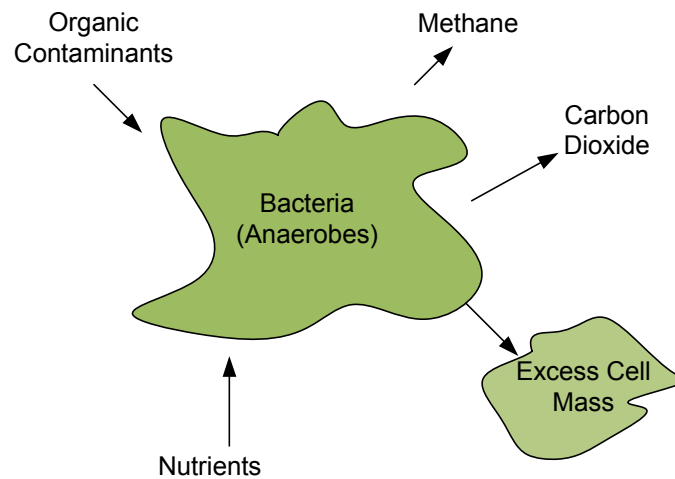


Figure 3 Anaerobic treatment principle [13].

1.4.2 Physical method

Physical methods of wastewater treatment accomplish removal of substances by use of naturally occurring forces, such as gravity, electrical attraction, and Van Der Waal forces, as well as by use of physical barriers. In general, the mechanisms involved in physical treatment do not result in changes in chemical structure of the target substances. In some cases, physical state is changed such as in vaporization, and often dispersed substances are caused to agglomerate, as happens during filtration. Physical methods of wastewater treatment include sedimentation, flotation, and adsorption, as well as barriers such as bar racks, screens, deep bed filters, and membranes[14].

Sedimentation: a physical water treatment process using gravity to remove suspended solids from water. Solid particles entrained by the turbulence of moving water may be removed naturally by sedimentation. The effectiveness depends on the size and weight of the particles. Suspended solids that have a specific gravity similar to water remain suspended while heavier particles settle [15]. The sedimentation process in wastewater treatment usually occurs in tanks of various shapes (i.e. Fig. 4 depicts a type of tank).

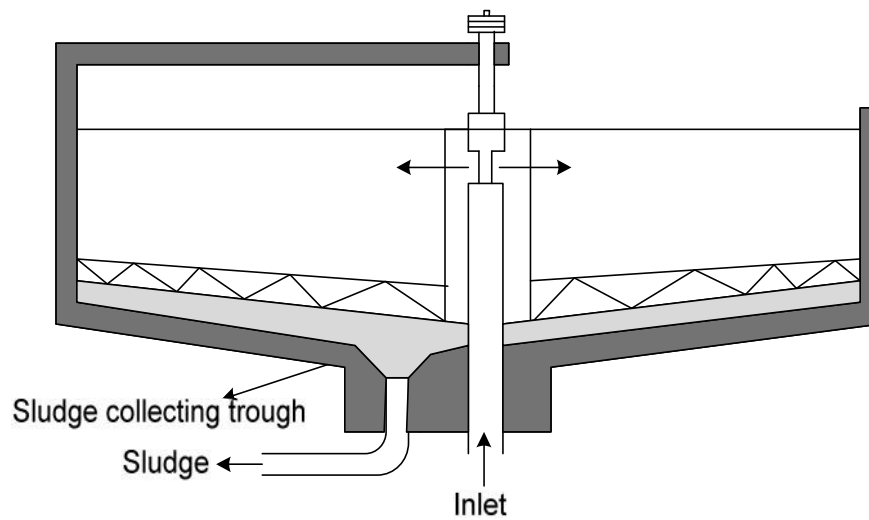


Figure 4 A type of sedimentation tank used in wastewater treatment [16]

Flotation: can be described as a gravity separation process, in which gas bubbles attach to solid particles to cause the apparent density of the bubble-solid agglomerates to be less than that of the water thereby allowing the agglomerates to float to the surface. The different methods of producing the gas bubbles give rise to different types of flotation processes which are electrolytic flotation, dispersed-air flotation and dissolved-air flotation (see its mechanisms in Fig. 5) [17].

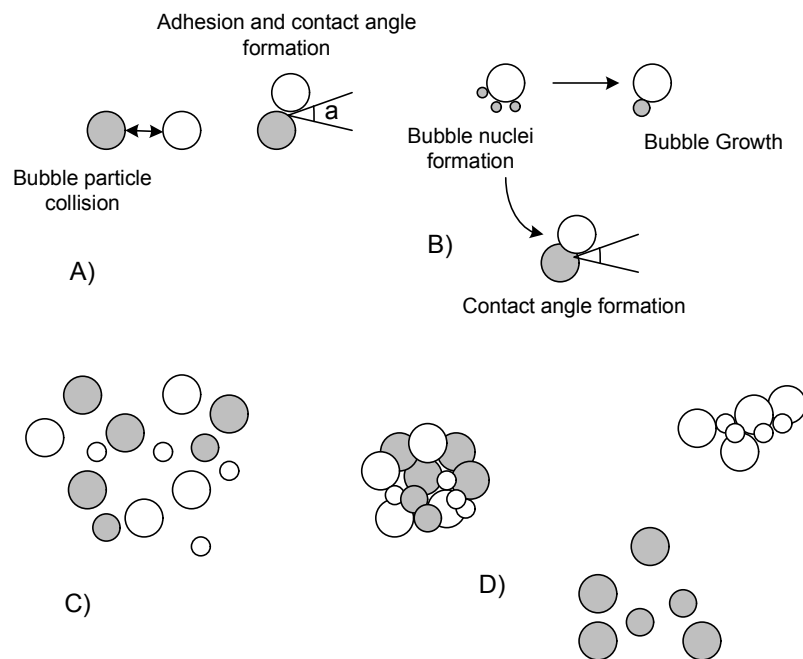


Figure 5 Bubble-particle mechanisms in dissolved air flotation: (a) particle–bubble collision and adhesion; (b) bubble formation at particle surface; (c) micro-bubble entrapment in aggregates; (d) bubbles entrainment by aggregates [18].

Adsorption: is a wastewater purification technique for removing a wide range of compounds from industrial wastewater. This method is most commonly implemented for the removal or low concentrations of non-degradable organic compounds from groundwater, drinking water preparation, process water or as tertiary cleansing after, for example, biological water purification. Adsorption takes place when molecules in a liquid phase bind themselves to the surface of a solid substance. The adsorption diagram is simply depicts in Fig. 6 [19].

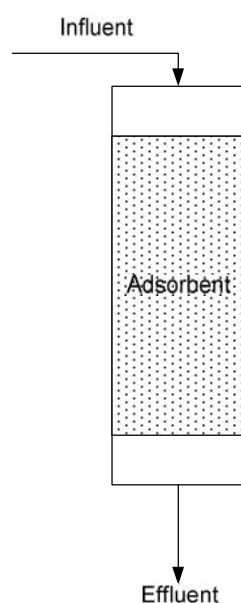


Figure 6 Adsorption diagram.

There are various adsorbents implemented for specific applications:

- Active carbon is by far the most commonly used adsorbent for industrial treatment and is particularly suited to the removal of polar compounds;
- Natural or synthetic zeolites (alumina-silicate-polymers): have a very homogenous pore distribution and polar bonding sites;
- Natural clay minerals: used for the adsorption of very polar organic and inorganic matter (in form of ions);
- Silica gel and activated aluminium: very polar adsorbents based on large affinity for water, used to remove water from polar medium;

1.4.3 Chemical method

In addition or in complement to physical or biological treatments, chemical treatments are used to mitigate the release of contaminants in receiving water bodies along with wastewater discharges. Different chemical processes are used to remove targeted contaminants or to

convert them into stable oxidized end products that can be safely disposed to receiving water streams without any adverse ecological effects. Different chemicals technologies such as chemically enhanced sedimentation (as known for the removal of suspended solids), chemical precipitation, adsorption (to remove selected contaminants) and disinfection (to inactivate bacteria and viruses) are commonly used [20]. Table 1 summarizes the main chemical processes used in water and wastewater treatment.

Table 1 A brief overview of chemical processes used in water and wastewater treatment [20].

Chemical-based processes	Description	Target contaminants
Coagulation	Destabilization of particles to facilitate aggregation during flocculation	Colloidal particles (particle size 0.01–1 μm)
Flocculation	Promoting the aggregation of small particles into larger ones to enhance removal by sedimentation	Total suspended solids
Neutralization	Control of pH	Not applicable
Chemical precipitation	Enhancement of removal of suspended solids and target contaminants by addition of chemicals	Phosphorus, heavy metals, total suspended solids and BOD
Disinfection / advanced oxidation	Use of strong oxidants (e.g. UV light, ozone, chlorine compounds, hydrogen peroxide) to inactivate bacteria and viruses (disinfection)	Bacteria and viruses (disinfection)
	Remove refractory organic contaminants (advanced oxidation)	BOD, COD and recalcitrant contaminants (advanced oxidation)
Ion exchange	Process in which ions of a given species are displaced from an insoluble exchange material by ions of a different species in solution (i.e. contaminants)	Wastewater: Ammonia, heavy metals and organic compounds Drinking water: Hardness due to calcium and magnesium and to a lesser extent aluminum, iron and other cations (water softening)

Adsorption	Process of accumulating contaminants that are in solution on an adsorbent	Organic compounds
------------	---	-------------------

In addition, considering that partial degradation, or only transformation, is often obtained rather than complete mineralization of the contaminants, AOPs-treated wastewaters may require further biological or polishing treatments [20].

1.5 The treatment methods in thesis

1.5.1 Chemical method (advanced oxidation processes)

AOPs were defined as processes that involve the generation of *in situ* hydroxyl radicals ($\bullet\text{OH}$), a chemical oxidizing agent with high oxidation potential able of removing organic and inorganic compound by means of oxidation, resulting in complete mineralization of these compounds as the result of the formation of carbon dioxide, water and inorganic salts, or their conversion into less aggressive products [21-23].

The advantage of AOPs is “environmental-friendly” method because they neither transfer pollutants from phase to the other (as in chemical precipitation, adsorption, and volatilization) nor produce massive amounts of hazardous sludge [24]. AOPs are considered as the promising processes for the wastewater treatment in 21st century [25].

1.5.1.1 Electrochemical oxidation

Electrochemical oxidation of pollutants in aqueous water can be oxidized by direct electron transfer on the anode surface (direct oxidation) or mediated by electro-generated oxidizing species, e. g. $\bullet\text{OH}$ radicals, $\text{S}_2\text{O}_8^{2-}$, H_2O_2 , Cl_2 and HClO etc [26] (called indirect oxidation) as described in Fig. 7.

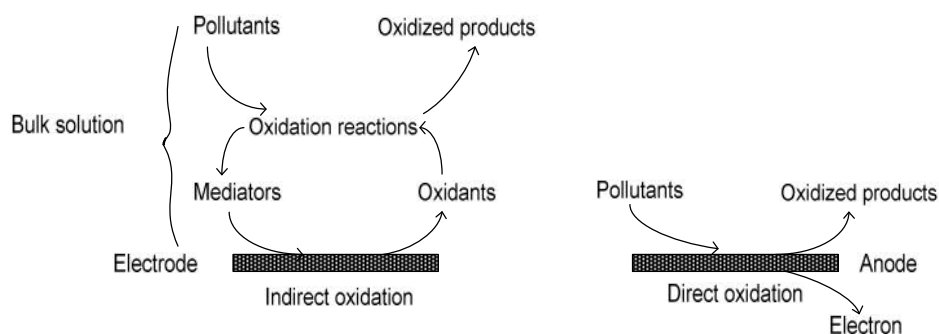


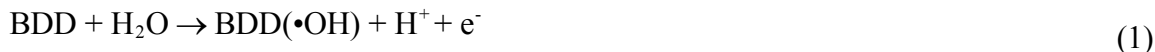
Figure 7 Pollutant removal pathways in electrochemical oxidation (indirect and direct oxidation) [27].

The electrochemical oxidation processes (EOPs) are considered one of the most powerful and clean methods for water and wastewater decontamination. It is well known that the performance of EOPs strongly depends on a variety of operating parameters, including anode material, reaction time, temperature, electrolyte type (chloride-free or chloride present), concentration, applied current density and initial organic load, of which the anode material has been regarded as the most important variable that governing the yield of generated oxidants (i.e. $\bullet\text{OH}$ radical) [28].

BDD electrode: Boron doped diamond (BDD) electrodes have been used in electrochemical experiments since 1983. BDD thin-films are mostly prepared by chemical vapor deposition (CVD) on silicon or metallic substrates under a hydrogen atmosphere yielding H-terminated surfaces [29]. Preparation techniques, characterization, surface modifications and electrochemical properties of BDD electrodes have been reported and reviewed elsewhere [30-35].

BDD electrodes have become attractive materials for electrochemical applications due to their wider potential window, low background currents, higher chemical inertness, high thermal conductivity, and high mechanical stability [29]. The high overpotential for both oxygen and hydrogen evolution are responsible for the wide potential window (the widest so far measured in aqueous electrolytes) and allows conversion of molecules with high oxidation and reduction potentials. Based on these properties, BDD is a well-known material which has some advantages i.e. low adsorption, resistance to (bio) fouling together with the extreme robustness and high resistance to corrosion, and thus BDD as an excellent electrode material for the anodic oxidation of organic wastes. This electrochemical technique is based on the

oxidation of organic pollutants by $\bullet\text{OH}$ radicals (Eq. (1)):



•OH radicals determination: The extremely large rate constants of reactions of $\bullet\text{OH}$ radicals with most compounds ensure that the lifetime of the hydroxyl radicals is in the nanosecond range (< 0.1 ns). For the investigation of these kinetics several methods have been developed including aromatic hydroxylation as one of the most sensitive methods to quantify $\bullet\text{OH}$ radical [36]. Although a variety of techniques (emission spectroscopy, laser induced fluorescence (LIF), electron spin resonance (ESR) spin trap, and chemical probes) is suitable for detection of hydroxyl radicals in the aqueous phase, the quantification of the hydroxyl radical is extremely still challenge [37-41]. However, it was reported that measurements of formed $\bullet\text{OH}$ radicals can be performed using a fluorescence technique [42]. In this method an organic molecule such as TA or coumarin effectively captures $\bullet\text{OH}$ radicals and generates highly fluorescent products which can be easily detected in a fluorescence spectrometer [43]. Comparing with coumarin, the advantage of using TA is the avoidance of isomer interferences, because only a single isomer (2-HTA) (see Fig. 3) is formed during the reaction with $\bullet\text{OH}$.

The fluorescence intensity as a result of formation 2-HTA is proportional to the amount of the $\bullet\text{OH}$ radicals, which many previous authors have observed in the photocatalytic oxidation process [44-47].

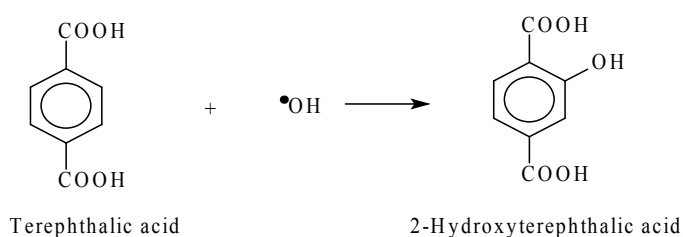


Figure 8 Formation of 2-hydroxyterephthalic acid by the reaction of terephthalic acid with $\bullet\text{OH}$ radicals.

1.5.1.2 Electro-Fenton process

Fenton process: Fenton's reagent is a solution of hydrogen peroxide and ferrous ions and was discovered by the chemical engineer Henry John Horstman Fenton in the 1890s. In the Fenton process the $\bullet\text{OH}$ radical is also produced by electron transfer between hydrogen peroxide (H_2O_2) and ferrous ions (Fe^{2+}) in acidic solution (Eq. (2)):



This method is an attractive oxidative system for wastewater treatment due to the fact that iron is very abundant and non toxic element and hydrogen peroxide is easy to handle and environmentally safe [48]. The oxidation using Fenton's reagent has proven a promising and attractive treatment method for the effective decolorization and degradation of dyes [49] as well as certain toxic contaminants [50].

The efficiency of the Fenton reaction depends mainly on H_2O_2 concentration, $\text{Fe}^{2+}/\text{H}_2\text{O}_2$ ratio, pH and reaction time. Initial concentration of the organics and its character as well as temperature, have a substantial influence on this efficiency. The H_2O_2 production rate is one of the crucial parameters of the process efficiency. It can be continuously supplied to the wastewater solution by feeding directly the electrode by O_2 gas or injected as compressed air (Eq. (3)):



Electro-Fenton process: Electrochemical regeneration of Fe^{2+} ions by electroreduction yields the so-called Electro-Fenton process developed in order to get higher efficiency of the plain Fenton process [51]. The Electro-Fenton process is enhanced using a one-compartment cell where pollutants can be simultaneously oxidized by $\bullet\text{OH}$ produced at the anode (Eq. (1)) and where said regeneration proceeds at the cathode. The diagram is described in Fig. 9.

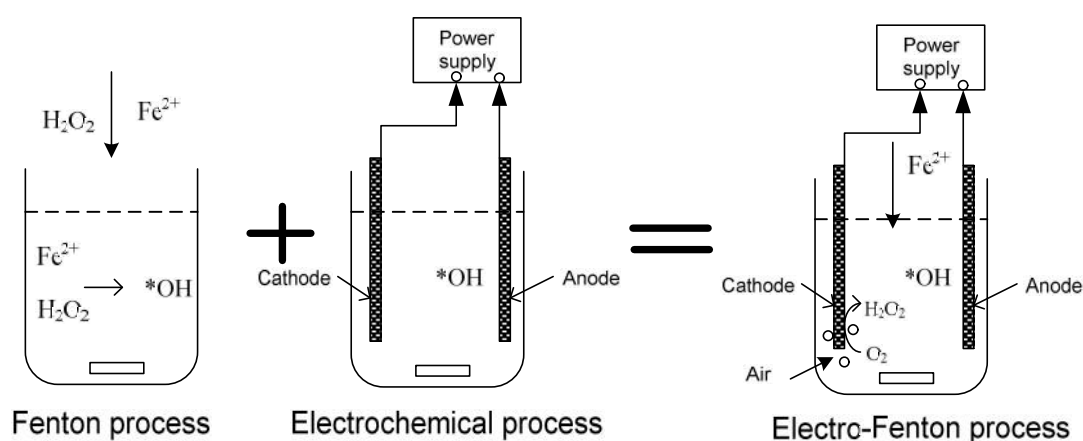


Figure 9 Schematic diagram for Fenton, Electrochemical and Electro-Fenton processes.

1.5.2 Physical method (adsorption process by granulated activated carbon)

Adsorption property: Activated carbon (AC) is one of the most common adsorbent for applied adsorption technology due to many advantages: adsorptive capacity, selectivity, regenerability, kinetics, compatibility and cheap cost [52]. AC comes in granular form with particle sizes in the range of 0.5 to 4 mm or powder with particle sizes $< 40 \mu\text{m}$. This method is effective in removing certain organics such as unwanted taste and odors, micro-pollutants, chloride, fluoride and radon from drinking-water or waste-water [53]. However, it is not effective for microbial contaminants, metal ions, nitrate and other inorganic contaminants [53]. The adsorption capacity of carbon materials is not related to a simple form with their surface area and porosity. The adsorption capacity depends on the accessibility of the organic molecules to the inner surface of the adsorbent, which depends on their size, and other operating parameters. Thus, under appropriate experimental conditions, small molecules such as phenol can access micropores, natural organic matter can access mesopores, and bacteria can have access to macropores. A polar substance (a substance which is well soluble in water) cannot be adsorbed or is only poorly removed meanwhile a non-polar substance can be adsorbed efficiently by AC.

Raw material: AC (including powdered and granular) is made from various types of carbonaceous raw materials: for example, coals (anthracite, bituminous, lignite), woods, peats and coconut shells, etc. Used AC can be regenerated or disposed. Fig. 10 shows the adsorption of organics by GAC.

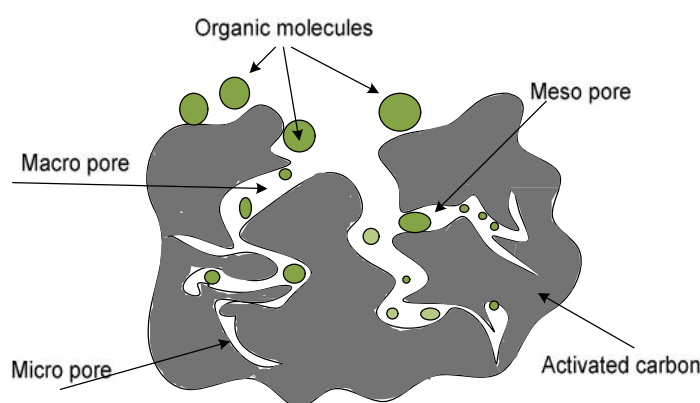


Figure 10 Structure of activated carbon adsorbing organic molecules [54].

AC structure: Activated carbon is highly heterogeneous, both in morphology and in surface characteristics. A typical elemental analysis indicated that the main elements in the activated

carbon framework are carbon (92 % w/w) and oxygen (7 % w/w) [55]. For commercial activated carbons, the amount of oxygen can vary between <1 % up to 16 %. Beyond carbon and oxygen other elements present in the structure can be hydrogen, nitrogen, phosphorus, and sulfur.

Structurally speaking AC is built from graphene layers also called “basal planes” [56]. Different functional groups containing oxygen, nitrogen and sulphur can be found at the basal plane edges as illustrated in Fig. 11 [55,57]. The quantity of functional groups in AC determined by temperature-programmed desorption method may differ depending on the raw material that AC is made from. A short introduction of this method as well as the content of functional groups for some GAC types can be found elsewhere [55].

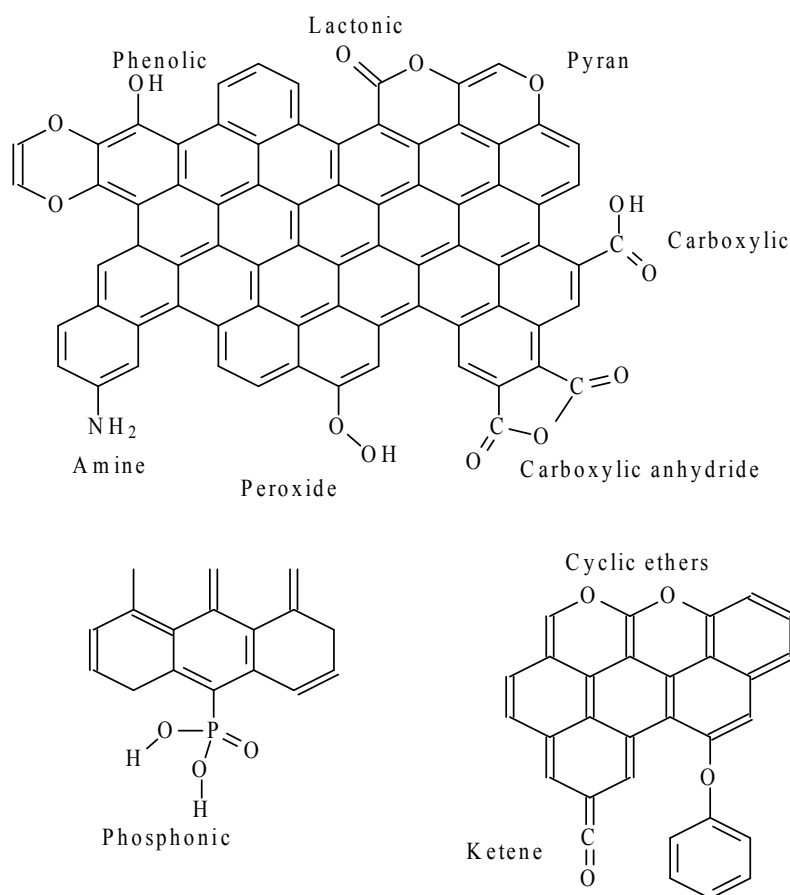


Figure 11 Carbon surface chemistry. Heteroatoms and groups commonly found in activated carbons [56].

1.6 Aims of the study (objectives)

Considering the extensive application of Cartap, it is very easy to cause environmental

pollution and hazardous accidents during usage. To avoid further accumulation of Cartap compounds in aquatic environments and to destroy these contaminants in water, it is necessary to perform degradation studies of Cartap. Nevertheless, a single alone might not be adequate for the treatment of bio-refractory organic compounds, and thus, many researchers are attempting the combination of two or more treatment methods for successful removal [58-60]. Due to the special electrochemical properties of the BDD electrodes and the efficiency of combination methods mentioned above and taking into account that up to our knowledge, this work aims:

1. To study the effect of operating conditions on trapping $\bullet\text{OH}$ radicals which is considered the main oxidizing agent in EOPs. This method is based on the measurement of fluorescence intensity of product (2-HTA) between $\bullet\text{OH}$ radicals and TA.
2. To investigate the electrochemical degradation of Padan 95SP (95% Cartap) on BDD electrode. Operating parameters such as applied current density, types of electrolyte and initial concentration of Padan 95SP were varied in order to determine their effects on the degradation efficiency of Cartap.
3. To investigate Electro-Fenton degradation of Padan 95SP (95% Cartap) and the effect of NaOCl on the process. The operating parameters such as the presence of NaOCl in pretreatment of process, H_2O_2 concentration, Fe^{2+} dosage, co-catalysts metals ion as well as solution pH were varied in order to determine their effects on the degradation efficiency of Cartap.
4. To evaluate the efficiency of the combination of electrochemical and adsorption techniques on the removal of Padan 95SP (95% Cartap). The influence of factors such as supporting electrolytes, flow rate, bed height, recycling number as well as initial concentration were varied in order to determine their effects on TOC removal.

CHAPTER 2 MATERIALS AND METHODS

2.1 Materials

Commercial pesticide Padan 95SP (95 % Cartap) was purchased from Japanese Sumitomo Chemical company branch in Vietnam. Ellman's reagent [5,5'-Dithiobis (2-nitrobenzoic acid) DTNB] purchased from Sigma–Aldrich was used to estimate the content of Cartap in Padan 95SP. Terephthalic acid, 2-Hydroxyterephthalic acid, 4-hydroxybenzoic acid (4-HBA) were also supplied by Sigma–Aldrich. Other chemicals (e.g.: NaCl, HCl, H₂SO₄, BaCl₂·2H₂O, NaNO₃, Na₂CO₃, Na₂SO₄, CH₃OH, K₂Cr₂O₇, H₃PO₄, K₂CrO₄, CH₃COOH, C₂H₅OH, NaOCl, H₂O₂, FeSO₄·7H₂O, glycerol, boric acid, etc) were also supplied by Sigma–Aldrich and Merck. BDD electrode (purchased from Neocoat, Switzerland) was used as working electrode with 3.8 cm² exposed surface area, the thickness of the diamond layer was 2.5–3 μm. Platinum foil and Ag/AgCl (3 M KCl) were used as counter and reference electrodes, respectively. Solutions were prepared using deionized ultrapure water (Seralpur Pro 90 C).

2.2 Experimental methods

2.2.1 Electrochemical experiment

Bulk electrolysis was carried out at room temperature (22 °C) in a 400 mL one-compartment electrochemical cell (see Fig. 12). BDD electrode was used as working electrode with 3.8 cm² exposed surface area of circle shape, the thickness layer of diamond was 2.5 - 3 μm according to manufacturer's information. The surface termination, the morphology and the elemental analysis of BDD electrode used in thesis can be seen in Fig. S1, Fig. S2 and Fig. S3 in *Supporting information section*, respectively. Platinum foil and Ag/AgCl (saturated KCl) were used as counter electrode and reference electrode, respectively. The 250 mL electrolytic system was continuously stirred by a magnetic bar throughout the process. Before the experiments started, the BDD electrode was ultrasonicated for 5 min to remove contaminants, and then washed with ultrapure water. The Pt electrode was also washed with ultrapure water. Padan 95SP-containing solutions with concentrations 100, 300, 500 and 700 mg·L⁻¹ were used. The pH values of the solution were adjusted by H₂SO₄ and NaOH using a pH-meter.

The influence of different salts (Na₂SO₄, Na₂CO₃, NaCl and NaNO₃) on the degradation of

Padan 95SP as well as the formation of 2-HTA was also investigated. The total time of electrochemical process was 120 min.

The electrochemical experiments were performed using IviumStat. Fig. 12 describes the setup of one-compartment glass cell and the holder of BDD electrode.

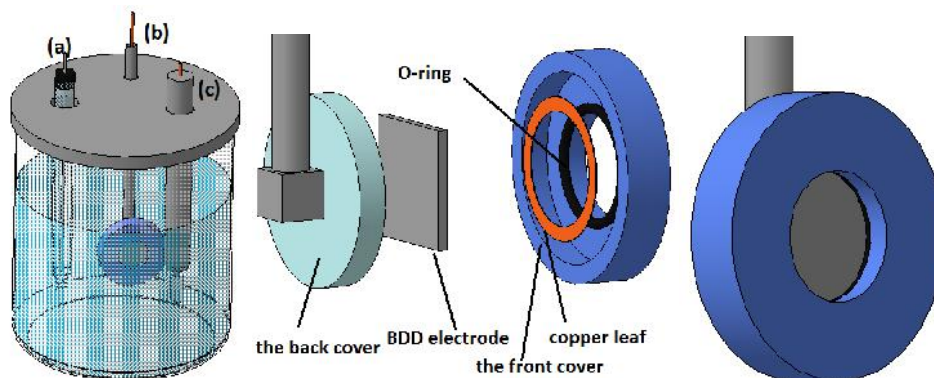


Figure 12 Arrangement of one-compartment glass cell and the Teflon holder for BDD, (a) reference electrode (Ag/AgCl), (b) BDD electrode, (c) counter electrode (platinum electrode).

2.2.3 Electro-Fenton experiment and pretreatment by sodium hypochlorite

The experimental setup for Electro-Fenton process is similar to the electrochemical setup (it can be seen in Fig. 9). In a part of this experiment, NaOCl was added into solution before running Electro-Fenton process to evaluate its effect on Cartap degradation and TOC decay in pretreatment and in Electro-Fenton process, respectively. The pH of solution after pretreatment by NaOCl was adjusted to 3 for Electro-Fenton process (because the presence of NaOCl changes the medium of solution into alkaline medium). The pH values of solution were adjusted by H_2SO_4 and NaOH using pH-meter. The operating parameters, e.g : electrodes, the volume of solution, electrolytic time of process, are similar as were in EC process in section 2.2.2 above. In this experiment, $\text{FeSO}_4 \cdot 7\text{H}_2\text{O}$ was added into solution as source of Fe^{2+} . H_2O_2 was also added into electrolytic solution instead of feeding directly the electrode by O_2 gas or injected as compressed air. 2 M NaOH was added into the samples to stop the Fenton reaction (Fenton reaction is diminished when pH is over 10). All samples were filtered using the filter paper with the pore size of 2.5 μm to eliminate the sludge before taking place the analysis steps.

The electrochemical process was stopped at the selected time intervals for recording the pH change.

2.2.4 The combination of electrochemical and adsorption processes

In adsorption process, GAC from Sigma–Aldrich. GAC was packed in glass column with an internal diameter of 2.8 cm. The treated solution from electrochemical section was subsequently passed into the columns through the valve on the top for controlling the flux flow rate. Sample fractions withdrawn from each treated column were analyzed for Cartap and TOC value. The whole setup is depicted in Fig. 13.

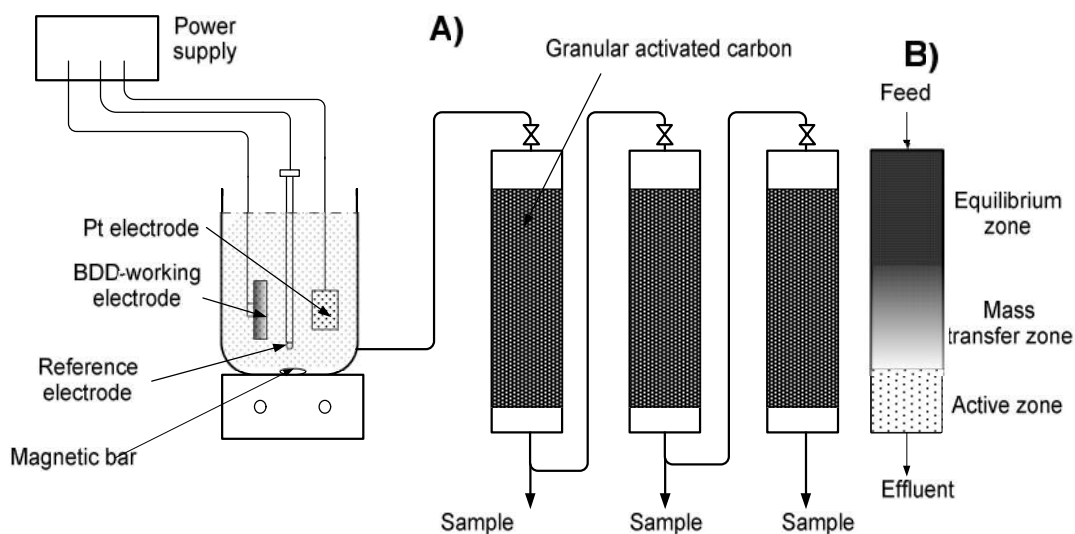


Figure 13 The combination setup of electrochemical and adsorption methods, b) Working zones in bed.

2.3 Analytical methods

2.3.1 Determination of Cartap content according to the 5,5-Dithiobis (2-nitrobenzoic acid) (DTNB) procedure [61-63]

The hydrolysis of Cartap is depicted in Fig. 14 and further detailed information can be found in reference [64]. The $-SCO(NH_2)$ group(s) of Cartap in the presence of DTNB generate the yellow 3-carboxy-4-nitrophenylthiolate anion [65] (see Fig. 15), which is detected at 412 nm wavelength of UV-Vis. Nereistoxin (NTX) (Fig. 14), which lacks a free thiol group, does not react with DTNB. The test solutions of 0.2 mL and 0.8 mL DTNB ($1 \text{ g} \cdot \text{L}^{-1}$) were kept in 4 mL of buffer solution ($\text{pH} = 9$) for the reaction time of 1 h before immediately recording UV-Vis spectrum. The calibration curve for Cartap was built up according to the procedure as described above [62]

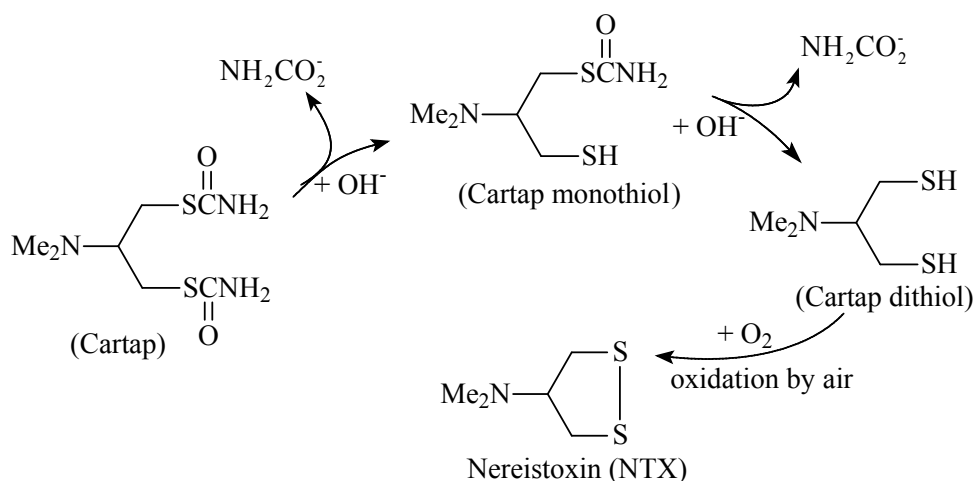


Figure 14 The hydrolysis of Cartap and its hydrolyzed products.

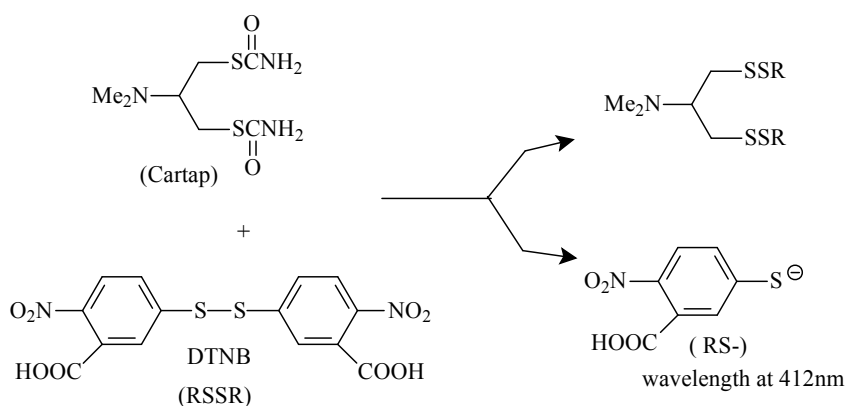


Figure 15 Reaction of Cartap with Ell'man reagent (DTNB).

2.3.2 Fluorescence spectrometer

TA at different concentrations (from 10^{-4} M to 10^{-3} M) was used as the scavenger for $\bullet\text{OH}$ radicals. The stock solution of TA with concentrations ranging from 0.001 M to 0.01 M NaOH was prepared for increasing the solubility of TA and investigating the effect of NaOH on $\bullet\text{OH}$ radicals formation. At various time intervals, samples were taken and immediately measured in the fluorescence spectrometer (FluoroMax-4 Spectrofluorometer, Horiba Jobin Yvon GmbH). The fluorescence of 2-HTA was detected as an emission peak at the maximum wavelength of 425 nm, with the excitation wavelength of 315 nm. All experiments were carried out twice for verification.

2.3.3 UV-Vis spectrometer, TOC analyzer and calculation of efficiency

Every time interval of investigation, the samples were picked up and immediately determined

the rest content of Cartap (according to the procedure [62]) in Getspec-2048-SPU spectrometer. The UV-Vis spectrum of 3-carboxy-4-nitrophenylthiolate anion detected at the maximum wavelength of 412 nm was proportional to the content of Cartap as can be seen in Fig. S4 of *Supporting information section*.

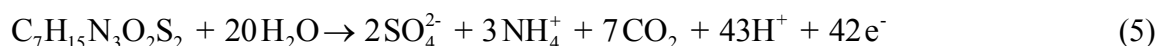
TOC of solutions was determined by standard nonpurgeable organic carbon (NPOC) method using the multi N/C 3100 (Analytik Jena) TOC analyzer. All samples were acidified with H₃PO₄ to remove inorganic carbon. The injection volumes were 0.5 mL and each sample was measured 3 times for verification.

The degradation efficiency of Cartap is calculated according to Eq. (4):

$$m = \frac{1-C}{C_0} \times 100\% \quad (4)$$

where C is the residual concentration of Cartap at a given electrolytic time and C_0 is the initial concentration of Cartap.

The theoretical mineralization of Cartap is proposed in Eq. (5):



The mineralization current efficiency (MCE) for each trial was estimated from Eq. (5) [66].

$$MCE(\%) = \frac{n \cdot F \cdot V \cdot \Delta(TOC)_{exp} \times 100}{4.32 \times 10^7 m \cdot I \cdot t} \quad (6)$$

where n is the number of electrons involved during Cartap mineralization ($n=42$ according to the reaction 5), F is Faraday constant (96 487 C mol⁻¹), $\Delta(TOC)_{exp}$ is the change in TOC value at the time interval (mg·L⁻¹), I is electric current (A), 4.32×10^7 is the factor for units homogenization (3600 s·h⁻¹ × 12000 mg·mol⁻¹), V is the volume of treated solution (L), m is number of carbon atoms in Cartap (7 atoms), t is electrolysis time (h).

In the electrical process, energy consumption is important factor when the electricity is the energy source. The specific energy consumption is calculated in Eq. (7):

$$SEC = \frac{U \times I \times t}{V_{solution} \times \Delta m_{cartap}} \text{ (Kwh} \bullet \text{kg}^{-1} \text{ Cartap)} \quad (7)$$

where U is cell voltage (V), I is electric current (A), t is electrolysis time (h), V_{solution} is the treated volume (L), Δm_{Cartap} is the content of Cartap removed ($\text{g}\cdot\text{L}^{-1}$).

2.3.4 HPLC

For by-products and TA measurement in section 3.1: Concentration of TA solution and its degradation products after electrochemical process were measured using a HPLC system (Knauer) equipped with an Eurospher 100 5 C8, 250 mm x 4.6 mm column and UV-Vis detector at temperature: 25 °C. The mobile phase consisted of water / acetonitrile (95/5, v/v) at a flow rate of $1 \text{ mL}\cdot\text{min}^{-1}$.

For by-products and Cartap measurement in sections 3.2 and 3.3: HPLC was used to analyze Padan 95 SP as well as products formed during electrochemical and Electro-Fenton processes. In case of Electro-Fenton process all samples of electrolyzed solutions were filtered using the filter paper with the pore size of $2.5 \mu\text{m}$, 2 M NaOH is added to the samples to stop the Fenton reaction (Fenton reaction is diminished when pH is over 10). The samples were then analyzed using HPLC system (model KNAUER Smartline). The chromatographic column was Eurospher 100 5 C8 column (250x4.6 mm). The detector was DAD 200-800 nm. The mobile phase consisted of 85 Vol % water and 15 Vol % acetonitrile with the flow rate of $1 \text{ mL}\cdot\text{min}^{-1}$ at 25 °C. The injection volume was 20 μL and the working wavelength for quantitative analysis was 210 nm.

2.3.5 GC-MS

Padan 95SP and by-products in section 3.3 (after being filtered using the filter paper with the pore size of $2.5 \mu\text{m}$) were carried out on the instrument SHIMADZU GC17A-QP5000 with the column WCOT CP-Sil 8-MS 30 m (L), 0.32 mm (ID), $1.0 \mu\text{m}$ (FT) – non-polar. The oven temperature was held at 50 °C for 5 min, elevated to 290 °C at $10 \text{ K}\cdot\text{min}^{-1}$, where it was held for 5 min for the total run time of 25 min. The samples were extracted by n-Hexane or Methyl acetate. The samples were injected in splitless mode with split 25:1 at 275 °C. The carrier gas was He with constant flow of $1.4 \text{ mL}\cdot\text{min}^{-1}$. The mass spectrometer was run in electron ionization (EI) mode with the electron energy of 70 eV. All experiments were carried out in duplication.

2.3.6 Anions concentration measurement

In Fenton process, hydrogen peroxide is added to generate $\bullet\text{OH}$ radicals for organics decomposition. The hydrogen peroxide concentration is then analyzed using the titanium sulfate spectrophotometric method [67].

Sodium hypochlorite (NaOCl), the active ingredient in household, is applied in pretreatment in Electro-Fenton process. Commercial grades of NaOCl contain about 10 % available chlorine. The hydrolysis of sodium hypochlorite in water is shown in Eq. (8):



The active chlorine (ClO^-) [68] and the concentration of $\text{S}_2\text{O}_8^{2-}$ in the solution samples were measured by the iodometric method. The concentration of NO_3^- and CO_3^{2-} were analyzed using spectrophotometric and alkalinity methods, respectively [68]. The concentration of Cl^- was measured by precipitation titration method [69,70], the concentration of SO_4^{2-} was measured by the turbidity method using Getspec-2048-SPU spectrometer.

2.3.7 Characterization of activated carbon

Fourier Transform Infrared (FTIR) spectra were recorded on Bruker Vector 22 spectrophotometer using direct GAC powder with a Platinum ATR unit. All spectra were collected between 5000 and 400 cm^{-1} , averaging the data of 64 successive scans.

The physical properties of the activated carbons such as surface area, average pore diameter were measured using a Thermo Sorptomatic 1990 according to the BET method.

CHAPTER 3 RESULTS AND DISCUSSION

3.1 Effect of operating conditions on trapping the $\bullet\text{OH}$ radicals via TA in the electrochemical process - the efficiency of this method

3.1.1 Calibration curve for 2-HTA

A calibration curve establishing the relationship between concentration of 2-HTA (and thus of $\bullet\text{OH}$ radicals) and fluorescence intensity in the range of relevant concentrations could be obtained based on the fluorescence spectra displayed in Fig. 16.

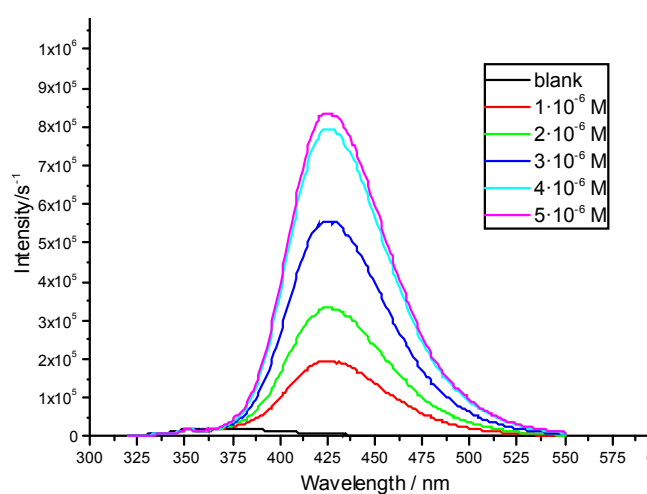


Figure 16 Fluorescence spectra measured at different concentrations (indicated in plot) of 2-HTA in water.

Fluorescence spectra obtained during further study in the presence of TA and NaOH did not differ from those shown in Fig. 16. The calibration plot relating concentration of 2-HTA is displayed in Fig. 17.

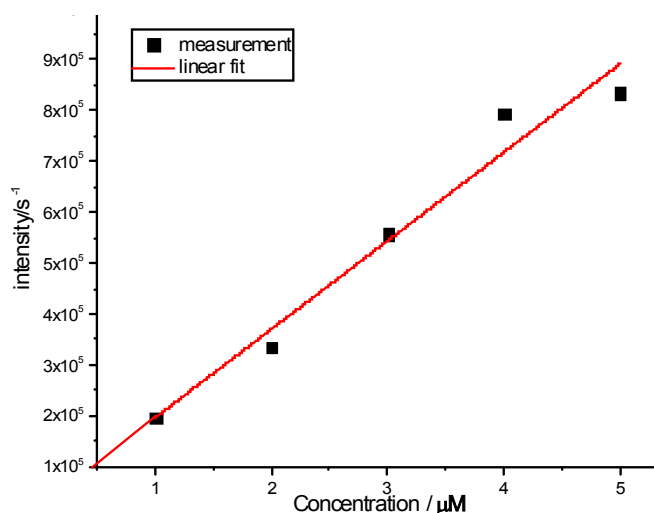


Figure 17 Calibration plot based on data of Figure 16.

3.1.2 Effect of applied current density

The applied current density j is a key experimental parameter in anodic oxidation because it regulates the amount of reactive $\bullet\text{OH}$ radicals produced [71]. Different current densities ranging from 5 to 20 $\text{mA}\cdot\text{cm}^{-2}$ were applied to study their effect on the formation of $\bullet\text{OH}$ (in 5 mM NaOH solution) in 0.05 M Na_2SO_4 electrolyte (Fig. 18).

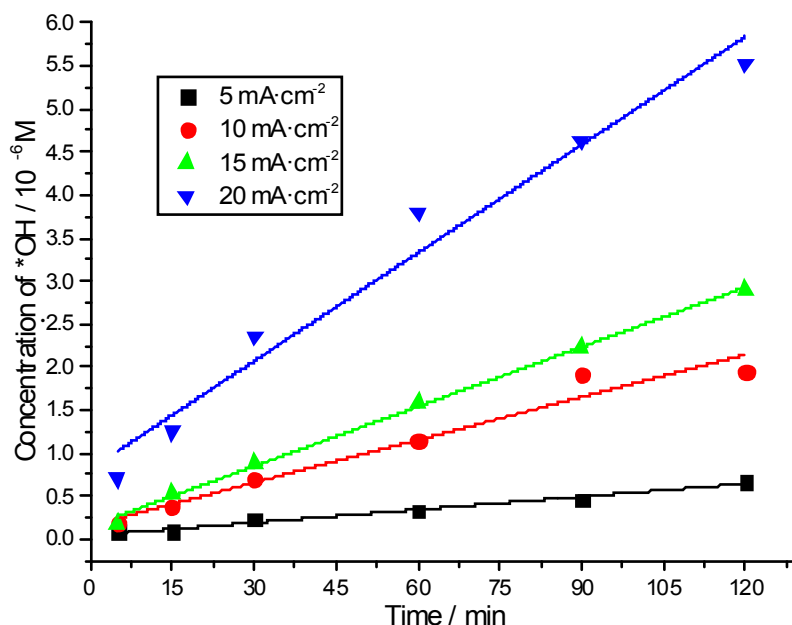


Figure 18 Concentration of $\bullet\text{OH}$ versus time t at various j , $[\text{TA}]_0 = 5 \times 10^{-4}\text{ M}$, 5 mM NaOH for increased solubility of TA, supporting electrolyte: 0.05 M Na_2SO_4 , initial concentration of $\bullet\text{OH}$ radicals was zero (not measured), this results in calculated high initial formation rates seen in Figure 19.

The $\bullet\text{OH}$ radicals react with TA to form 2-HTA (see Fig. 8). As expected, the concentration of $\bullet\text{OH}$ increases with growing current densities but not proportional to the increase of current densities. With lowest applied current density ($j = 5 \text{ mA}\cdot\text{cm}^{-2}$), the concentration of $\bullet\text{OH}$ is determined below $0.7\cdot 10^{-6} \text{ M}$ after 120 min. On the other hand, the concentration of $\bullet\text{OH}$ reaches $5.5\cdot 10^{-6} \text{ M}$ at 4-fold current density ($j = 20 \text{ mA}\cdot\text{cm}^{-2}$).

While the formation rates of $\bullet\text{OH}$ (see Fig. 19) for $j = 5$ and $15 \text{ mA}\cdot\text{cm}^{-2}$ remain stable, a slight decrease in the formation rate for $j = 20 \text{ mA}\cdot\text{cm}^{-2}$. To compare the efficiency of $\bullet\text{OH}$ generation at various j , the insert of Fig. 19 shows the accumulation of $\bullet\text{OH}$ radicals per unit of current density ($1 \text{ mA}\cdot\text{cm}^{-2}$) at various j . It is surprising that at highest current density ($j = 20 \text{ mA}\cdot\text{cm}^{-2}$) this specific formation rate of $\bullet\text{OH}$ reaches the highest value. It is generally expected that at high current densities and the associated high electrode potentials side reactions tend to diminish the actual rate of product ($\bullet\text{OH}$) formation as the result in oxygen evolution (Eq. (9)) occurs on the BDD surface [72], and thus blocking active sites on the electrode. However, in our research the specific formation rate of $\bullet\text{OH}$ at $j = 20 \text{ mA}\cdot\text{cm}^{-2}$ is higher than those at the lower current densities.

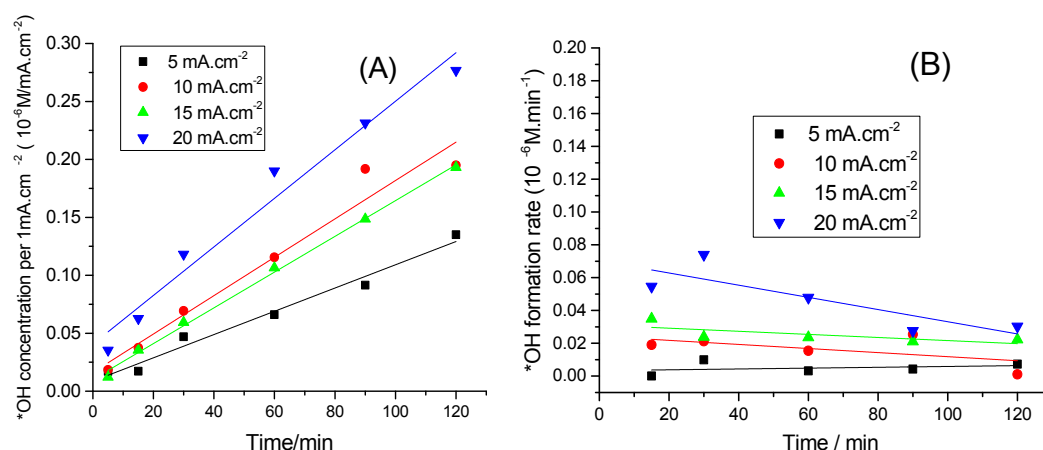


Figure 19 Insert A: Formation rate of $\bullet\text{OH}$ radicals at different current densities, $[\text{TA}]_0 = 5\cdot 10^{-4} \text{ M}$ with 5 mM NaOH added for increased solubility of TA, supporting electrolyte: 0.05 M Na_2SO_4 . Insert B: Concentration of $\bullet\text{OH}$ per $1 \text{ mA}\cdot\text{cm}^{-2}$ versus time t at various j .

This observation contradicts previous studies. Because so far no study of the specific rate of $\bullet\text{OH}$ radical formation has been published we can look for trends in e.g. degradation of

organic compounds with BDD electrodes presumably proceeding via $\bullet\text{OH}$ radicals. For example, Zhang et al. [73] have pointed out that the degradation efficiency of ethidium bromide dropped progressively with increasing current density. They reported that the rate constant degradation only rose 6-fold when the applied current density was increased 18-times, indicating a lower efficiency for reasons not given (see also [74]). The contradictions above may suggest also that the current efficiency (at different applied current densities) could depend on the presence of organic compounds in aqueous solution. It should also be kept in mind that an increase in current density may result in more production of other reactive oxygen-containing species like $\text{S}_2\text{O}_8^{2-}$ (Eq. 10) [75], which could also oxidize TA and promote the formation of 2-HTA:



3.1.3 Effect of different electrolyte anions

The efficiency of BDD electrode-based electrolysis is known to depend strongly on the type of supporting electrolyte [76]. Fig. 20 shows the influence of supporting electrolytes (Na_2SO_4 , Na_2CO_3 , NaNO_3 and NaCl) on the formation of $\bullet\text{OH}$ at $j = 20 \text{ mA} \cdot \text{cm}^{-2}$.

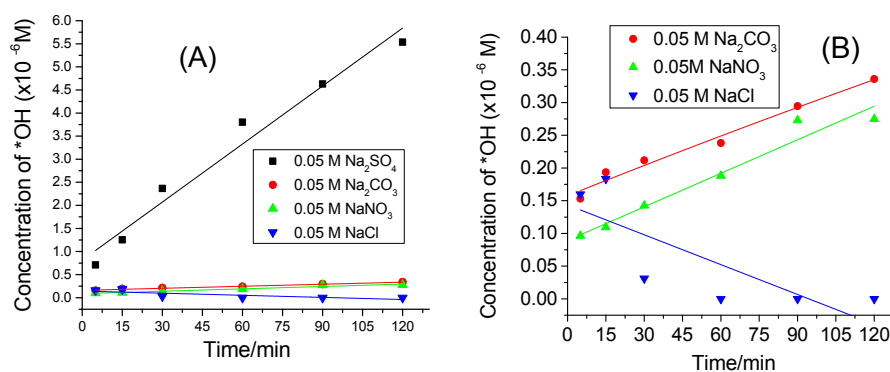
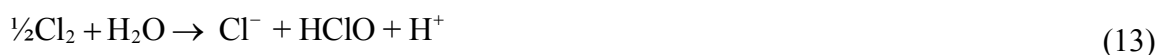


Figure 20 Influence of supporting electrolytes on the accumulation of $\bullet\text{OH}$ during 120 min on BDD electrode (insert A), $[\text{TA}]_0 = 5 \cdot 10^{-4} \text{ M}$ in 5 mM NaOH , $j = 20 \text{ mA} \cdot \text{cm}^{-2}$. Insert B: increased scale from (A).

The obtained results clearly demonstrate the impact of different inorganic anions on the formation of $\bullet\text{OH}$. It is surprising that the concentration of $\bullet\text{OH}$ radicals measured via formation of 2-HTA is higher when using Na_2SO_4 as supporting electrolyte than with the other salts, which cannot be explained straightforwardly taking into account conceivable

differences in properties of the anions and any effects (e.g. stabilizing $\bullet\text{OH}$ or 2-HTA) they might have. To be more specific, the insert of Fig. 20 shows that the concentration of $\bullet\text{OH}$ radicals in case of Na_2CO_3 and NaNO_3 slowly increases from $0.15 \cdot 10^{-6}$ M to $0.35 \cdot 10^{-6}$ M and $0.1 \cdot 10^{-6}$ M to $0.25 \cdot 10^{-6}$ M after 120 min, respectively. On the other hand, the concentration of $\bullet\text{OH}$ in case of NaCl significantly collapses to zero after 60 min. Perhaps chlorine and/or HClO formed by electro-oxidation of chloride degrade 2-HTA and keep its concentration at a very low level. In addition it should be mentioned that degradation efficiency of organics with NaCl is actually higher sometimes [73,77,78]. For example, Zhang et al. [73] have reported that the quickest removal of ethidium bromide is found with NaCl , this can be related to the existence of dissolved Cl_2 and HClO , generated from the oxidation of Cl^- at the BDD electrode, as shown in Eqs. 11 – 13 [58]:



Because of its reactivity Cl_2 is expected to react quickly with organic species and to form stable chlorinated organic intermediates instead of degrading these species oxidatively (i.e. to mineralize them) and these compounds are mostly carcinogenic [79]. Given these arguments NaCl as supporting electrolyte is not helpful to follow the concentration of $\bullet\text{OH}$.

Among the electrolytes studied, Na_2SO_4 was found to be the best supporting electrolyte and was chosen for further studies.

3.1.4 Effect of different concentrations of Na_2SO_4

The influence of Na_2SO_4 concentration on electrochemical generation of $\bullet\text{OH}$ was investigated within the range of 0.01 M to 0.1 M (see Fig. 21). It can be clearly seen that the concentration of $\bullet\text{OH}$ increases gradually when increasing the concentration of supporting electrolyte Na_2SO_4 up to 0.05 M, at 0.1 M the increase is less than expected (e.g. $6.8 \cdot 10^{-6}$ M after 120 min). In contrast, at the lowest concentration 0.01 M Na_2SO_4 , BDD electrode generated only a small amount of $\bullet\text{OH}$ (e.g. $0.62 \cdot 10^{-6}$ M $\bullet\text{OH}$) after 120 min. On the other hand, unusual significant increase in $\bullet\text{OH}$ concentration observed at the beginning of the time interval (here: 5 min) can be also found in the study of T. Tryba et al. [80] or of Y.L. Jiang et

al. [81] (after 10 min) without any reasons disclosed. More surprisingly, in the study of M. Janus et al. [46] the fluorescence intensity was remarkably high at the first interval time of 60 min.

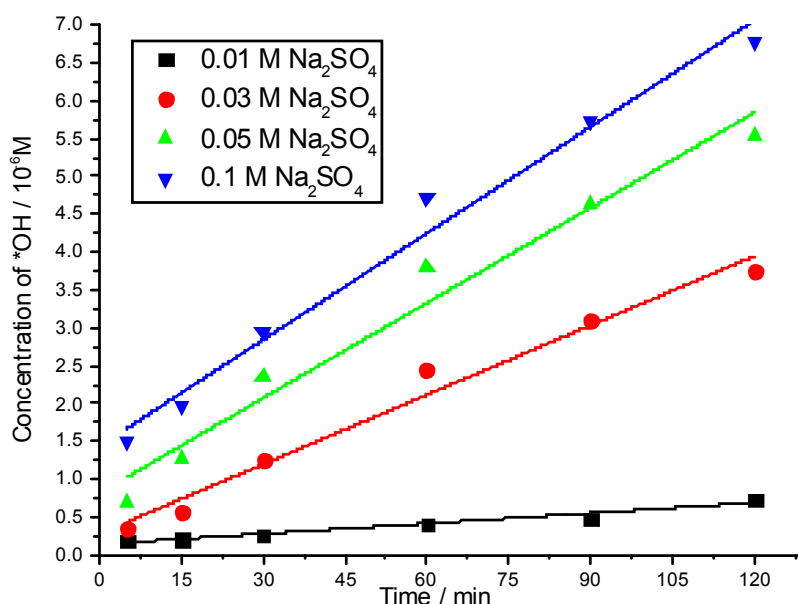


Figure 21 Influence of Na₂SO₄ concentration on the •OH radical concentration, [TA]₀ = 5 · 10⁻⁴ M in 5 mM NaOH, current density : $j = 20 \text{ mA} \cdot \text{cm}^{-2}$.

The formation rates of •OH (Fig. 22) in case of high concentration of Na₂SO₄ (from 0.03 M to 0.1 M Na₂SO₄) decrease during 120 min. This experimental result is agreed with other study [82], in which the formation of H₂O₂ (i.e. thus of •OH) reached the steady-state at various current densities as a function of time, indicating the loss of formation rate of •OH as a function of time. In general, the decreased formation rate of product versus time is due to the decrease in reactants concentration and the increase of products concentration. It is explained by a lower concentration of reactants leads to less effective collisions per unit time, leading to a decreasing reaction rate (except for zero-order reactions). Similarly, a higher concentration of products tends to be associated with a lower reaction rate. However, the TA concentration of this investigation is redundant to capture all of •OH radicals and the formation of 2-HTA via reaction between •OH and TA is obeyed the zero-order reaction due to the independence of the initial TA concentrations (see more detail in section 3.1.5). The higher formation rate of •OH (via 2-HTA formation) at the early stages (5 min) might be due to the generated •OH radicals is rather consumed for 2-HTA formation than the unexpected consumptions of •OH such as by-products formation and/or degradation of by-products due to their low amount at the beginning times.

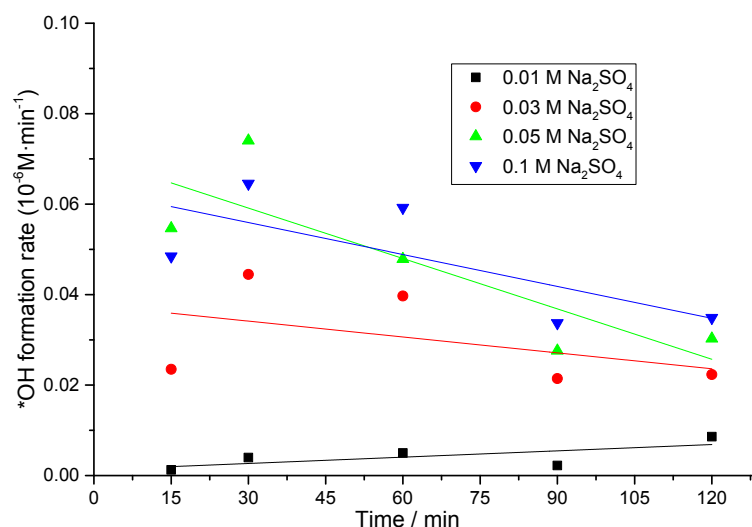


Figure 22 •OH formation rate at different concentration of Na₂SO₄ versus time, [TA]₀ = 5·10⁻⁴ M in 5 mM NaOH, current density: $j = 20 \text{ mA} \cdot \text{cm}^{-2}$.

3.1.5 Effect of initial terephthalic acid concentration

Four different initial TA concentrations (0.1 mM, 0.5 mM, 0.7 mM and 1 mM) were tested to investigate the effect of initial TA concentration on the formation of •OH at 20 mA·cm⁻². Fig. 23 shows the effect of initial TA concentration on the formation of •OH during 120 min. As can be observed in Fig. 23, there is a slight variation in the •OH formation trend at various initial TA concentrations. After 120 min the accumulation of •OH as can be seen slightly higher for higher concentration. To be more specific, at the lowest concentration (i.e. 0.1 mM TA) the concentration of •OH reaches 3.6·10⁻⁶ M meanwhile increasing this value 10 times (i.e. up to 1 mM) accelerates the concentration of •OH to 4.1·10⁻⁶ M at 120 min.

In general, an increase of initial concentration of a compound increases its concentration gradient and mass transfer across the diffusion layer [83] and thus resulting in an increase of the collision between the generated •OH radicals with the TA molecules. In our study, various initial TA concentrations with the range of 0.1 mM – 1.0 mM do not cause any significant difference in the •OH formation trend. Therefore, the range of the initial TA concentration above can be feasible for this investigation.

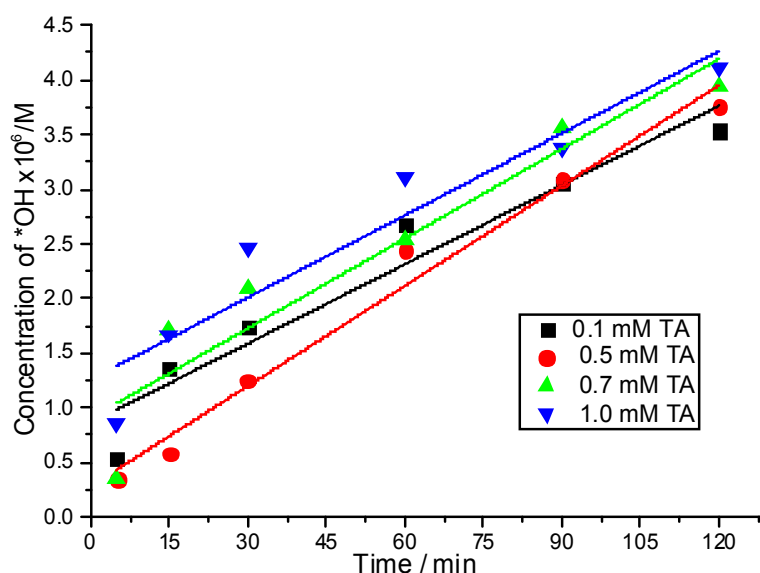


Figure 23 The formation of $\bullet\text{OH}$ at various initial concentrations of TA during 120 min, concentration of electrolyte: 0.03 M Na_2SO_4 , 5 mM NaOH, current density: $j = 20 \text{ mA}\cdot\text{cm}^{-2}$.

The effect of initial concentrations of scavenger was also investigated by previous researchers using photocatalytic techniques for $\bullet\text{OH}$ estimation [44,45]. Regarding K. Ishibashi et al. [45], when the concentration of aromatic compound (i. e. scavenger) is low (less than 1 mM) they can be oxidized by $\bullet\text{OH}$ [44,84-86]. In the study of K. Ishibashi et al. [45], around the 1 mM range of coumarin, no change in fluorescence intensity of hydroxylation product was observed. Under the experimental conditions of presumably 0.1 – 1 mM probe molecules, hydroxylation reactions of coumarin or TA were undergone mainly by $\bullet\text{OH}$ [45], this result also agrees with our study.

3.1.6 Effect of NaOH concentration

Because of poor solubility of TA in neutral medium, NaOH was added to dissolve TA. However, the presence of NaOH significantly affects the formation of $\bullet\text{OH}$. Thus, the concentrations of NaOH in the range of 0.005 M to 0.015 M were tested. Fig. 24 shows the effect of NaOH concentration on the $\bullet\text{OH}$ formation during 120 min.

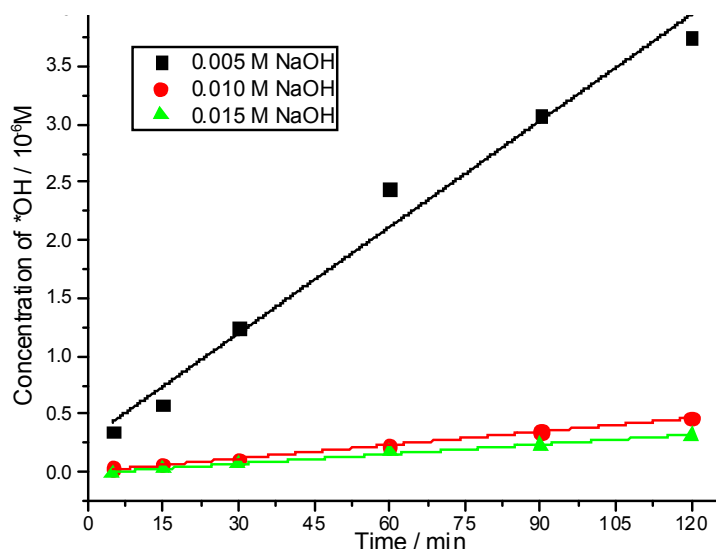


Figure 24 The formation of $\bullet\text{OH}$ versus different concentrations of NaOH during 120 min, concentration of electrolyte: 0.03 M Na_2SO_4 , $[\text{TA}]_0 = 0.5$ mM, current density: $j = 20 \text{ mA} \cdot \text{cm}^{-2}$.

It can be clearly seen that the concentration of $\bullet\text{OH}$ decreases significantly when increasing the NaOH concentration, particularly, for 0.01 M and 0.015 M NaOH the concentration of $\bullet\text{OH}$ is estimated below $0.5 \cdot 10^{-6}$ M after 120 min. At the lower concentration (i.e. 0.005 M NaOH), the formation of $\bullet\text{OH}$ is much higher comparing to 0.01M and 0.015 M. This result may be caused by the recombination reaction with hydroxide ions normally occurring in alkaline solutions (Eq. 14) [87] to form water:



Similar trends have been reported in previous study by Y. Nakabayashi et al. [88], they investigated the influence of pH on $\bullet\text{OH}$ formation using photo-electrochemical oxidation with rutile TiO_2 single crystals. They reported that the concentration of 2-HTA reduced approximately 3 times when pH value increased from 9.6 to 12.5 for both TiO_2 electrodes with (100) and (110) facets. The same result was also found in the study of Jiang et al. [81], they have pointed out that the concentration of $\bullet\text{OH}$ decreased gradually when increasing the pH value from 7 to 9.

3.1.7 By-products and the reliability of $\bullet\text{OH}$ determination technique

According to the literature [89] the main products of TA hydroxylation are 2-HTA and 4-hydroxybenzoic acid (4-HBA), however only 2-HTA is highly fluorescent. It is necessary to know the transformation pathway of TA for optimal experimental condition. In this study,

HPLC was used to trace the decomposition of TA and the formation of electrochemical by-products.

In Fig. 25 the increasing trends of 2-HTA detected by both techniques (HPLC and fluorescence spectroscopy) are very similar. It can be concluded that the yield of 2-HTA can be also determined by HPLC. Nevertheless, the fluorescence spectroscopy can be more commonly used for evaluation of $\bullet\text{OH}$ radicals because 2-HTA is the main product of TA hydroxylation and the fluorescence technique is quickly and a very sensitive method for its detection with very low concentration of fluorescent product.

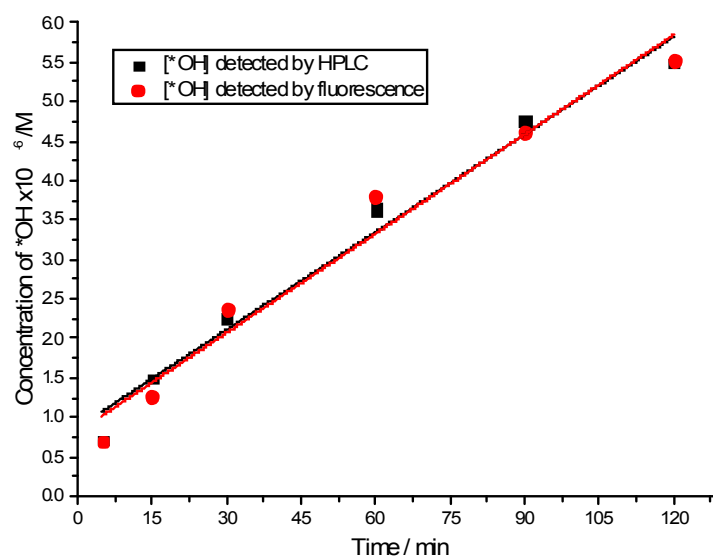


Figure 25 Comparison of 2-HTA concentration detected by HPLC and fluorescence spectroscopy during 120 min, $[\text{TA}] = 5 \cdot 10^{-4} \text{ M}$, concentration of electrolyte: 0.05 M Na_2SO_4 in 5 mM NaOH solution, current density $j = 20 \text{ mA} \cdot \text{cm}^{-2}$.

The formation of products and the degradation of TA during 120 min of electrochemical generation of $\bullet\text{OH}$ are shown in Fig. 26. The mechanism formation of products is shown in Fig. 28. Taking into account that the concentration of TA ($5 \cdot 10^{-4} \text{ M}$) and other parameters were optimal using fluorescence technique above. Beside two products (2-HTA and 4-HBA), a new by-product at the retention time of 3.9 min was found in HPLC. It is surprising that the increase of 2-HTA is slightly higher than that of 4-HBA. Thus, both 2-HTA and 4-HBA are the main products in this condition. Moreover, the linear TA decrease by $130 \cdot 10^{-6} \text{ M}$ (i.e. from $500 \cdot 10^{-6} \text{ M}$ down to approximately $370 \cdot 10^{-6} \text{ M}$) after 120 min is much higher than the increase in the formed products. Thus, based on the significant loss of TA concentration we can assume that TA or those products are probably decomposed by the oxidizing species (e.g. $\bullet\text{OH}$, $\text{S}_2\text{O}_8^{2-}$) to form other products which might not be obtained in HPLC, or furthermore, to

release the end products (CO_2 and H_2O) (see reaction pathways in Fig. 28). As the result, the total content of all products obtained by HPLC is much lower than the loss of the large amount of TA ($11 \cdot 10^{-6} \text{ M}$ versus $130 \cdot 10^{-6} \text{ M}$).

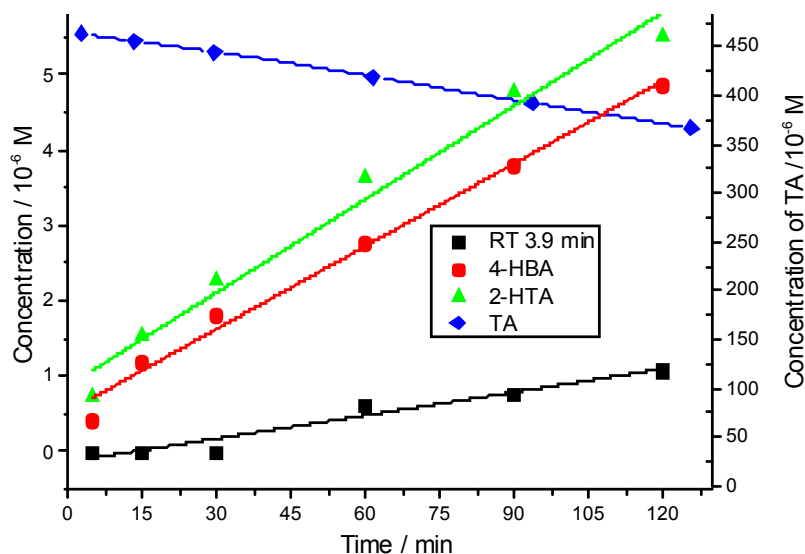


Figure 26 Formation of products and TA degradation detected by HPLC during 120 min, initial concentration of TA: $5 \cdot 10^{-4} \text{ M}$, concentration of electrolyte: $0.05 \text{ M Na}_2\text{SO}_4$ in 5 mM NaOH , current density: $j = 20 \text{ mA} \cdot \text{cm}^{-2}$, RT 3.9 min (by-product at retention time of 3.9 min).

The same result was also found in a previous study by Bubacz et al. [44]. They have pointed out that after 80 min of UV irradiation time the linear TA reduction of $15 \text{ mg} \cdot \text{dm}^{-3}$ (from $70 \text{ mg} \cdot \text{dm}^{-3}$ to approximately $55 \text{ mg} \cdot \text{dm}^{-3}$) was 3 times higher than the total formation of all products ($15 \text{ mg} \cdot \text{dm}^{-3}$ versus $5 \text{ mg} \cdot \text{dm}^{-3}$). In the study of G.L. Newton and J.R. Milligan [90], the trapping efficiency of $\bullet\text{OH}$ formed on TiO_2 photocatalysis was estimated about 4.7 % by the photoluminescence technique using coumarin as probe molecule. This implies that the photoluminescence method only detects a small part of the generated $\bullet\text{OH}$ and the formation rate of $\bullet\text{OH}$ is actually underestimated [91]. Peralta et al. [36] have suggested that $\bullet\text{OH}$ radicals were not only consumed to produce the hydroxylation products but also are being consumed in their mineralization when using salicylic acid as scavenger.

From the observed experimental result above, the efficiency of trapping the $\bullet\text{OH}$ radicals can be established. The $\bullet\text{OH}$ consumption is not only from the hydroxylation products (HPs) but also for their mineralization. Based on this suggestion, Fig. 27 shows the calculation of $\bullet\text{OH}$ radicals via 2-HTA and the total hydroxylation products. As can be seen in Fig. 27, the consumption of $\bullet\text{OH}$ for HPs almost doubles that for 2-HTA, therefore, we can propose the

quantitative formula of the $\bullet\text{OH}$ radicals by fluorescence technique in our investigation:

$$\bullet\text{OH}_{\text{exp}} = 2 \times \bullet\text{OH}_{2\text{-HTA}} + m \quad (15)$$

Where $\bullet\text{OH}_{\text{exp}}$ is the concentration of $\bullet\text{OH}$ generated by electrochemical process, $\bullet\text{OH}_{2\text{-HTA}}$ is the concentration of $\bullet\text{OH}$ measured by fluorescence technique, m is the $\bullet\text{OH}$ radicals consuming for mineralization (it can be assumed via COD or TOC values).

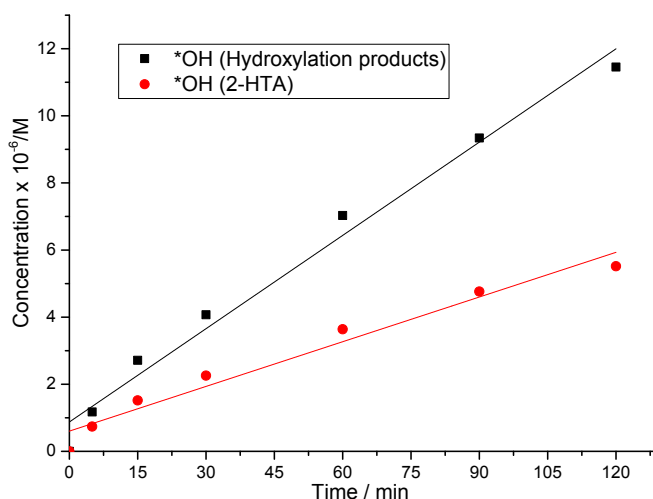


Figure 27 $\bullet\text{OH}$ estimation and their linear fitting via 2-HTA and the total hydroxylation products on BDD electrode, initial concentration of TA: $5 \cdot 10^{-4}$ M, 0.05 M Na_2SO_4 in 5 mM NaOH, current density: $j = 20 \text{ mA} \cdot \text{cm}^{-2}$.

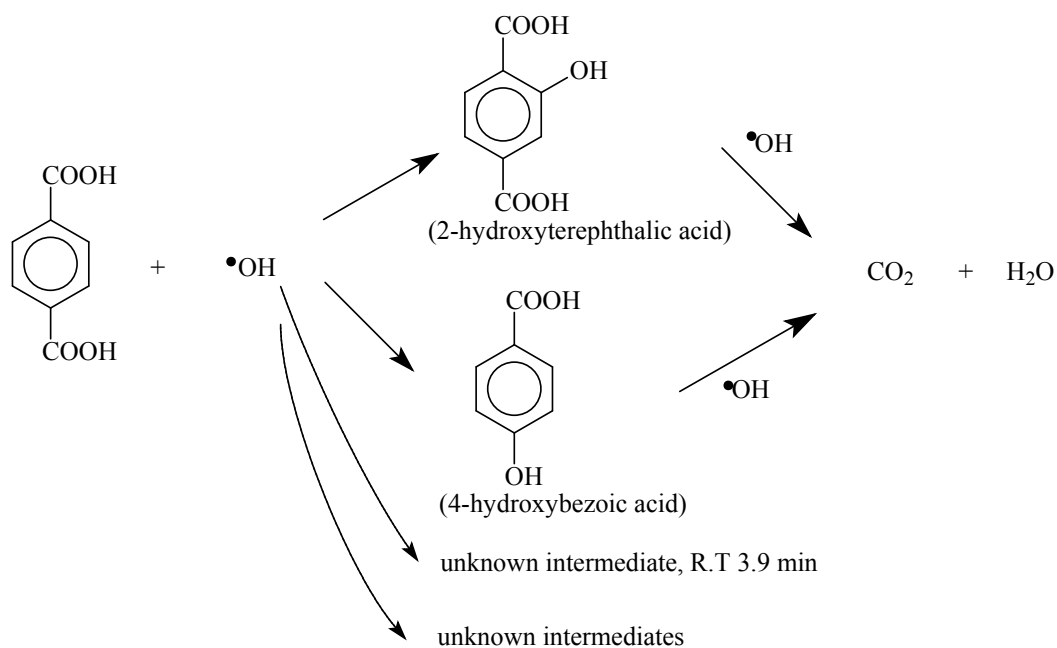


Figure 28 Mechanism reaction of terephthalic acid and hydroxyl radical.

3.1.8 Conclusions

Fluorescence spectroscopy is a sensitive technique used to indirectly quantify the low concentration $\bullet\text{OH}$ radical production when using terephthalic acid as scavenger.

The optimal condition for $\bullet\text{OH}$ radical measurement was established: concentration of electrolyte: 0.05 M Na_2SO_4 , initial concentration of TA: 0.1 mM, concentration of NaOH: 5 mM, current density: $j = 20 \text{ mA}\cdot\text{cm}^{-2}$. At that condition the concentration of $\bullet\text{OH}$ gradually increases to $5.5\cdot 10^{-6}$ M after 120 min of electrolysis.

The main product (2-HTA) was observed slightly higher than by-product (4-HBA) during the optimal condition. The amount of $\bullet\text{OH}$ radicals generated is not only consumed for conversion of TA into products but also attends in the degradation of those products to CO_2 and H_2O . As suggested, the amount of generated $\bullet\text{OH}$ radicals is theoretically much higher than the amount of 2-HTA formed. Thus, we should take into account the simulated calculation which relates to the reaction pathways of TA and $\bullet\text{OH}$ radicals.

3.2 Electrochemical process for Padan 95SP degradation

3.2.1 Analysis of ingredients in pesticide Padan 95SP

Due to the content of 5 % of additives (in commercial pesticide Padan 95SP), which might cause some effects to the stability of Cartap in investigated experiments, GC-MS was applied to determine their chemical structures. As can be seen in Fig. 29 and 30, the compound depicted at retention time of 7 min is very similar to an amino alcohol, whose structure corresponds to the Fig. 30(A) with the base peak of 44 (m/z). The second signal at 11 min can be a sulfur containing compound, which is suggested by chemical structures in Fig. 30(B) or Fig. 30(C) with the base peak of 45 (m/z). The mass spectrum of the peak at 14.2 min (see Fig. 29) is similar to that, which is stored for Cartap in the library with the base peak of 70.95 (m/z) (see Fig. 30(D)). The last retention time at 15 min could be Nereistoxin, which can be formed in ethanolic solution or in the injector of the GC due to decomposition of the starting solution.

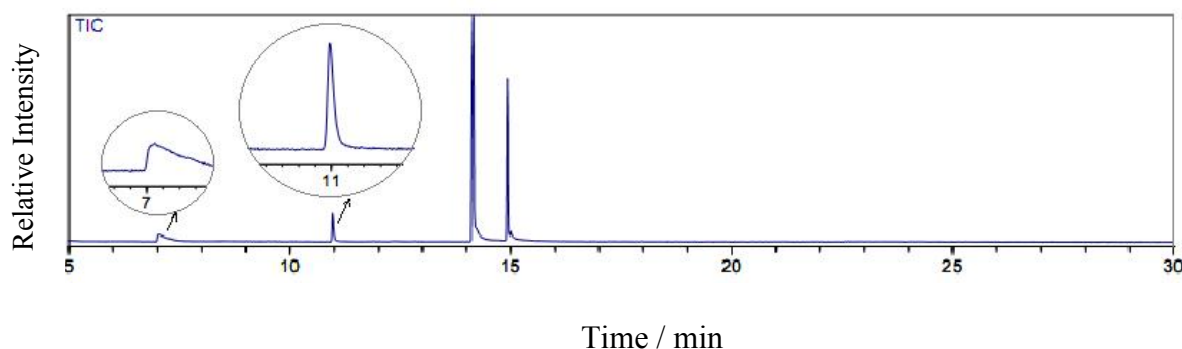


Figure 29 GC-MS profile of Padan 95SP in methanol.

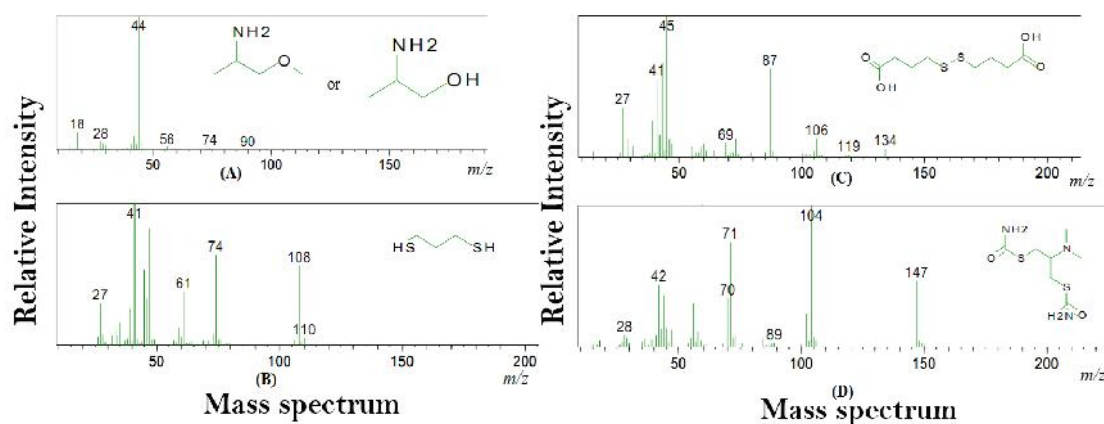


Figure 30 The mass spectrum of ingredients in Padan 95SP.

3.2.2 Effect of pH on hydrolysis rate of Cartap in Padan 95SP

It is important to note that pure Cartap is hydrolyzed quickly in neutral and alkaline mediums to form different hydrolysis products [61,92]. Thus, the investigation of the pH effect on hydrolysis rate of Cartap (in Padan 95SP) before the electrochemical degradation is necessary to evaluate the interferences from itself hydrolysis process.

The influence of different pH values (from 3 to 9) on hydrolysis of $300 \text{ mg}\cdot\text{L}^{-1}$ Padan 95SP was investigated in this study (see Fig. 31). It is surprising that Cartap from Padan 95SP is stable with pH (from 3 to 9) for 6 h indicating no loss of the bound thiol of Cartap in different mediums. However, via determination of the remaining Cartap at various pH Cartap hydrolyzed for several days with different rate (insert A and B of Fig. 31). To be more specific, at pH 7 or 9, the hydrolysis of Cartap completes after 4 days meanwhile it need more than 5 days and 6 days (predictably) for completely hydrolyzing at pH 5 and 3, respectively. Instead, the hydrolysis product (i.e. NTX) is formed. These results contracted to the previous researcher [61]. S.J. Lee et al. [61] has reported that Cartap generated 1.8 equiv of free thiol at pH 7.4 or 9.0, and the reaction appeared to be essentially completed in 120 min. Normally, the hydrolysis reaction of Cartap will be followed by the first-order process as also can be seen in the study of Y. Asani and T. Yoshida [93]. And they assumed that the half-life for Cartap (25 °C) at pH 5, 7, 9 were 19 h, 11 min and 1.1 min, respectively. In our investigation, the first-order process can be seen until the 3rd day (see insert C of Fig 31). After that time, for example, on the 4th day this law is not observed anymore.

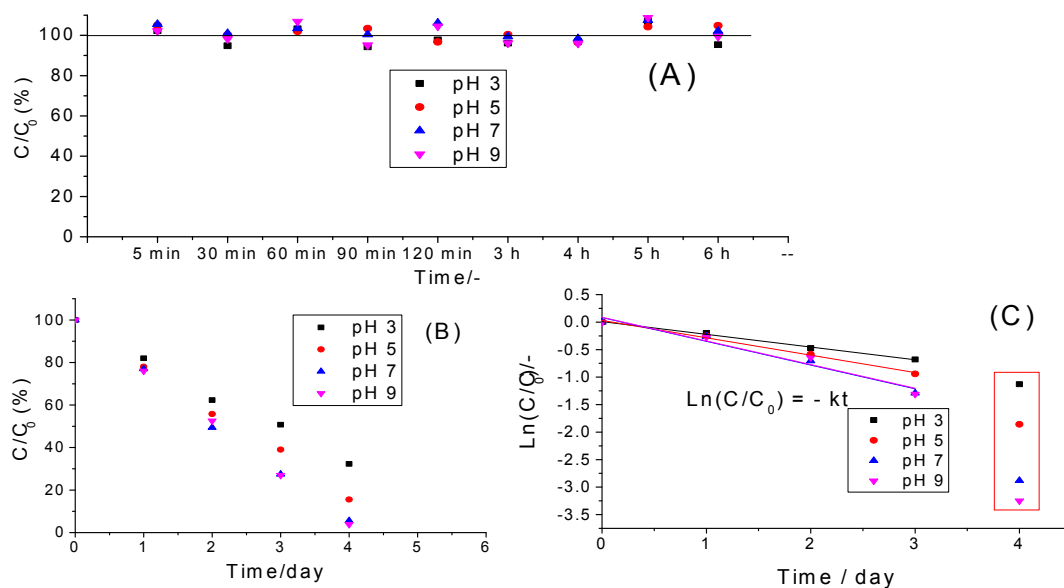


Figure 31 Insert (A) and (B) shows the remaining Cartap (including mono/di-thiol Cartap) vs time at pH = 3, 5, 7 and 9, initial concentration of Padan 95SP (95% Cartap) : $300 \text{ mg}\cdot\text{L}^{-1}$, C_0 , C : concentration of Cartap (including mono/di-thiol Cartap) at 0 min and at the time interval, respectively. Insert (C) shows the Pseudo-first-order reaction based on hydrolysis of Cartap.

It is important to note that Cartap in commercial pesticide Padan 95SP consists of 95 % per weight and there are also 5 % of additives, which could be assumed to increase the stability of Padan 95SP in aqueous solution. As the result, Cartap (in Padan 95SP) is much more slowly hydrolyzed than pure Cartap.

3.2.3 Effect of applied current density

The applied current density (j) is a key experimental parameter in anodic oxidation because it regulates the amount of reactive $\bullet\text{OH}$ radicals produced [71]. The different current densities ranging from 5 to $20 \text{ mA}\cdot\text{cm}^{-2}$ were applied to study their effect on the degradation of $300 \text{ mg}\cdot\text{L}^{-1}$ Padan 95SP in $0.05 \text{ M Na}_2\text{SO}_4$ (Fig. 32 A). The degradation of Cartap in electrochemical process is occurred under the first-order kinetic as shown in Fig. 32 B.

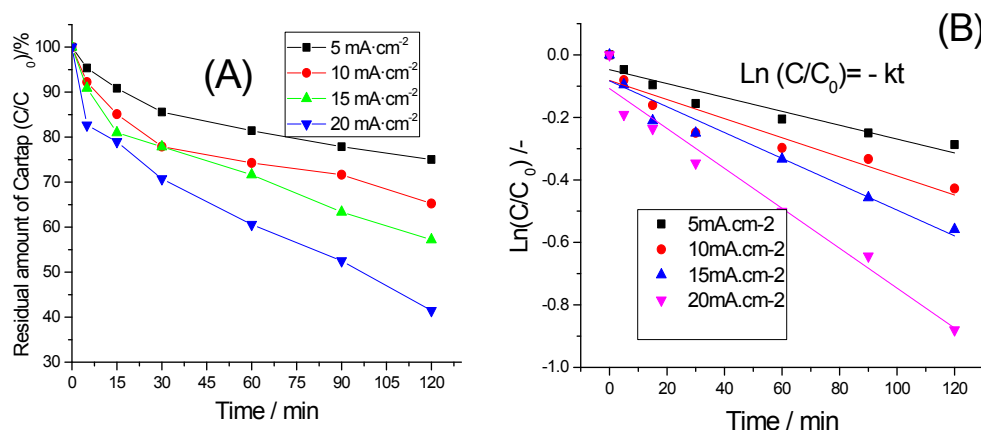


Figure 32 Effect of current densities on Cartap degradation at j from 5 to 20 mA·cm⁻² (insert A), initial concentration of Padan 95SP (95% Cartap): 300 mg·L⁻¹, supporting electrolyte: 0.05 M Na₂SO₄, pH = 3. Insert B: The Pseudo-first-order process of Cartap degradation.

As expected, the degradation of Cartap increases with rising current density. This proves that under constant applied current density, the electro-generation of •OH at BDD surface is uniform and it is greatly enhanced with increasing current density, thus promoting the oxidation of Cartap. It is surprising that more than 5 % and 15 % of Cartap are decomposed at the beginning of 5 min at 5 mA·cm⁻² and 20 mA·cm⁻², respectively. However, after 120 min of electrochemical oxidation, Cartap in solution remained approximately at 75 % and 41 % when increasing current density 4-folds (from 5mA·cm⁻² to 20 mA·cm⁻²). Increasing j (from 5 mA·cm⁻² to 20 mA·cm⁻²) does not proportionally to enhanced Cartap oxidation. It can be explained that at high applied current, side reactions such as oxygen evolution (Eq. (5)) occurs at the BDD surface [94] leading to produce a greater of gas on the surface of electrode, and thus minimizing the number of active side electrode:



As the result, the current efficiency of the process drops significantly with rising current density (see insert of Fig. 33). The high MCE at the early stage of 5 min for all cases may be attributed to a larger accumulation of pollutants in the vicinity of electrode surface during the initial stage of electrolysis [75]. As shown in Fig. 33, lower TOC decay comparing with Cartap decomposition can also be explained by the consumption of oxidizing species (i.e. •OH radical and S₂O₈²⁻) not only for Cartap decomposition but also for the mineralization of

intermediates.

Some previous studies have also shown the same trends. For example, C. Zhang et al. [73] have pointed out that the degradation efficiency of ethidium bromide dropped progressively with increasing current density. They reported that the current efficiency only raised 6–folds when the applied current density increased 18-times.

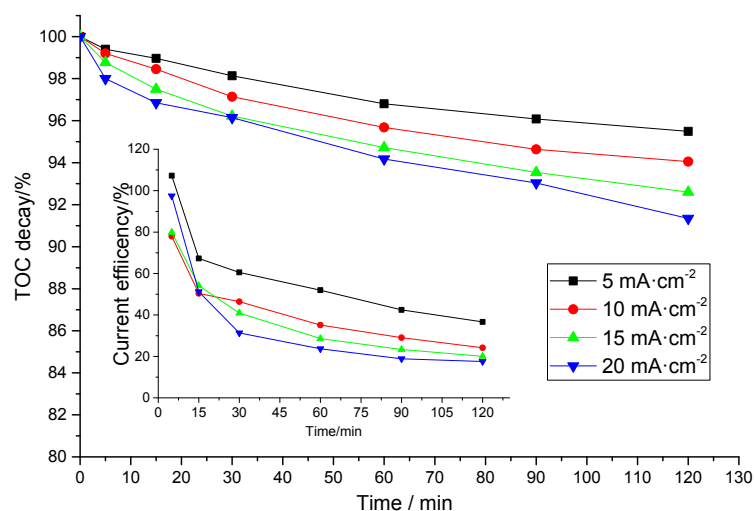


Figure 33 The TOC decay at various current densities, initial concentration of Padan 95SP (95% cartap): $300 \text{ mg}\cdot\text{L}^{-1}$, supporting electrolyte: $0.05 \text{ M Na}_2\text{SO}_4$, $\text{pH} = 3$. Insert: mineralization current efficiency (MCE) at different current densities versus electrolytic time.

3.2.4 Effect of different electrolyte anions

The efficiency of BDD electrode is well-known to be strongly dependent on the type of supporting electrolyte [73]. Fig. 34 shows the influence of supporting electrolyte (Na_2SO_4 , Na_2CO_3 , NaNO_3 and NaCl) on the degradation efficiency of Cartap (at $j = 20 \text{ mA}\cdot\text{cm}^{-2}$). The results obtained clearly demonstrate the effect of different electrolytes on the degradation of Cartap at $j = 20 \text{ mA}\cdot\text{cm}^{-2}$.

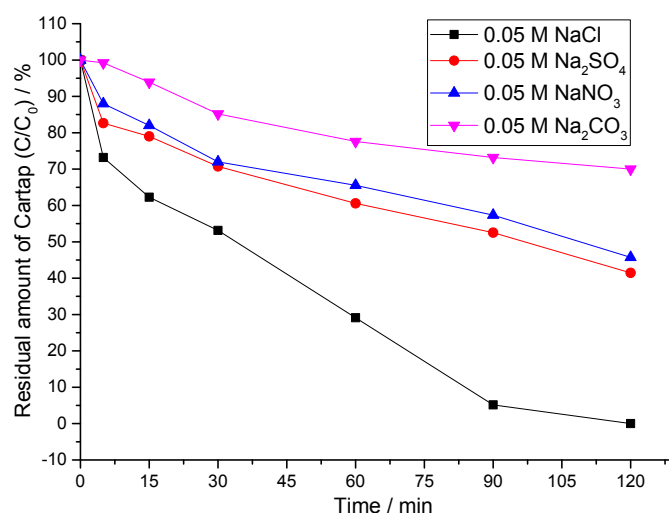


Figure 34 Cartap degradation versus various supporting electrolytes in electrochemical process, $[\text{Padan 95SP}]_0 = 300 \text{ mg}\cdot\text{L}^{-1}$, $V_{\text{treated solution}} = 250 \text{ mL}$, $\text{pH} = 3$ (except the case of Na_2CO_3 , which was added into electrolytic solution with the initial pH of deionized water), $j = 20 \text{ mA}\cdot\text{cm}^{-2}$.

To be more specific, Cartap is completely destroyed after 120 min in case of NaCl meanwhile approximately 41 % of Cartap is remained in treated solution for the case of Na_2SO_4 and the much more remaining Cartap content is found in case of Na_2CO_3 with 75 % (note that the solution with the presence of Na_2CO_3 changes pH of the solution to alkaline medium, thus the electrochemical process was performed in alkaline medium). Although the previous studies [61,91] concluded that Cartap is quickly hydrolyzed in alkaline medium, in our investigation Cartap (as the main compound in Padan 95 SP) remains stable at various pH from 3 to 9 without any loss of hydrolysis during the experimental time (at least 6 h in the presence of Na_2CO_3). This might be due to the presence of impurities or somehow cannot be straightforward explained that contradiction.

The highest performance of NaCl as supporting electrolyte is also reported in previous studies [73, 94]. This is because the formation of active chlorine (ClO^\cdot) generated from the oxidation of Cl^- on the BDD electrode accelerates the oxidation efficiency of organics, as shown in Eqs. (11-13) [95]. Next, the less degradation efficiency of Cartap can be found in case of Na_2SO_4 and the rest electrolytes. N. Rabaaoui et al. [96] have pointed out that the formation of persulfate ($\text{S}_2\text{O}_8^{2-}$) (see Eq. (10)) from SO_4^{2-} can also accelerate the oxidation of organics, comparing to other supporting electrolytes. However, in our case the degradation of Cartap for the case of Na_2SO_4 is not much higher than NaNO_3 . This is because the low formation of

persulfate (as weaker oxidizing specie) does not accelerate the degradation of Cartap as much higher than that for NaNO_3 .

In contrast, carbonates are much easier to form peroxodi-carbonates results in the less efficiency of oxidation due to the invalid consumption of $\bullet\text{OH}$ [97]. Therefore, it could be concluded that the difference in the behavior between these electrolytes may due to the oxidizing species being formed by the respective electrochemical oxidations.

The effects of supporting electrolytes on the current efficiency and on the TOC decay are depicted in Fig. 35 and insert of Fig. 35, respectively. The highest degradation of Cartap in case of NaCl also results in the highest TOC removal among these electrolytes, i.e. 14 % of TOC is removed after 120 min. A rapid decrease in MCE at the beginning of most experiments is observed, suggesting the quick destruction of initial compound that is more easily oxidizable than the immediate products. At long electrolysis time the current efficiency always undergoes a dramatic fall (as can be seen clearly in cases of NaCl and Na_2SO_4) due to the gradual formation of intermediates that are more difficultly destroyed or consumed oxidant species. Moreover, at long electrolysis time the collision between $\bullet\text{OH}$ radicals and easy oxidized organic molecules is decreased due to the mass transport limitations because of the presence of small concentration of that in solution. For example, the maximum MCE of 97 % for NaCl at the early stages of 5 min decreases to below 60 % after 15 min. Respectively, Na_2CO_3 shows the lowest result of MCE with the value below 10 %.

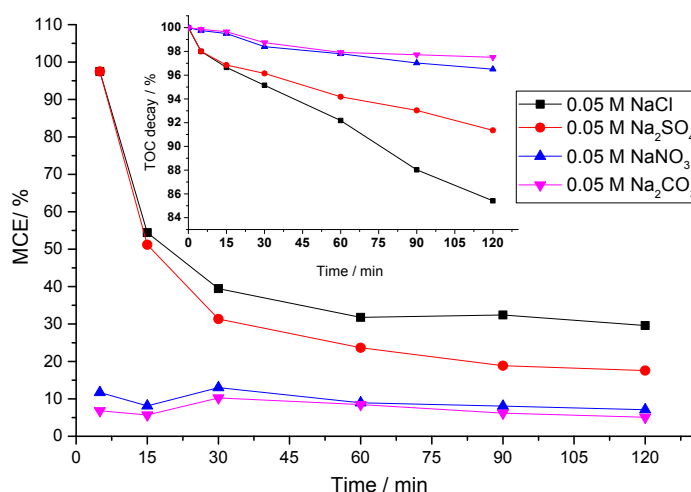


Figure 35 Mineralization current efficiency (MCE) calculated from Eq. (6) versus various supporting electrolytes in electrochemical process. Insert: TOC decay for the runs of Fig. 34. $[\text{Padan } 95\text{SP}]_0 = 300 \text{ mg}\cdot\text{L}^{-1}$, $V_{\text{treated solution}} = 250 \text{ mL}$, $\text{pH} = 3$ (except the case of Na_2CO_3 ,

which was added into electrolytic solution with the initial pH of deionized water), $j = 20 \text{ mA} \cdot \text{cm}^{-2}$.

3.2.5 Effect of Na_2SO_4 concentration

In the present work, the influence of Na_2SO_4 concentration on the decay of Cartap was investigated with the range from 0.01 M to 0.1 M. As seen in Fig. 36, the beneficial effect of increasing Na_2SO_4 from 0.01 M to 0.1 M increases Cartap decomposition from 70 % to 30 % after 120 min, respectively. In our study, an increase in concentration of Na_2SO_4 results in the larger formation of persulfate (see Eq. (10)) which is called indirect oxidation by persulfate. The indirect oxidation does not depend on current density, but rather on Na_2SO_4 concentration.

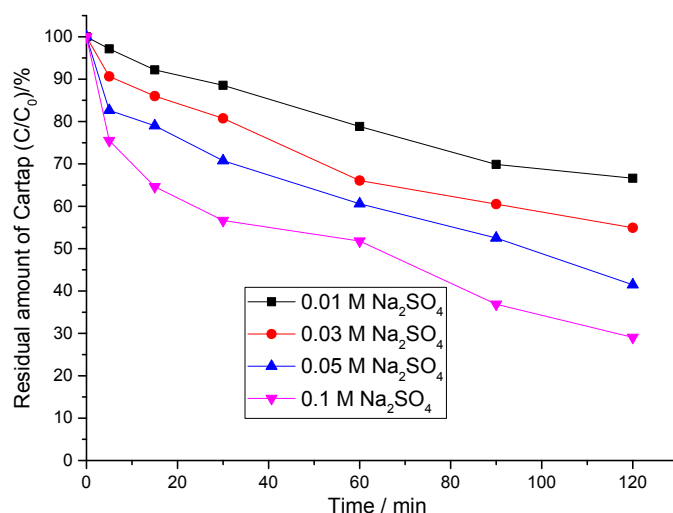


Figure 36 Cartap degradation versus various concentration of Na_2SO_4 in electrochemical process, $[\text{Padan 95SP}]_0 = 300 \text{ mg L}^{-1}$, $V_{\text{treated solution}} = 250 \text{ mL}$, $\text{pH} = 3$, $j = 20 \text{ mA} \cdot \text{cm}^{-2}$.

It can be seen that an increase in the Na_2SO_4 concentration gradually increases the Cartap decomposition (but only up to 0.05 M Na_2SO_4) and its further increase (up to 0.1 M) does not have much effect as expected. This is because the addition of excess SO_4^{2-} can also consume $\bullet\text{OH}$ radicals to form weaker oxidizing species than $\bullet\text{OH}$ radicals, thus 0.05 M Na_2SO_4 is the optimal value for this process.

On the other hand, the supporting electrolyte is added to the solution in order to increase its electrical conductivity, i.e. to decrease its electrical resistance and thus the energy consumption (see Fig. 37). As can be seen in Fig. 37, the energy consumption decreases

significantly from 62 to over 20 $\text{Kwh}\cdot\text{kg}^{-1}$ Cartap when increasing the concentration of Na_2SO_4 from 0.01 M to 0.05 M. Further increase of Na_2SO_4 concentration to 0.1 M has a slight effect on decrease of energy consumption. Thus, 0.05 M of Na_2SO_4 is assumed to be an optimal concentration in this study.

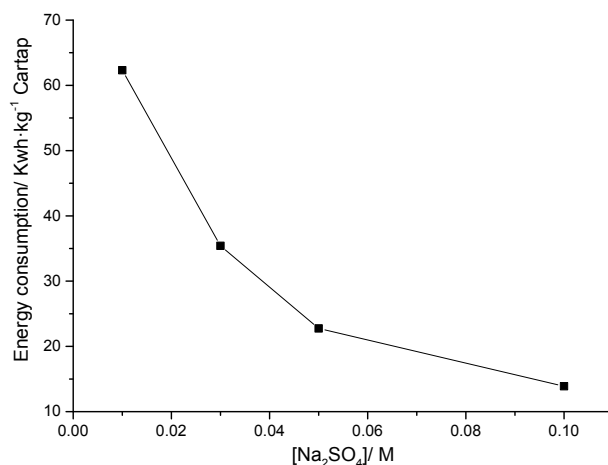


Figure 37 The effect of electrolyte concentration on energy consumption, $[\text{Padan 95SP}]_0 = 300 \text{ mg}\cdot\text{L}^{-1}$, $V_{\text{treated solution}} = 250 \text{ mL}$, $\text{pH} = 3$, $j = 20 \text{ mA}\cdot\text{cm}^{-2}$.

3.2.6 Effect of initial Padan 95SP concentration

The experiment was performed with different initial Padan 95SP concentrations. The results are indicated in Fig. 38 and 39. As can be seen in Fig. 38, the degradation efficiency of Cartap decrease with an increase of its initial concentration. i.e: Cartap remained at 18.5 %, 41 %, 51 % and 60 % for 100, 300, 500 and 700 $\text{mg}\cdot\text{L}^{-1}$ (after 120 min), respectively. It is clearly that when increasing the concentration of Cartap, the amount of $\bullet\text{OH}$ radicals is also required higher for their oxidation and mineralization. However, under galvanostatic conditions, the amount of $\bullet\text{OH}$ radicals generated is similar at the same operating conditions and have nonselective reactivity in relation to the adsorbed intermediates [83]. Thus, the Cartap degradation and TOC decay decrease with an increase in the initial Padan 95SP concentration (100–700 $\text{mg}\cdot\text{L}^{-1}$).

On the other hand, the increase of initial concentration of a compound increases its concentration gradient and mass transfer across the diffusion layer and thus its degradation on electrode [83]. As the result, the amount of Cartap removed as well as the TOC value removed (which are not shown) increase with increasing Padan 95SP concentration. This assumption is clearly proved by an increase in MCE when increasing the initial concentration

of Padan 95SP (see Fig. 39).

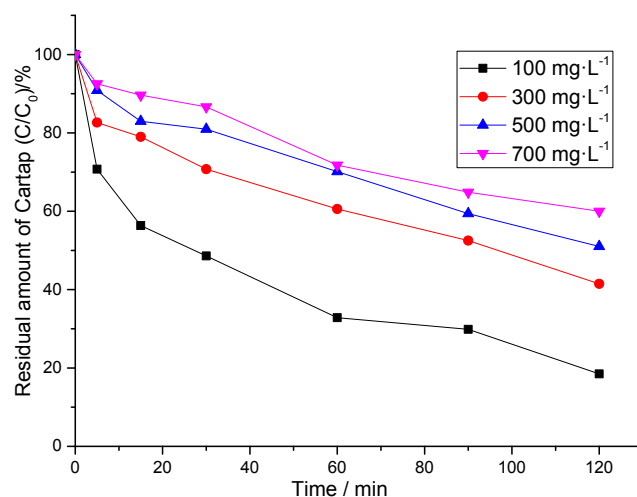


Figure 38 Influence of initial concentrations of Padan 95SP on Cartap degradation, ($[\text{Padan}]_0 = 100 \text{ mg}\cdot\text{L}^{-1}$, $300 \text{ mg}\cdot\text{L}^{-1}$, $500 \text{ mg}\cdot\text{L}^{-1}$ and $700 \text{ mg}\cdot\text{L}^{-1}$), concentration of electrolyte: $0.05 \text{ M Na}_2\text{SO}_4$, $V_{\text{treated solution}} = 250 \text{ mL}$, $\text{pH} = 3$, current density: $j = 20 \text{ mA}\cdot\text{cm}^{-2}$.

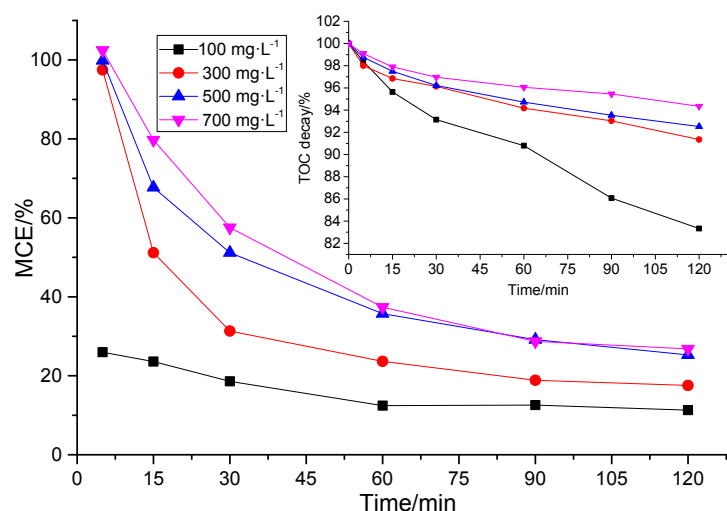


Figure 39 Mineralization current efficiency (MCE) calculated versus initial concentration of Padan 95 SP. ($[\text{Padan}]_0 = 100 \text{ mg}\cdot\text{L}^{-1}$, $300 \text{ mg}\cdot\text{L}^{-1}$, $500 \text{ mg}\cdot\text{L}^{-1}$ and $700 \text{ mg}\cdot\text{L}^{-1}$) Insert: TOC decay for the runs of Fig. 38, $V_{\text{treated solution}} = 250 \text{ mL}$, $\text{pH} = 3$, $j = 20 \text{ mA}\cdot\text{cm}^{-2}$.

3.2.7 By-products and their release

The formation of intermediates during Cartap degradation was monitored with HPLC. It was observed that most of these intermediates are initial oxidation products resulting from the initial oxidation of Cartap.

To have an overall view on the rate of the release of those intermediates for various supporting electrolytes (i. e: Na_2SO_4 , NaCl , NaNO_3 and Na_2CO_3), the method of relative area ratio (RAR) comparison is applied. Four peaks are observed in HPLC chromatograms as shown in Figs. 40-43, their relative area ratios at the electrolytic time intervals are depicted in Fig. 44.

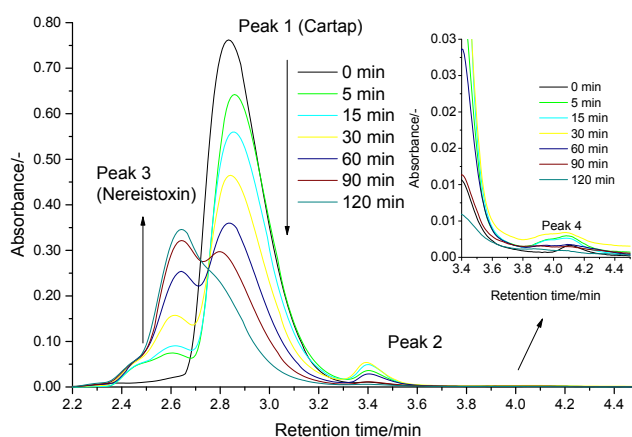


Figure 40 HPLC chromatogram for intermediates in electrochemical process: $[\text{Padan 95SP}]_0 = 300 \text{ mg}\cdot\text{L}^{-1}$, $V_{\text{treated solution}} = 250 \text{ mL}$, $j = 20 \text{ mA}\cdot\text{cm}^{-2}$, $[\text{NaCl}] = 0.05 \text{ M}$, $\text{pH} = 3$.

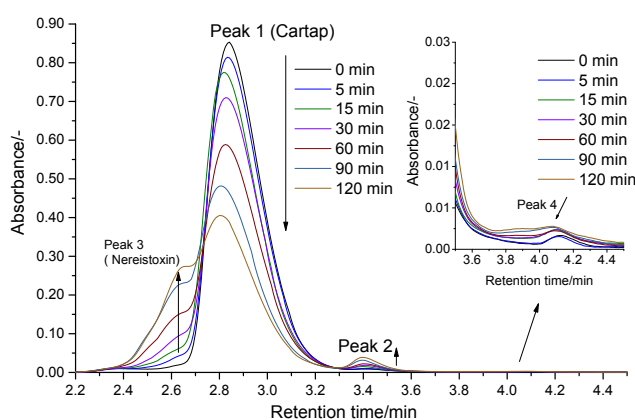


Figure 41 HPLC chromatogram for intermediates in electrochemical process: $[\text{Padan 95SP}]_0 = 300 \text{ mg}\cdot\text{L}^{-1}$, $V_{\text{treated solution}} = 250 \text{ mL}$, $j = 20 \text{ mA}\cdot\text{cm}^{-2}$, $[\text{Na}_2\text{SO}_4] = 0.05 \text{ M}$, $\text{pH} = 3$.

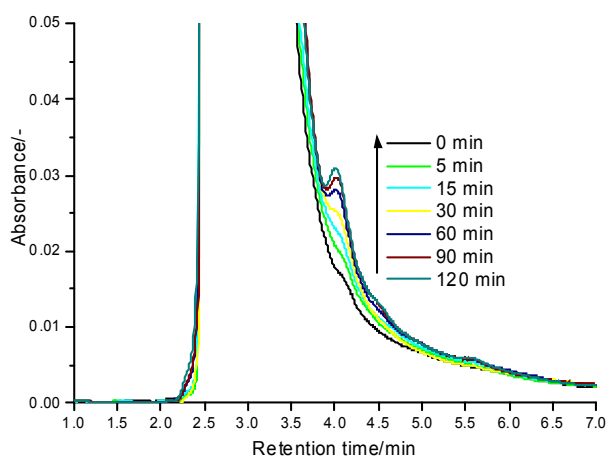


Figure 42 HPLC chromatogram for intermediates in electrochemical process: $\text{Padan 95SP}_0 = 300 \text{ mg}\cdot\text{L}^{-1}$, $V_{\text{treated solution}} = 250 \text{ mL}$, $j = 20 \text{ mA}\cdot\text{cm}^{-2}$, $[\text{NaNO}_3] = 0.05 \text{ M}$, $\text{pH} = 3$.

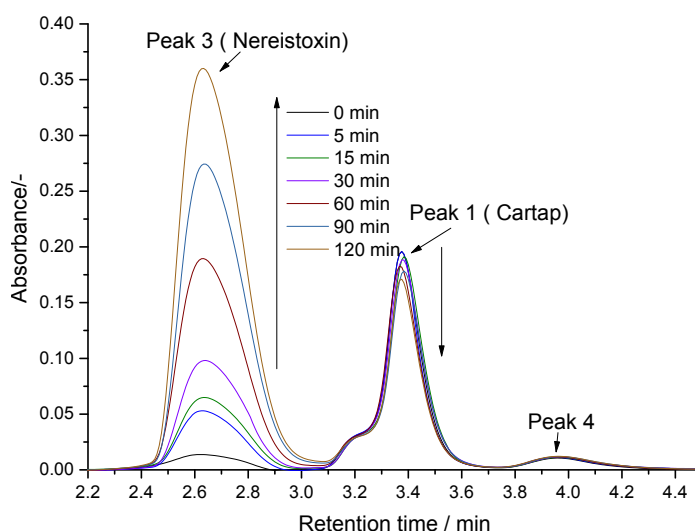


Figure 43 HPLC chromatogram for intermediates in electrochemical process: $[\text{Padan 95SP}]_0 = 300 \text{ mg}\cdot\text{L}^{-1}$, $V_{\text{treated solution}} = 250 \text{ mL}$, $j = 20 \text{ mA}\cdot\text{cm}^{-2}$, $[\text{Na}_2\text{CO}_3] = 0.05 \text{ M}$.

In HPLC chromatograms obtained with samples prepared with NaCl and Na_2SO_4 as electrolyte peaks appeared at the same retention times. Peak 1 is attributed to Cartap ($t_r = 2.9 \text{ min}$) and peak 3 to nereistoxin ($t_r = 2.6 \text{ min}$) partly overlapping each other.

As seen in Figs. 40-41, the peak of Cartap in case of NaCl as the supporting electrolyte decreases more rapidly than with Na_2SO_4 , resulting in higher RAR of nereistoxin for NaCl than for Na_2SO_4 . Peak 2 ($t_r = 3.4 \text{ min}$) appears to reach the maximum value at 30 min and then diminishes at 120 min in case of NaCl meanwhile it increases slowly in case of Na_2SO_4 (see Fig. 44). Nevertheless, peak 4 could be neglected due to its low intensity. This peak might be caused by the additives in Padan 95 SP.

HPLC chromatograms for the case of NaNO_3 show a shoulder on the main peak and no further peaks possibly indicating intermediates. Perhaps, the presence of NO_3^- in treated samples causes some interference with that signal. A very different result can be also seen for the case of Na_2CO_3 as an electrolyte: For example, the peak for Cartap shifts to $t_r=3.4$ min, resulting in the disappearance of peak 2 (see Fig. 42). Nereistoxin accumulates gradually during process, resulting in the significant increase of its RAR.

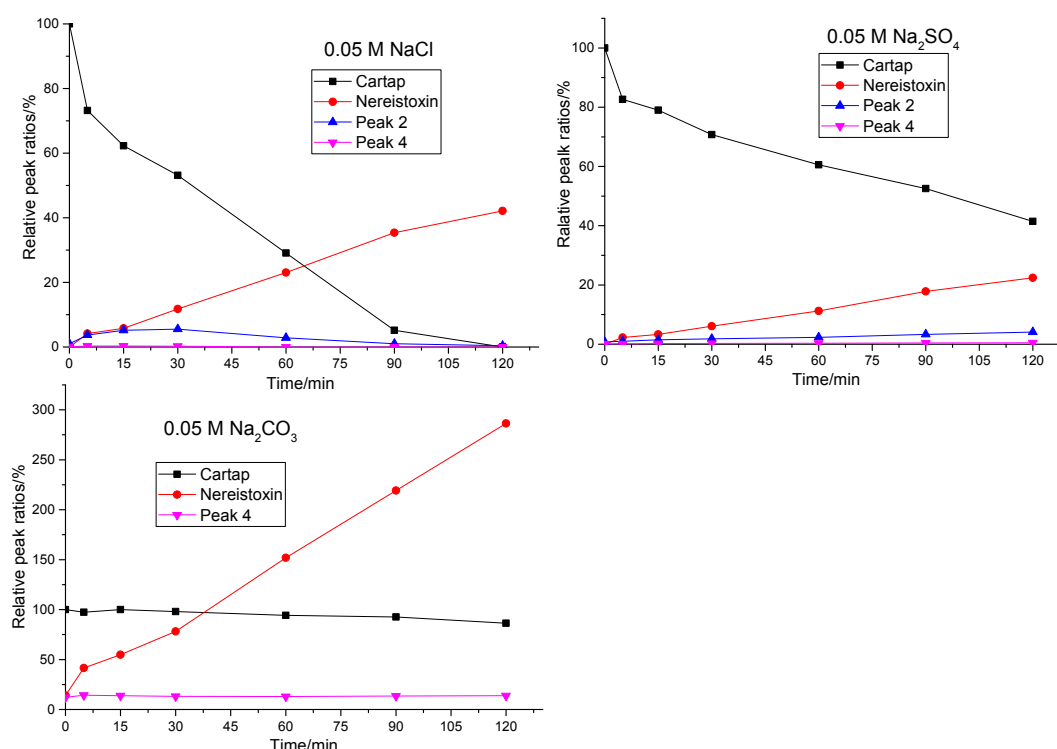


Figure 44 Relative peak ratios of Cartap and its degradation products versus time with various supporting electrolytes based on HPLC chromatograms, $[\text{Padan 95SP}]_0 = 300 \text{ mg}\cdot\text{L}^{-1}$, $V_{\text{treated solution}} = 250 \text{ mL}$, $j = 20 \text{ mA}\cdot\text{cm}^{-2}$, $\text{pH} = 3$ (except the case of Na_2CO_3 , which was added into electrolytic solution with the initial pH of deionized water).

3.2.8 Time-dependent concentrations of oxidizing ions and the influence of inorganic anions as supporting electrolytes

During the electrochemical oxidation process less strongly oxidizing species such as ClO^- related to the existence of dissolved Cl_2 and HClO generated from the oxidation of Cl^- as shown in Eqs. (11-13)) and $\text{S}_2\text{O}_8^{2-}$ (Eq. (10)) from the oxidation of SO_4^{2-} at the BDD electrode

are formed. Their accumulation is recorded in Fig. 45. The continuous gradual increase in concentration of active chlorine once again demonstrates the higher efficiency of NaCl for Cartap decomposition than of Na₂SO₄. In Fig. 45, the accumulation of ClO⁻ reaches 0.55 mM after 120 min meanwhile the concentration of S₂O₈²⁻ remains < 0.1 mM. Many previous researchers [58,60,98] have also detected the formation of active chlorine in electrochemical process. For example, in the study of D. Rajkumar et al. [58] there was no chlorine/ hypochlorite detected during the initial period of electrolysis, but the concentration of hypochlorite continuously increased thereafter. M. Santhanam et al. [60] found the concentration of chlorine and hypochlorite, respectively to increase gradually after the disappearance of color in solution.

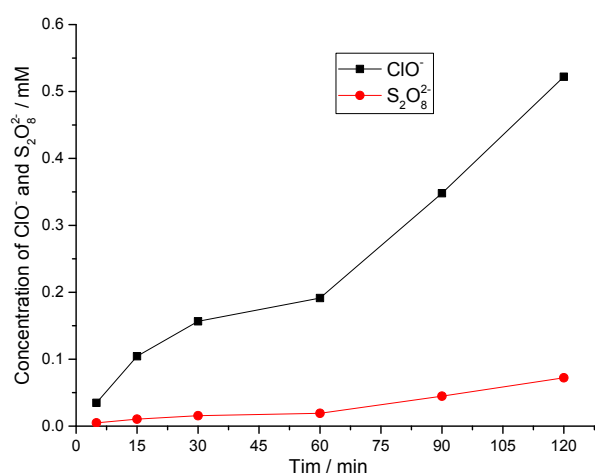


Figure 45 ClO⁻ and S₂O₈²⁻ concentrations in case of 0.05 M NaCl and 0.05 M Na₂SO₄ during electrochemical oxidation, [Padan 95SP]₀ = 300 mg·L⁻¹, $V_{treated\ solution} = 250\text{ mL}$, $j = 20\text{ mA}\cdot\text{cm}^{-2}$, pH = 3.

To evaluate the change in concentration of electrolyte anions, their concentration are displayed in Fig. 46. Note that the degradation of Cartap releases inorganic ions such as SO₄²⁻, NO₃⁻ [11,12] which may also contribute to the change of their concentration. . In case of Na₂CO₃, there is no significant change in concentration of salt anions, meanwhile the trace for Cl⁻ shows a slight decrease. Although degradation of Cartap releases SO₄²⁻, the concentration of SO₄²⁻ decreases significantly within the initial 30 min and decreases further thereafter. In contrast, the concentration of NO₃⁻ increases to approximately 0.055 M after 120 min, this is due to the release of NO₃⁻ from decomposing Cartap.

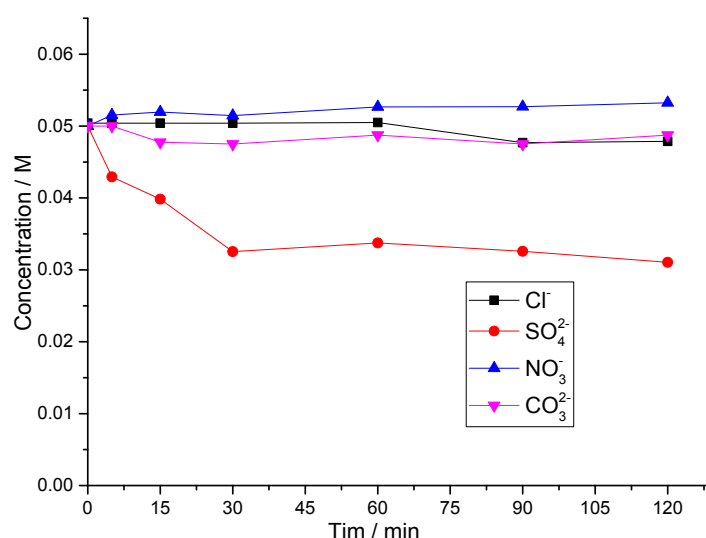


Figure 46 The change of concentration of supporting electrolytes during electrochemical oxidation at 0.05 M initial concentration of electrolytes, $[\text{Padan 95SP}]_0 = 300 \text{ mg}\cdot\text{L}^{-1}$, $V_{\text{treated solution}} = 250 \text{ mL}$, $j = 20 \text{ mA}\cdot\text{cm}^{-2}$, $\text{pH} = 3$ (except for Na_2CO_3 , which was added into electrolytic solution with the typical pH of deionized water around 6 - 6.5).

3.2.9 Conclusion

In fact, Cartap in Padan 95SP is stable in different mediums from acid to alkaline (pH from 3 to 9) for 6 h. The hydrolysis rate of Cartap in Padan 95SP undergoes slowly for several days and depends on the pH value.

The degradation efficiency of Cartap in Padan 95SP strongly depends on operating parameters such as current density, supporting electrolytes and initial concentration of Padan 95SP. The optimal condition for Cartap degradation in electrochemical oxidation are established: current density: $j = 20 \text{ mA}\cdot\text{cm}^{-2}$, concentration of electrolyte: 0.05 M Na_2SO_4 at the initial concentration of Padan 95SP of $300 \text{ mg}\cdot\text{L}^{-1}$. The concentration of supporting electrolyte is also found to be an important role not only for decrease of energy consumption but also an acceleration of Cartap degradation. In addition, the study shows that MCE continuously drops down due to the competitive formation of intermediates which is considered to be more difficult to oxidize than Cartap.

3.3 Electro-Fenton process and effect of NaOCl on this process

3.3.1 Padan 95SP degradation with NaOCl

The removal capability of sodium hypochlorite was tested with a solution containing 700 mg L⁻¹ Padan 95SP (TOC = 215 mg·L⁻¹). Remaining concentrations of NaOCl in solutions with different starting concentrations are shown in Fig. 47, progress of Cartap degradation is displayed in Fig. 48. For example, the NaOCl concentrations decreased to 3.5 mM and 0.8 mM after 2 min and further more slowly to 2 mM and 0.2 mM during 60 min at initial NaOCl concentrations of 22 mM and 8 mM, respectively (see Fig. 47).

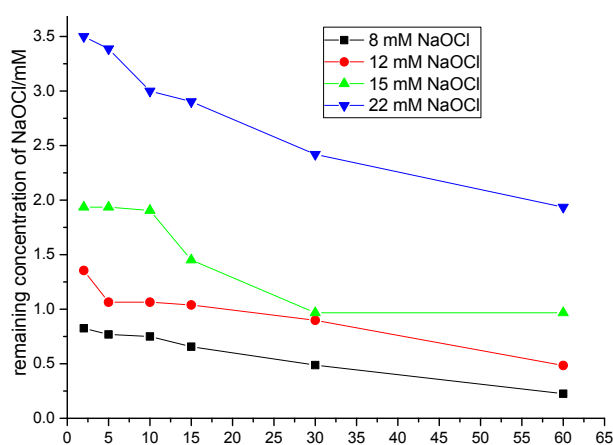


Figure 47 Concentration of NaOCl at various initial concentrations versus time after adding into solution containing Padan 95SP, [Padan 95SP]₀ = 700 mg·L⁻¹, $V_{\text{solution}} = 250$ mL.

Fig. 48 shows that Cartap decomposition starts immediately after adding NaOCl but there is no more decomposition after 2 min (in case of low concentrations 8 and 12 mM NaOCl) although NaOCl still remains in solution (as can be seen in Fig. 47). Cartap remains in treated solution at 20 and 45 % of its initial value for the cases of 12 mM and 8 mM NaOCl meanwhile it is totally decomposed after 2 min with 15 mM and 22 mM NaOCl.

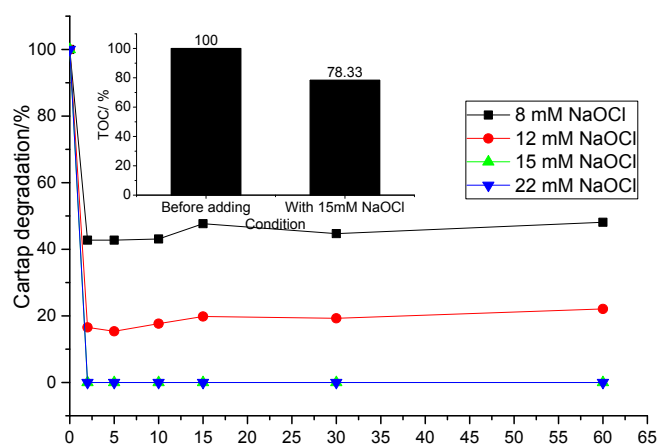


Figure 48 Cartap degradation after adding various concentrations of NaOCl, $[\text{Padan } 95\text{SP}]_0 = 700 \text{ mg}\cdot\text{L}^{-1}$, $V_{\text{solution}} = 250 \text{ mL}$. Insert: TOC reduction in case of a solution containing 15 mM NaOCl after 60 min.

Thus, 15 mM NaOCl is the optimal value to remove Cartap completely in a test solution containing $700 \text{ mg}\cdot\text{L}^{-1}$ Padan 95SP. In this case TOC remained at 78.33 % (insert of Fig. 4). It can be concluded that NaOCl is a very efficient bleaching agent which needs only a short time to decompose Cartap by releasing free chlorine (“active chlorine” ClO^- and HOCl). The reactions are shown in Eq. (17) and (18):



3.3.2 Effect of H_2O_2 addition

Electro-Fenton oxidation treatment was tested by electrolyzing 700 mg L^{-1} Padan 95SP solutions (equivalent to $215 \text{ mg}\cdot\text{L}^{-1}$ of TOC) of $\text{pH} = 3$ at $j = 20 \text{ mA}\cdot\text{cm}^{-2}$ at room temperature for 120 min with the addition of H_2O_2 instead of feeding the cathode with O_2 for H_2O_2 generation. Thus, Cartap is almost decomposed quantitatively after 5 min at various H_2O_2 concentrations; 0.2 M H_2O_2 can be chosen as the optimal value regarding Cartap degradation (see Fig. 19).

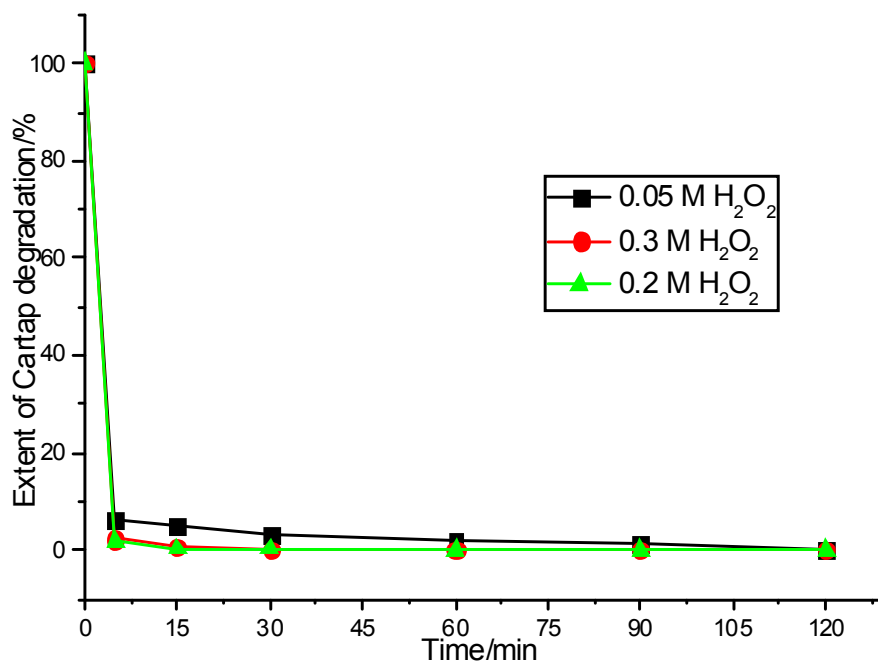


Figure 49 Cartap degradation at various H₂O₂ additional concentrations versus time in the Electro-Fenton process, [Padan 95SP]₀ = 700 mg·L⁻¹, V_{solution} = 250 mL, [Fe²⁺] = 15 mM, [Na₂SO₄] = 0.05 M, pH = 3, j = 20 mA·cm⁻².

Fig. 50 shows the remaining concentration of H₂O₂ after its addition to the electrolyte solution. In all cases approximately 50 % of the initial H₂O₂ concentration has been consumed after 5 min, a further gradual consumption is observed. After 120 min the concentration of H₂O₂ remains at 6.5 mM for cases of 0.2 and 0.3 M and 2 mM in case of 0.05 M initial H₂O₂ initial concentration. The large extent of removal of Cartap and the rapid consumption of H₂O₂ during the initial 5 min show that •OH generated according to from Eq. (2) plays the main role in Cartap degradation. As the result of rapid decomposition of Cartap, the pH-value of solution (see insert of Fig. 50) decreases rapidly from 3 to 2.2 after 5 min and does not change thereafter. It can be assumed that the formation of organic acids resulting from the degradation of Cartap reduces pH of the treated solution.

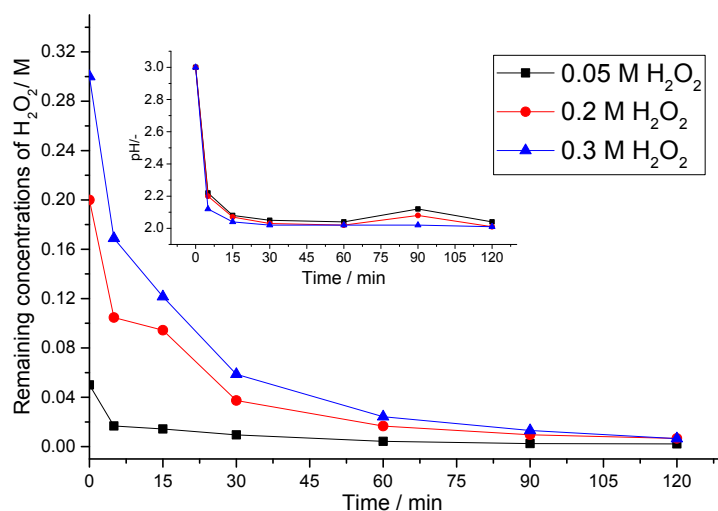


Figure 50 The decrease of H_2O_2 at various initial concentrations versus time after adding into solution containing Padan 95SP, $[\text{Padan 95SP}]_0 = 700 \text{ mg}\cdot\text{L}^{-1}$, $j = 20 \text{ mA}\cdot\text{cm}^{-2}$, $[\text{Na}_2\text{SO}_4] = 0.05 \text{ M}$, $[\text{Fe}^{2+}] = 15 \text{ mM}$, $V_{\text{solution}} = 250 \text{ mL}$, $\text{pH} = 3$. Insert: Change of pH versus time.

The TOC reduction in the Electro-Fenton process and the effect of pretreatment with 15 mM NaOCl are presented in Fig. 51.

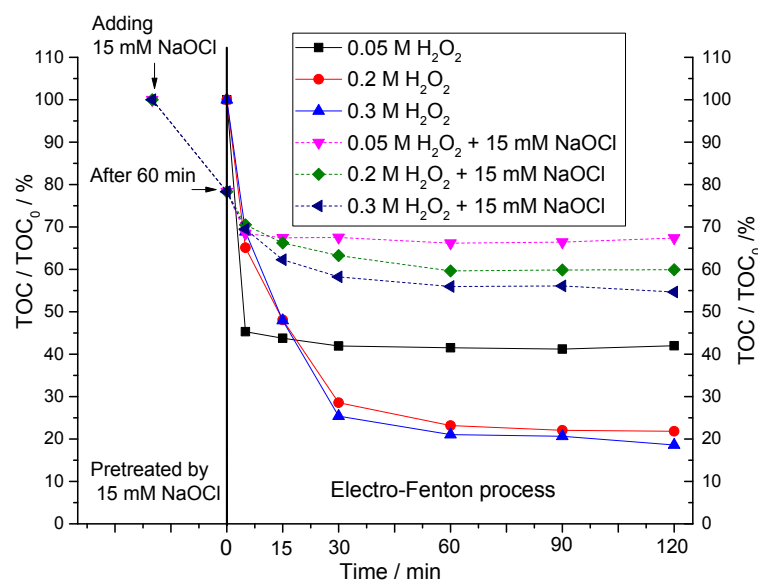


Figure 51 TOC decay at different operating conditions, $[\text{Padan 95SP}]_0 = 700 \text{ mg}\cdot\text{L}^{-1}$, $V_{\text{solution}} = 250 \text{ mL}$, $j = 20 \text{ mA}\cdot\text{cm}^{-2}$, $[\text{Na}_2\text{SO}_4] = 0.05 \text{ M}$, $[\text{Fe}^{2+}] = 15 \text{ mM}$ and $\text{pH} = 3$ for Electro-Fenton process.

It is surprising that at lowest H_2O_2 concentration TOC decreases approximately to 42 % after

5 min and then remains constant time whereas TOC decreases for the cases of 0.2 M and 0.3 M H₂O₂ are very similar, only reach to below 70 % after 5 min. However, TOC for all cases decreases rapidly for 30 min after start of the experiment and decrease slowly to 22 % and 18 % for 0.2 and 0.3 M H₂O₂, respectively at the end of process. It can be concluded that a lower concentration of H₂O₂ (0.05 M) results in higher efficiency of TOC removal than higher ones (0.2 and 0.3 M) in the initial of 5 min. This may be due to the possibility that excess H₂O₂ at the early stage (5 min) can also scavenge •OH to produce weaker oxidative species like •OOH (Eq. (19)) [99] or can undergo competing reactions (Eqs. (20-21)) [100,101] which results in the loss of oxidative capability.

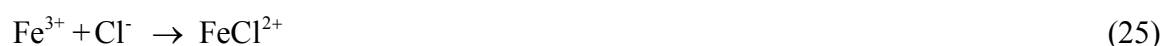


This may also explain why the highest concentration of H₂O₂ (0.3 M) does not cause much higher TOC removal compared with lower concentration (0.2 M).

Results of an investigation whether pretreatment of solution with NaOCl has positive impact on the Electro-Fenton process are also depicted in Fig. 51. Although the TOC value remains at 78 % after treatment with 15 mM NaOCl, further treatment by the Electro-Fenton process does not result in further degradation. Obviously, the presence of Cl⁻-ions formed from the OCl⁻ decomposition by organics (Eq. (22)) [102] has a negative impact on the Fenton process.



The interaction of chloride with the Fenton mechanism may be explained by two possible pathways: (i) the complexation of Fe²⁺/Fe³⁺ with Cl⁻ (Eqs. (23-26)) [103], (ii) scavenging of hydroxyl radicals (Eq. (27)) [104, 105] resulting in generation of chloride radicals Cl• (Eq. (28)) which are less reactive than the hydroxyl radical [106, 107] or generation of Cl⁻ ion (Eq. (29)) [107].





3.3.3 Effect of metal ion catalysts

It is well known that the Fenton reaction is catalyzed by several metal ions [99]. In order to investigate the influence of metal ions on the Electro-Fenton process was investigated in the presence of three different metal ions: Mg^{2+} , Al^{3+} and Cu^{2+} . The initial metal ion concentration was 5 mM.

As shown in Fig. 52, the Electro-Fenton process is effective up to 60 min. Although Al^{3+} or Mg^{2+} as co-catalysts slow down the process within the interval time 5 to 60 min, more than 80 % TOC removal can be achieved after 120 min.

Fig. 52 shows that adding 5 mM Cu^{2+} can accelerate TOC removal in the initial 30 min and only 35 % of TOC remain in the treated solution after 5 min already. Further treatment can reduce the TOC value only to 22 %.

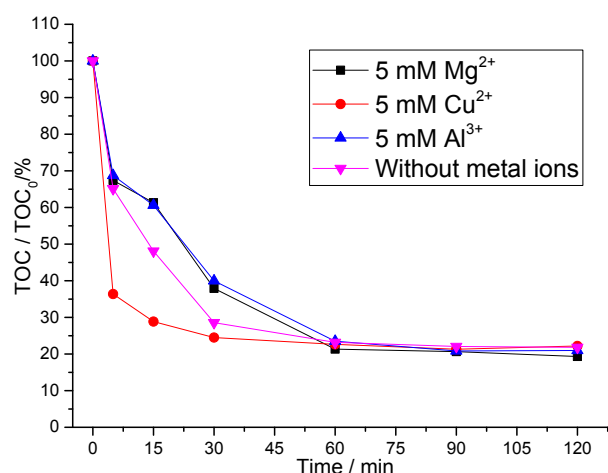


Figure 52 TOC decay with different metal catalysts in Electro-Fenton process, $[\text{Padan 95SP}]_0 = 700 \text{ mg}\cdot\text{L}^{-1}$, $V_{\text{solution}} = 250 \text{ mL}$, $j = 20 \text{ mA}\cdot\text{cm}^{-2}$, $[\text{Na}_2\text{SO}_4] = 0.05 \text{ M}$, $[\text{Fe}^{2+}] = 15 \text{ mM}$, $\text{pH} = 3$, $[\text{H}_2\text{O}_2]_0 = 0.2 \text{ M}$.

This positive synergetic effect is due to the fast destruction of complexes of Cu^{2+} with carboxylic acids [108,109] and the enhanced generation of $\bullet\text{OH}$ from the redox couple

$\text{Cu}^{2+}/\text{Cu}^+$ (Eq. (32)) [108,110], in which Cu^+ is formed from Cu^{2+} with HO_2^\bullet (Eq. (31)) (weaker oxidants produced in the electrolytic system), followed by regeneration of Cu^{2+} by oxidation of Cu^+ with H_2O_2 from the Fenton-like reaction (32) [111]:



It can be concluded that although co-catalysts have some impact (positive/negative) at the early stages (less than 60 min), TOC/TOC_0 in all cases is the same at around 20 % at the end of the process.

3.3.4 Effect of Fe^{2+} concentration

According to several studies, the dosage of Fe^{2+} plays an important role on the efficiency of the Electro-Fenton process [112 - 115]. As shown in Fig. 53, the TOC decreases with increasing Fe^{2+} concentration.

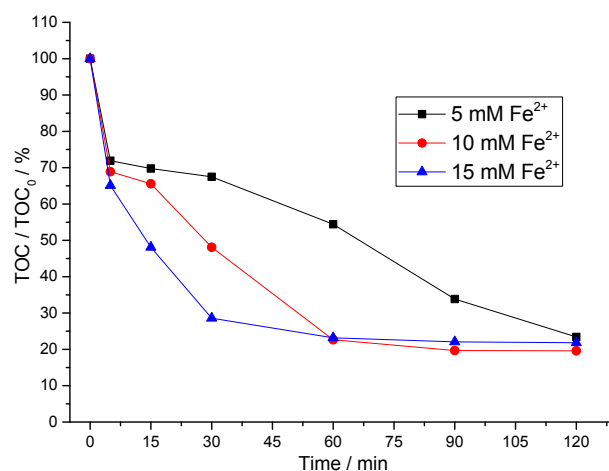


Figure 53 TOC decay versus various concentrations of Fe^{2+} in Electro-Fenton process, $[\text{Padan } 95\text{SP}]_0 = 700 \text{ mg}\cdot\text{L}^{-1}$, $[\text{TOC}]_0 = 215 \text{ mg}\cdot\text{L}^{-1}$, $V_{\text{solution}} = 250 \text{ mL}$, $j = 20 \text{ mA}\cdot\text{cm}^{-2}$, $[\text{Na}_2\text{SO}_4] = 0.05 \text{ M}$, $\text{pH} = 3$, $[\text{H}_2\text{O}_2]_0 = 0.2 \text{ M}$.

Meanwhile TOC decreases continuously during 120 min in case of 5 mM Fe^{2+} , there is no considerable reduction in TOC for the cases of 10 mM and 15 mM after 60 min. However, in

all cases the same value of TOC at approximately 20 % is reached after 120 min of treatment time. This can be explained by assuming that in the early stages (less than 60 min) the higher Fe^{2+} concentration promotes production of $\bullet\text{OH}$ radical leading to faster decrease of the TOC value. Further treatment time does not contribute remarkably to TOC decay. This may be due to the formation of recalcitrant products that are difficult to be destroyed by BDD ($\bullet\text{OH}$) and/or the Fenton reagent ($\bullet\text{OH}$).

On the other hand, several previous studies [116-118] have pointed out that the use of excess Fe^{2+} influences the process negatively, which can be explained in Eqs. (33-35) [99]:



Thus, using high concentration of Fe^{2+} should be considered, because the ferrous ions not only generate hydroxyl radicals but also are scavengers of $\bullet\text{OH}$.

3.3.5 Effect of pH

The pH of the solution is a very important parameter in the Fenton process. It affects directly the mechanism of oxidation, because a change in pH of the solution involves a variation of the concentration of Fe^{2+} , and therefore the formation rate of $\bullet\text{OH}$ radicals is affected. At high pH ($\text{pH} > 4$), the generation of $\bullet\text{OH}$ becomes slower due to the formation of various iron oxide hydroxide species; the complexes would further form $[\text{Fe}(\text{OH})_4]^-$ when pH in treated solution is higher than 9.0 [119].

On the other hand, at very low pH values (< 2.0) the reaction is slowed down by the formation of complex species $[\text{Fe}(\text{H}_2\text{O})_6]^{2+}$, which react more slowly with peroxide as compared to $[\text{Fe}(\text{OH})(\text{H}_2\text{O})_5]^{2+}$. In addition, the peroxide gets solvated in the presence of high concentration of H^+ ions to form stable oxonium ions $[\text{H}_3\text{O}_2]^+$ [120]. The oxonium ion makes peroxide more electrophilic enhancing its stability and presumably reduces substantially the reactivity with Fe^{2+} ion [121,122].

Many previous studies [100,101,123] have pointed out that $\text{pH} = 3$ is the optimal value for the

Fenton reaction. Therefore, the experiment was run at initial pH of 3 and at controlled pH of 3 during process for comparison.

The influence of pH on TOC removal is depicted in Fig. 54. As seen in insert of Fig. 50, pH of solution remains at 2.1 after 5 min. With initial pH =3 the TOC value (see Fig. 54) gradually decreases to 23 % and there is no significant change of the TOC value after 60 min. It is surprising that keeping pH of the solution at 3 results in only 5 % of TOC decay (from 75 % at 5 min to 70 % at 120 min). As can be seen in Fig.54, any addition of OH⁻ for reaching the initial pH value of solution (pH = 3) slow down the TOC decay, in comparison with the case of initial pH of 3. It can be assumed that the OH⁻ ions consumed is not for changing the pH value of solution but it is firstly consumed for decomposing H₂O₂ or precipitate Fe²⁺ as described in Eq. (36).

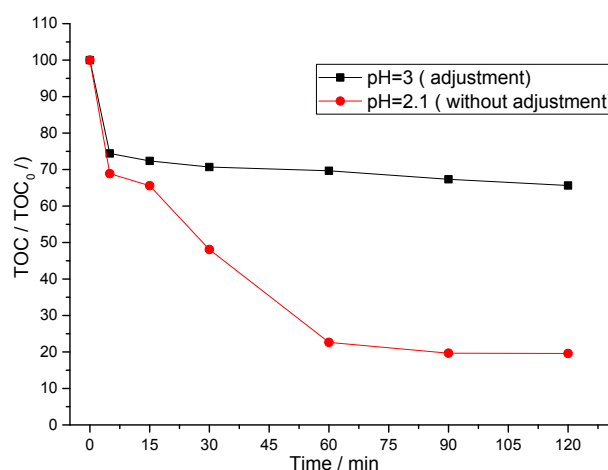
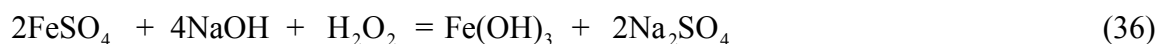


Figure 54 TOC decay versus pH, [Padan 95SP]₀ = 700 mg L⁻¹, [TOC]₀ = 215 mg·L⁻¹, V_{solution} = 250 mL, $j = 20 \text{ mA} \cdot \text{cm}^{-2}$, [Na₂SO₄] = 0.05 M, pH = 3, [H₂O₂]₀ = 0.2 M, [Fe²⁺] = 10 mM.

In previous studies this range of pH values (from 2 to 3) was also maintained. For example, in the study of El-Ghenymy et al. [124] TOC decays are very similar for pH = 2 and 3 at 83 and 85 % of TOC removed, respectively. The same result can be also found elsewhere [111] noting no difference in TOC decay between pH = 2 and 3. On the other hand, the study [125] showed that more than 90 % of TOC removal was achieved at pH=3 meanwhile approximately 50 % of that at pH=2 after 120 min.

Obviously it is recommend not to adjust of pH by addition of OH⁻ ions during the Fenton process.



3.3.6 Identification of intermediates and proposed degradation pathway

Fig. 55 depicts the degradation of Cartap and intermediates during 120 min. Note that the content in Padan 95 SP is 5 % additives and assumed that their presence does not cause any significant interference in determination of the intermediates from degradation of Cartap. As can be seen in Fig. 55 Cartap ($t_r = 3.1$ min) is decomposed almost after 5 min. Besides, the new peaks appear and then fade with reaction time. All peaks are present at retention times less than 5 min and their retention times are close to each other. Therefore, it is difficult to identify a single peak.

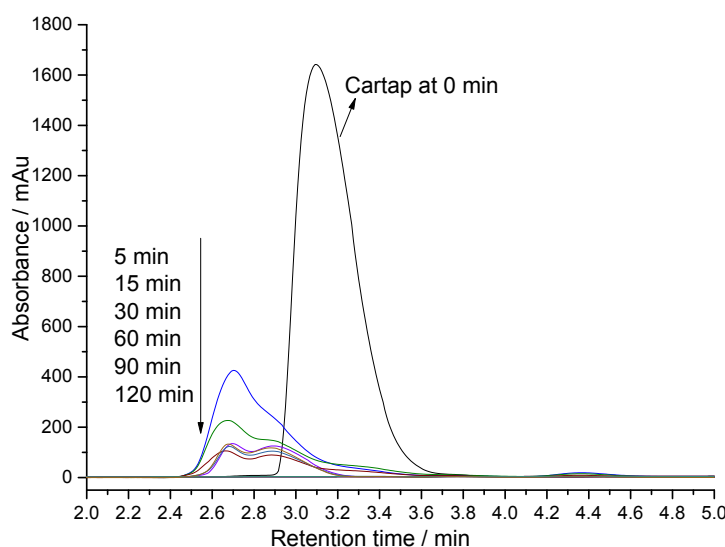


Figure 55 HPLC signal of intermediates in Electro-Fenton process: $[\text{Padan 95SP}]_0 = 700 \text{ mg}\cdot\text{L}^{-1}$, $V_{\text{solution}} = 250 \text{ mL}$, $j = 20 \text{ mA}\cdot\text{cm}^{-2}$, $[\text{Na}_2\text{SO}_4] = 0.05 \text{ M}$, $\text{pH} = 3$, $[\text{H}_2\text{O}_2]_0 = 0.2 \text{ M}$, $[\text{Fe}^{2+}] = 10 \text{ mM}$.

The reaction intermediates were further examined by GC–MS based on the molecular ion measurement. The FID–GC analysis (see Fig. 56) of the Electro-Fenton process of Padan 95SP degradation shows the formation of several intermediate products. However, the volatilities of some intermediates are seemingly too small to be eluted out under the gas chromatographic conditions, and some compounds cannot be obtained by GC–MS due to their significant polarity [126126].

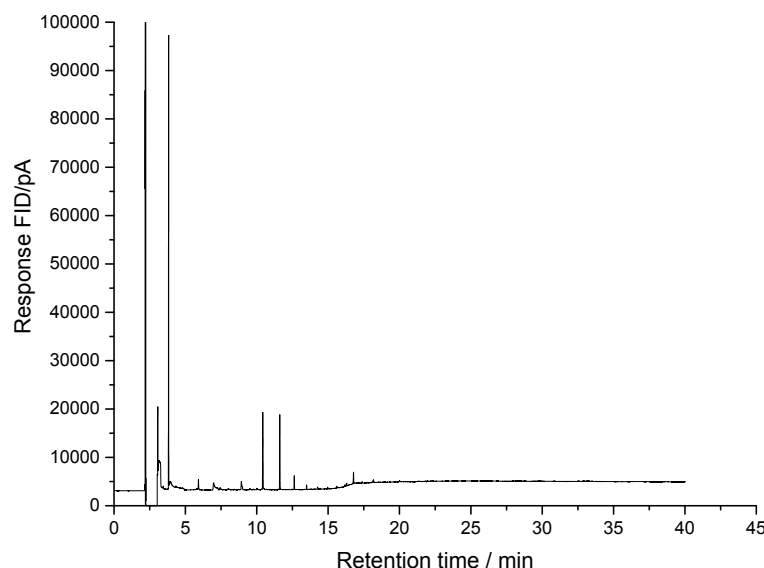


Figure 56 FID –GS signal of by-products in Electro-Fenton process: $\text{Padan 95SP}]_0 = 700 \text{ mg} \cdot \text{L}^{-1}$, $V_{\text{treated solution}} = 250 \text{ mL}$, $j = 20 \text{ mA} \cdot \text{cm}^{-2}$, $[\text{Na}_2\text{SO}_4] = 0.05 \text{ M}$, $\text{pH} = 3$, $[\text{H}_2\text{O}_2]_0 = 0.2 \text{ M}$, $[\text{Fe}^{2+}] = 10 \text{ mM}$.

The high volatility and hydrophilic characteristics of short chain acids make the detection of them difficult and GC-MS can be a suitable technique, offering advantages for the detection of volatile compounds. Such highly polar species need to be derivatized for proper GC-MS analysis. Before measuring in GC-MS the reaction solution at 120 min in Fig. 55 was esterified by n-propanol for tracing the derivatives of short chain acids. Fig. 56 depicts the GC spectrum of reaction products after esterification. Fig. 57 indicates that several peaks for derivative of oxalic acid in standard solution and that for derivative in sample were present at the same retention times. Therefore, it can be concluded that oxalic acid formed in Electro-Fenton process above. Unfortunately, the peaks for the derivatives of other acids (e.g.: formic and acetic acid) do not match any peaks in sample.

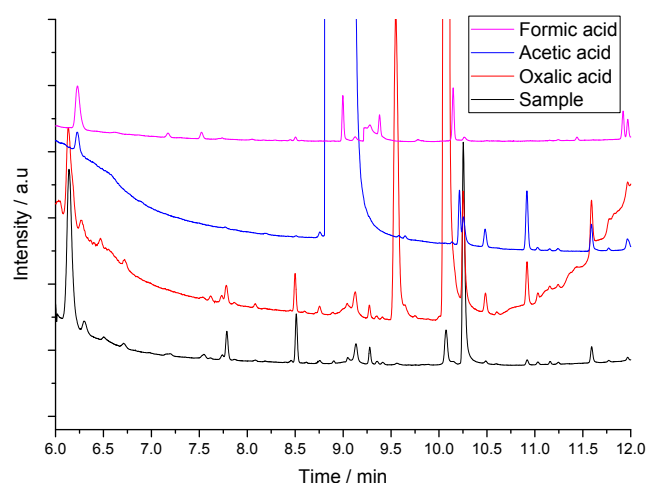


Figure 57 GC spectrum for derivatives of short chain acids esterified by n-propanol. The sample for derivatization was similar as in Fig. 55 at 120 min.

However, based on the previous study [12] and some proposed pathways of the organics [126-130] which have the chemical bonds of S, N and O in structure similar to Cartap, the proposed degradation pathway of Cartap in Electro-Fenton process once again can be obtained [Fig. 58].

Because Cartap is an ionic compound, HCl is freely liberated into the solution, consequently Cartap changed into compound A in the solution [12]. The long alkane chain is easily degraded into small molecule organic acids [12]. The amino group at the end of the Cartap chain is oxidized into a nitro group as proposed by product B. The attack of $\bullet\text{OH}$ can also break the bond N-C in the main chain to release smaller molecules (products C and D). The same phenomenon can be seen in previous studies [131**Error! Bookmark not defined.**,132]. The compound D can be consequently oxidized into products E and F or G, and followed by gas CO_2 and inorganic ions (NO_3^- and NH_4^+). The C-S chemical bond in compound C is broken out to form product J and release SO_2 , CO_2 , H_2O_2 and SO_4^{2-} . On the other side, product B can also subsequently be converted into product H to release NO and then the C-S chemical bond from H is destroyed for producing sulfuric acid in solution. Product I subsequently liberates the amine group to form malonic acid. According to the previous study [133], malonic acid is decomposed to acetic acid and formic acid.

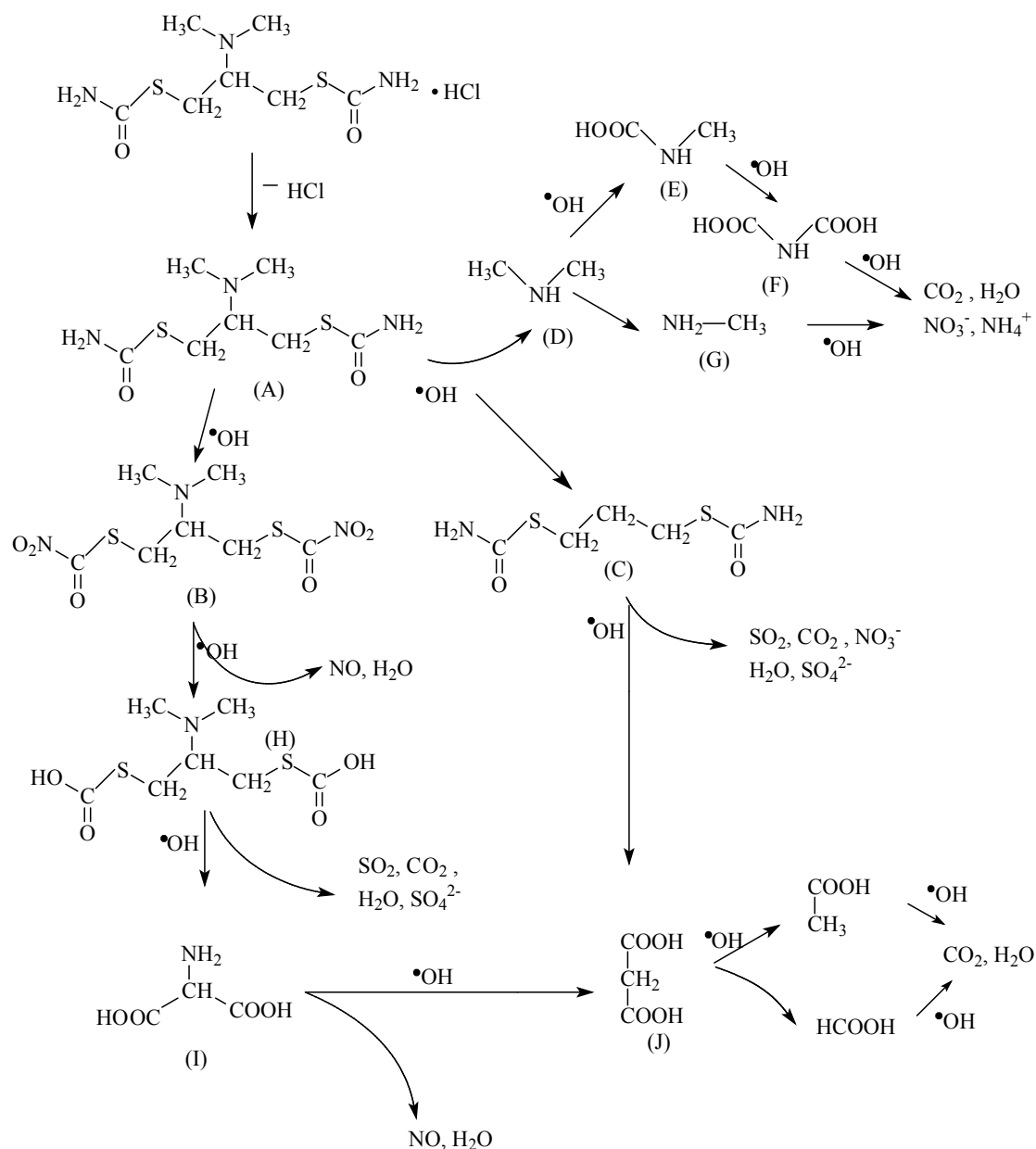


Figure 58 Proposed degradation pathway of Cartap in Electro-Fenton process.

It should be mentioned that the final degradation products were mineral ions such as NH_4^+ , SO_4^{2-} , NO_3^- , which are in the substituent groups of the initial molecule [131,132,134,135].

3.3.7 Conclusions

In this study, pretreatment with 15 mM NaOCl can effectively remove Cartap in $700 \text{ mg}\cdot\text{L}^{-1}$ Padan 95SP at very short reaction time and lead to decrease of 22 % in TOC due to active chlorine, but it results in negative impact on Electro-Fenton process because of the remaining of Cl^- ions in solution. The concentration of H_2O_2 and the dosage of Fe^{2+} are considered as the

main parameters in Fenton process. However, the excess of both of them does not lead to increase in TOC removal. Using Cu^{2+} can also enhance the TOC removal at the early stages but does not increase the effectiveness of process after 120 min of treatment. This is due to the refractory by-products which cannot be decomposed by the attack of further $\bullet\text{OH}$ radicals. In addition, this study also shows that the decrease of pH from 3 to 2.1 is the result of releasing organic acids and keeping the pH remained at 3 doesn't remarkably increase TOC removal. In the optimal condition ($[\text{Padan 95SP}]_0 = 700 \text{ mg}\cdot\text{L}^{-1}$, $V_{\text{solution}} = 250 \text{ mL}$, $j = 20 \text{ mA}\cdot\text{cm}^{-2}$, $[\text{Na}_2\text{SO}_4] = 0.05 \text{ M}$, $\text{pH} = 3$, $[\text{H}_2\text{O}_2]_0 = 0.2 \text{ M}$, $[\text{Fe}^{2+}] = 10 \text{ mM}$), 20 % of TOC still remained in solution. In order to get higher TOC decay, we suggest the support of UV light on process or the treated solution could be recycled again in the subsequent stage as the same condition. A mechanism pathway of Cartap mineralization is proposed based on the previous studies as well as our observations.

3.4 The combination of electrochemical and adsorption techniques

The influent of the adsorption section is the treated solution from the electrochemical (EC) process. The operating parameters in EC section are based on optimized conditions ($\text{pH} = 3$, $[\text{Na}_2\text{SO}_4] = 0.05 \text{ M}$, current density $j = 20 \text{ mA}\cdot\text{cm}^{-2}$, electrolysis time $t = 120 \text{ min}$). The combination scheme can be seen in Fig. 13.

Further details can be found in Figs. S5-S7 and Table S1 in *Supporting information section*.

3.4.1 Effect of flow rate on TOC removal

The use of GAC is an effective and economical way to remove taste, odor, color and other undesirable organics including toxic substances on a continuous basis without much capital investment costs [58]. Based on these advantages, GAC was chosen for TOC reduction in this study. The treated solution from EC process was passed into the adsorption section. The effect of flow rate on TOC removal was studied. As shown in Fig. 59, TOC still present after EC process (i.e: 91.3 %) is subsequently reduced to 27 - 32 % in the adsorption section at various flows rate of influent. In general, an increase in flow rate results in a decrease of adsorption of organics onto adsorbent due to the decrease of contact time between liquid and adsorbent. For example, the maximum removal of adsorbable organic halogens was achieved when flow rate was maintained at the lowest value ($5 \text{ mL}\cdot\text{min}^{-1}$) [58]. It is surprising that in the range of $5 \text{ mL}\cdot\text{min}^{-1}$ to $20 \text{ mL}\cdot\text{min}^{-1}$ the higher TOC reduction can be obtained at higher flow rates when usually at higher flow rate the adsorption capacity is decreased due to the reduction of contact time between adsorbate and adsorbent. Thus, controlling the flow rate is the important parameter to achieve high removal efficiency as well as to reduce the operating time of process.

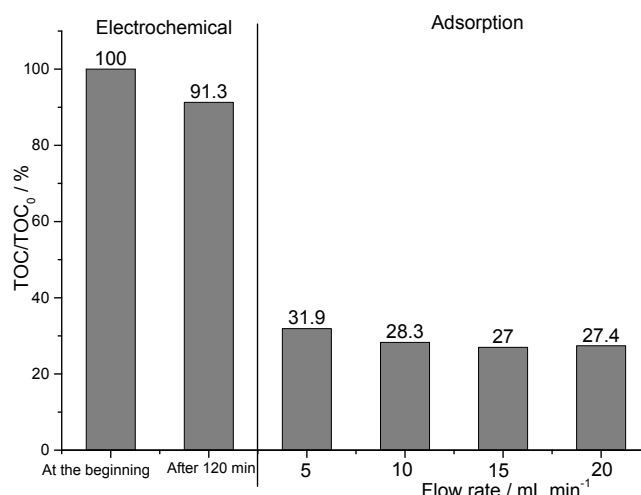


Figure 59 TOC decay in electrochemical process ($[\text{Padan 95SP}]_0 = 300 \text{ mg}\cdot\text{L}^{-1}$, $V_{\text{treated solution}} = 250 \text{ mL}$, $j = 20 \text{ mA}\cdot\text{cm}^{-2}$, $\text{pH} = 3$, $[\text{Na}_2\text{SO}_4] = 0.05 \text{ M}$) and in adsorption process (bed height: 10 cm, inner diameter of column: 2.8 cm, diameter of particles: 2.5 mm, $V_{\text{treated solution}} = 50 \text{ mL}$).

3.4.2 Effect of bed height

According to AC columns plant design [136], the optimal ratio of AC bed height/column diameter is approximately 10 for practical application. However, in the scale of experimental lab we only arranged the bed height from 8-14 cm together with the inner diameter of 2.8 cm. It is clear that an increase in bed height will result in higher adsorption capacity due to the increased number of adsorbent particles and thus the more available adsorption sites. However, in Fig. 60 the TOC/TOC₀ ratio only decreases by 5 % (from 30.1 % to 25.7 %) when increasing the bed height to 175 % (from 8 cm to 14 cm). About 61.2 % of TOC is removed in case of 8 cm bed height in adsorption section. It can be concluded that most of organics in solution is removed on the top layer of adsorbent and the very small content of them is further adsorbed in the next zone (i.e. mass transfer zone or active zone) as depicted in Fig. 13(b).

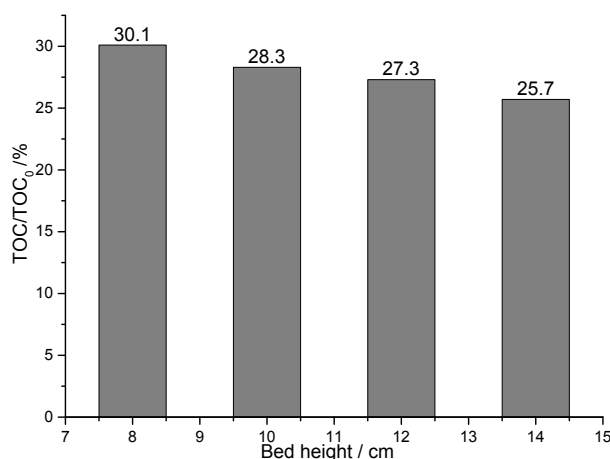


Figure 60 TOC removal versus bed height in adsorption process after EC (operating parameters in EC process can be seen in description of Fig. 59), diameter of particles: 2.5 mm, $V_{treated\ solution} = 100\text{ mL}$, inner diameter of column: 2.8 cm, flow rate: $10\text{ mL}\cdot\text{min}^{-1}$).

3.4.3 Effect of electrolyte anions from EC process on the adsorption process

Generally, chloride, sulfate, nitrate and carbonate are not only used as supporting electrolytes, they can also be found in wastewater. The presence of them in the influent can cause a negative effect on the adsorption behavior of organics [137]. Although the supporting electrolytes have different influence on TOC removal in EC process as can be seen in Figs. 34-35 in section 3.2.4, the finally left TOC in the presence of those electrolytes is very similarly (24 % to 29.5 %). Note that the effect of anions depends on the nature of ion (i.e.: monovalent and divalent ions) and the hydration energy of the target ions. The value of hydration energy (molar enthalpies) of nitrate was higher than that of other anions [138-141]. Thus, nitrate ion lower the adsorption capacities as compared to other anions. For example, in the study of Wilaimgam et al. [137] the nitrate ion had a stronger negative effect on the adsorption capacity for perfluorohexanoic acid by GAC than chloride. The same phenomenon can also be observed in the study of Galamos et al. [138] when using activated carbon to adsorb pertechnetate.

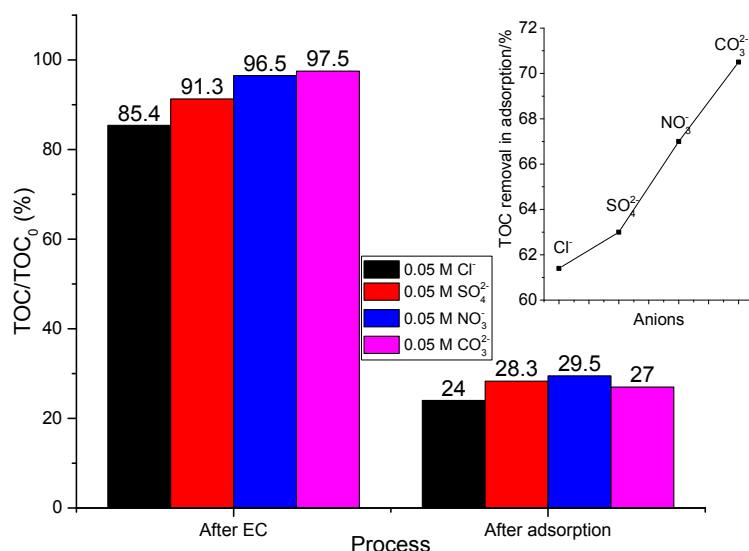


Figure 61 Remaining TOC with various inorganic anions in electrochemical ($[\text{Padan 95SP}]_0 = 300 \text{ mg}\cdot\text{L}^{-1}$, $V_{\text{treated solution}} = 250 \text{ mL}$, $t = 120 \text{ min}$, $j = 20 \text{ mA}\cdot\text{cm}^{-2}$, $\text{pH} = 3$ (except for Na_2CO_3 electrolyte with pH not adjusted) and adsorption processes ($V_{\text{treated solution}} = 100 \text{ mL}$, diameter of particles: 2.5 mm , bed height: 10 cm , flow rate: $10 \text{ mL}\cdot\text{min}^{-1}$). Insert: TOC removal after EC in adsorption column.

3.4.4 Effect of treated volume

To evaluate the effect of treated volume on TOC removal, 10 runs were set up with the treated solution volume of each run being 50 mL . It is clear that the saturation of adsorbent depends on the amount of sorbate onto/inside adsorbent. Therefore, the adsorption capacity will be decreased after several times of usage. It is surprising that TOC/TOC_0 slightly decreases from 28.3% to 23.7% after 10 runs in adsorption section (see Fig. 62), and thus, the average TOC value remained at 25% after 500 mL loading volume of influent. The volume of treated solution of 500 mL may be too small to indicate any loss of adsorption capacity possibly caused by the accumulation of adsorbate on/in the GAC surface. Consequently we do not calculate the lifetime of bed. Nevertheless, this study suggests the long term use of GAC for pesticide removal due to the stability and high removal efficiency of GAC.

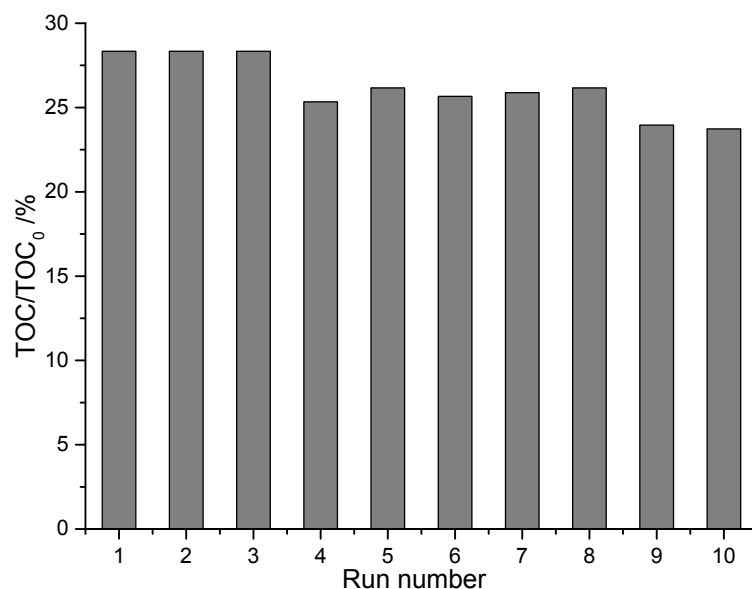


Figure 62 TOC removal versus the run number in adsorption process after EC, $[\text{Padan 95SP}]_0 = 300 \text{ mg}\cdot\text{L}^{-1}$, $V_{\text{run}} = 50 \text{ mL}$, diameter of particles: 2.5 mm, bed height: 10 cm, inner diameter of column: 2.8 cm, flow rate: $10 \text{ mL}\cdot\text{min}^{-1}$).

3.4.5 Effect of initial Padan 95 SP concentration

To investigate the effect of initial concentration of Cartap and the TOC removal in both methods four different initial Padan 95SP concentrations ($100 \text{ mg}\cdot\text{L}^{-1}$, $300 \text{ mg}\cdot\text{L}^{-1}$, $500 \text{ mg}\cdot\text{L}^{-1}$ and $700 \text{ mg}\cdot\text{L}^{-1}$) were tested. The degradation of Cartap in EC process decreases when increasing the initial Padan 95 SP concentration (Fig. 63). For example, 18 % of Cartap remained in case of $100 \text{ mg}\cdot\text{L}^{-1}$ meanwhile 60 % Cartap remained for the case of $700 \text{ mg}\cdot\text{L}^{-1}$. It should be noted that the increase of initial concentration of a compound increases its concentration gradient and mass transfer across the diffusion layer and thus increases its degradation at the electrode [142], resulting in an increased amount of organic molecules decomposed. However, the degradation efficiency is decreased at higher concentration of Cartap. The effect of initial concentrations was also investigated by previous researchers [142,143] using electrochemical techniques for decomposing organic pollutants. In most cases an increase in concentration of organic pollutants reduces their removal percentage.

Cartap and degradation intermediates still remained in the first adsorption column (Fig. 63, Fig. 64), the treated solutions should be subsequently passed through the next column. In subsequent adsorption process, with different concentrations of the remaining Cartap from EC, the results show: (i) the removal of Cartap is slightly higher at higher initial concentration, except the lowest initial concentration of Cartap, (ii) Cartap is almost

completely removed in the first run with the remaining content being below 10 %. It can be concluded that the remaining Cartap (here: below 10 %) in effluent is independent of the initial concentration of Padan 95 SP. After reaching the maximum adsorption in the first column, the remaining Cartap cannot be removed in the subsequent columns. Because adsorption is often reversible, adsorbed compounds may desorb and appear in the effluent when the influent concentrations of those compounds are lower [144]. Thus, the remaining Cartap cannot be adsorbed on GAC below a certain low concentration.

Fig. 64 depicts TOC removal in both processes. In EC process 95 % and 82 % of TOC still remain for the case of $700 \text{ mg}\cdot\text{L}^{-1}$ and $100 \text{ mg}\cdot\text{L}^{-1}$, respectively. Note that TOC decay (see Fig. 64) is lower than Cartap removal by adsorption (see Fig. 63). This is because by-products still remain in treated solution. For example, about 45 %, 35 % and 20 % of TOC remain in the first run of the adsorption step for the cases of $700 \text{ mg}\cdot\text{L}^{-1}$, $500 \text{ mg}\cdot\text{L}^{-1}$ and $100 \text{ mg}\cdot\text{L}^{-1}$, respectively. Cartap cannot be removed in the second column when TOC can be subsequently removed till reaching the minimum values of approximately 25 % in the 2nd and 4th cycles for $500 \text{ mg}\cdot\text{L}^{-1}$ and for $700 \text{ mg}\cdot\text{L}^{-1}$, respectively. This similar phenomenon can be found in the study of K. Ranani et al [145], in which TOC removal can be achieved partly in the second and third columns. This phenomenon can be also explained by assuming reversible adsorption, adsorbed compounds may desorb and appear in the effluent when the influent concentrations of those compounds decrease [144]. Moreover, some compounds may be nonadsorbable or very weakly adsorbable as the result of approximately 25 % of the remaining TOC.

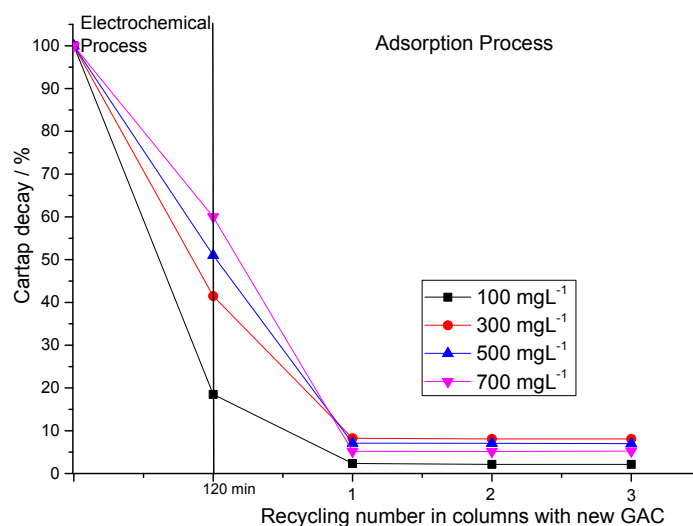


Figure 63 Cartap decay in electrochemical process ($V_{\text{treated solution}} = 250 \text{ mL}$, $j = 20 \text{ mA}\cdot\text{cm}^{-2}$, $\text{pH} = 3$, $[\text{Na}_2\text{SO}_4] = 0.05 \text{ M}$, $t = 120 \text{ min}$) and adsorption process after EC (bed height: 10 cm, inner diameter of column: 2.8 cm, diameter of particles: 2.5 mm, $V_{\text{treated solution}} = 100 \text{ mL}$, flow rate: $10 \text{ mL}\cdot\text{min}^{-1}$).

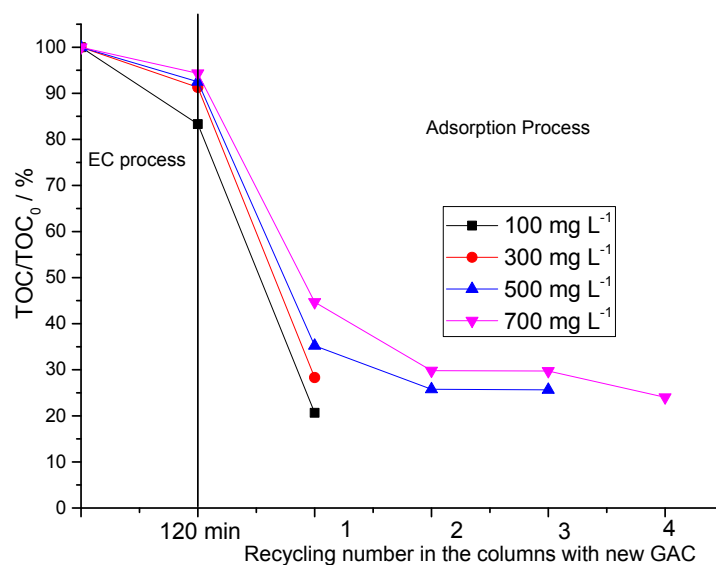


Figure 64 TOC decay in electrochemical process ($V_{\text{treated solution}} = 250 \text{ mL}$, $j = 20 \text{ mA}\cdot\text{cm}^{-2}$, $\text{pH} = 3$, $[\text{Na}_2\text{SO}_4] = 0.05 \text{ M}$) and adsorption process after EC (bed height: 10 cm, inner diameter of column: 2.8 cm, diameter of particles: 2.5 mm, $V_{\text{treated solution}} = 100 \text{ mL}$, flow rate: $10 \text{ mL}\cdot\text{min}^{-1}$).

3.4.6 FT-IR analysis of GAC

The removal of organics by GAC treatment is due to a physical affinity between hydrophilic

organic molecules and GAC (e.g., van der Waals, electrostatic forces) as well as to chemical adsorption forces [146]. The FT-IR method has been widely used to characterize the surface groups of different oxides, and also applied to various types of carbon and carbonaceous materials [147]. Thus, FT-IR spectroscopy was employed in order to verify the differences between GAC before and after adsorption (as shown in Fig. 65). GAC after adsorption shows a band in the vicinity of 1445 cm^{-1} , tentatively assigned to C–H deformation vibration either in $-(\text{CH}_3)_2$ or in methylene group $(-\text{CH}_2-)$. In addition, there is a weak peak at 874 cm^{-1} , suggesting the C–H possibly caused by a vibrational mode in the center of the Cartap molecule.

Table 1 FT-IR spectral band assignments [148]

Band position/ cm^{-1}	Assignment
1612, 1631, 1656, 1657, 1695, 1732	C=O stretching vibration in ketone
1559, 1570, 1585	C=O stretching vibration in aromatic
1467	C–H deformation vibration in methylene group
1439	C–H deformation vibration in $-\text{C}(\text{CH}_3)_3$
1418	C–H deformation vibration in alkane
1161, 1206, 1218	C–O stretching vibration in alcohol
< 900	C–H vibration

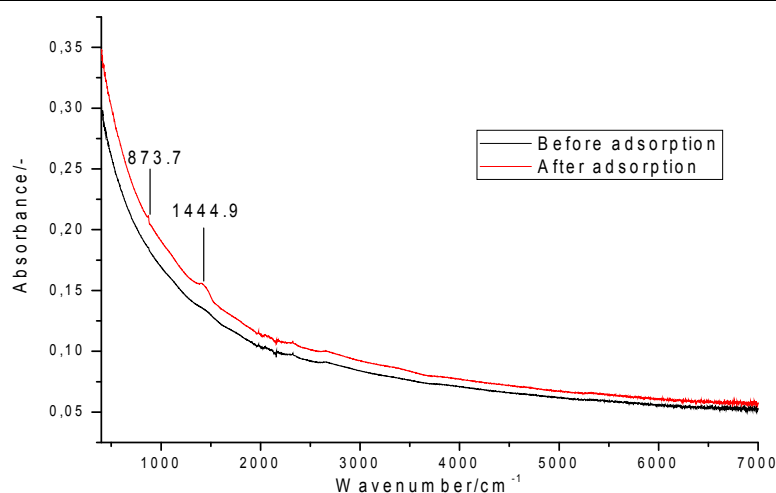


Figure 65 FT-IR spectra of GAC before and after adsorption.

3.4.7 Adsorption mechanism of Cartap

It is well known that surface groups of the adsorbent can interact with the organic adsorbate and affect the adsorption of the latter. That means the hydrophilic and hydrophobic groups on the surface of AC may interact with hydroxyl groups and organic moieties of adsorbate, respectively [149].

Mohammad et al. [150] have suggested that adsorption of the pesticide Oxamyl which has a structure similar to that of Cartap was considered to take place mainly by dispersion forces between electrons in the pesticide structure and electrons in the Silkworm feces activated carbon (SFAC) surface. The adsorption of Oxamyl on SFAC may be mainly due to dispersion forces and electrostatic interaction. Hence, Cartap could also be subject to the same interaction mechanism of hydrogen-bonding interaction as mentioned above in the study of Mohammad et al. [150]. Moreover, hydrogen-bonding interaction between certain functional groups such as $-\text{COOH}$, $-\text{OH}$ and $-\text{NH}_2$ of adsorbate and the hydrophilic groups (e.g: $-\text{COOH}$ groups and $-\text{OH}$ groups) of the tested activated carbons was suggested in [151,152]. The interaction mode of Cartap onto activated carbon is proposed in Fig. 66.

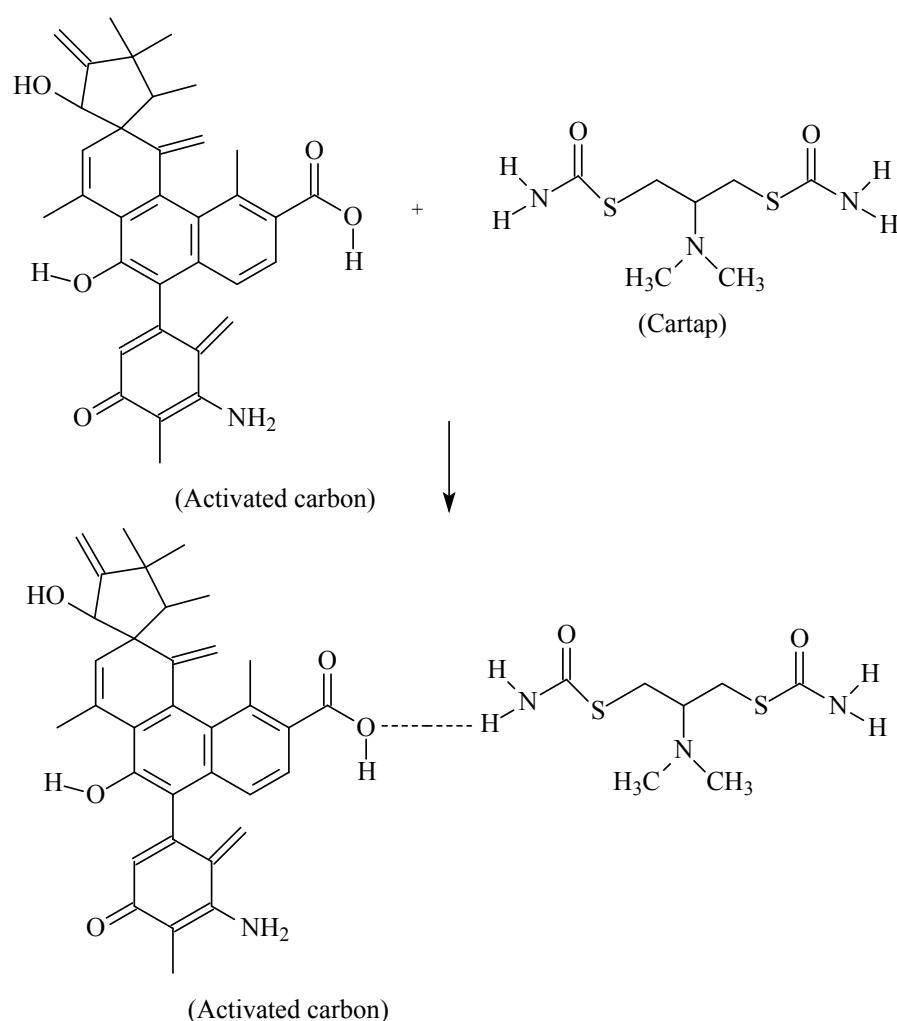


Figure 66 Interaction mechanism of activated carbon with Cartap via hydrogen bond.

According to [152], covalent bonds may be formed between organic chemicals and carbon nanotubes (CNTs) if both the chemicals to be adsorbed and CNTs have functional groups such as $-\text{COOH}$, $-\text{OH}$, $-\text{NH}_2$ suitable for covalent bond formation. Thus, based on the

structural formulas of GAC and Cartap above, a hypothesis for covalent bonds between them may also occur.

3.4.8 Conclusions

In this study, various supporting electrolytes show the differences in the release of by-products. Among of them, NaCl performs better than other electrolytes in term of TOC removal and by-products release. This might due to the contribution of activated chlorine on organics decomposition. It is surprising that the decrease in flow rate of influent and increase in bed height of column do not improve TOC removal gradually as expected. We did not see any losses of adsorption capacity after 10 runs of the total volume of 500 mL. On the other hand, a slight increase in TOC removal shows a long term usage of this adsorbent. With various initial concentrations of Cartap in effluent less than 10 % of Cartap remained after the 1st run and further recycles do not contribute to the Cartap removal meanwhile TOC can be slightly removed for the cases of higher initial concentrations (500 mg L⁻¹ and 700 mg L⁻¹ of Padan 95SP).

CHAPTER 4 CONCLUSION AND RECOMMENDATIONS FOR FUTURE WORKS

4.1 Conclusion

This research has demonstrated the laboratory-scale experimental study on Padan 95 SP removal. Moreover, the trapping efficiency of $\bullet\text{OH}$ radicals generated on BDD electrode in the electrochemical process via TA was also established.

The efficiency of indirect determination of $\bullet\text{OH}$ radicals content strongly depends on the scavengers, operating parameters and the environment of solution. For example, using NaCl as supporting electrolyte has less efficiency than Na_2SO_4 . This is because the formation of other oxidizing species (ClO^- or HClO) results in the effective degradation of organic compound. As the result, the formed 2-HTA molecules are further decomposed leading to the decrease of $\bullet\text{OH}$ radicals versus electrolytic time. NaOH is necessary for diluting TA in aqueous solution, but it also reduces the efficiency of process due to the decomposition of $\bullet\text{OH}$ radicals by OH^- ions.

In a part of EC process we have demonstrated that Cartap in Padan 95 SP is more stable than pure Cartap. There is no clue to disclose for this result though we have tried to investigate 5 % of ingredient in Padan 95 SP. The work has showed the efficiency of electrochemical process on Padan 95 SP removal by mean of MCE. It is obvious that MCE decreased when increasing current density and decreasing the concentration of Padan 95 SP. It can be explained by: (i) by-reaction at BDD electrode (e.g. oxygen evolution) at high current density resulting in lower $\bullet\text{OH}$ radicals generation, (ii) the decrease of initial concentration of a compound decreases its concentration gradient and mass transfer across the diffusion layer and thus leading to lower degradation on electrode. Moreover, MCE decreased versus electrolytic time due to the consumption of oxidizing species for by-products decomposition which is more hardly decomposed, comparing to the Cartap molecules. As shown in this work, NaCl has a better performance than other supporting electrolytes, in term of Cartap and TOC removals. But the usage of NaCl should be considered regarding the toxic by-products release.

To boost TOC removal, Electro-Fenton method was applied in this work. NaOCl is well-known as bleaching reagent, thus it was used to quickly decompose Cartap and reduce partly

TOC in pretreatment. However, the release of Cl^- ion from NaOCl restricts Fenton reaction. The investigated range of H_2O_2 concentration of 0.05 M to 0.3 M, Fe^{2+} (from 5 mM to 15 mM) and even 5 mM Cu^{2+} has showed the efficiency on the TOC removal at the early stage of process, however, roughly 20 % of TOC still remained after 120 min due to the formation of refractory by-products.

In this work, the combination of EC and adsorption methods was an option for increasing both Cartap and TOC removal. As can be seen the detailed study above, GAC has a good performance due to durable and long term usage. As the same result in Electro-Fenton method, about 20 % of TOC still remained in effluent after adsorption section.

4.2 Recommendation for future works

EC process was proved to be useful as a pretreatment in a system coupled with AC sorption for treating aqueous solution containing Padan 95 SP. In the future works, this is a need to perform real wastewater containing Padan 95 SP. Moreover, 20 % of TOC remained in both Electro-Fenton method and EC/GAC adsorption combination could be completely reduced by sequencing biological treatments or by other methods. The absolute rate constants for oxidation of TA or Cartap by hydroxyl radicals determined by competition kinetics method (it can be found elsewhere [51]) as a criteria to compare the reaction time between hydroxyl radicals and organics would be a parameter applied to the next research after Ph.D degree.

It should be mentioned that supporting electrolyte is needed for EC treatment but it could also inhibit the biological treatment at too high concentration, and thus, the salinity of solution should be monitored before applied biological.

The toxicity of initial compounds and by-products in EC or Electro-Fenton process were still not investigated in this thesis. As have been conducted by previous studies [51,153], the toxicity measurement performed with marine *Vibrio fischeri* is suggested for the future work.

The application of EC or Electro-Fenton processes always require extra treatment in industrial application such as anions (i.e: SO_4^{2-} as supporting electrolyte) and cations ($\text{Fe}^{2+}/\text{Fe}^{3+}$ as catalyst) elimination before discharged into environment. Thus, in laboratory scale further

studies regarding to treating solution after EC/Ectro-Fenton processes would be needed for the future work.

In the future, the final goal is to develop this work at pilot scale and furthermore at industrial scale. The performance of electrodes would need to be studied for this scale (i. e: surface size, life duration as well as distance between electrodes, etc). The dead zone in adsorption section should be avoided taking into account the high/diameter ratio of column.

CHAPTER 5 SUPPORTING INFORMATION

The contact angle of BDD with water was measured using Optical Tensiometer TL 100A. As can be seen, hydrophobic surface displays water contact angles as high as 97° at the beginning of water drop (Fig. S1(a)). In this study, the contact angle after several using was observed about 28° (Fig. S1(b)). The mechanism of growing H-terminated BDD (as showed in Fig. S1(c)) can be explained in hot filament Chemical vapor deposition process (HFVCD) [154-156].



Figure S1 (a) Contact angle measurement of H-terminated BDD surface before (a) and after (b) electrolysis), (c) H-terminated BDD surface.

The morphology of BDD electrode characterized by scanning electron microscopy (SEM) is depicted in Fig. S2. Fig. S2 (a) shows the specific crystal morphology of BDD with the average layer thickness of $2.5\ \mu\text{m}$ - $3\ \mu\text{m}$. As can be seen, the film consists of many grains with an average grain size of $300\ \text{nm}$ and the grains are randomly oriented diamond crystallites.

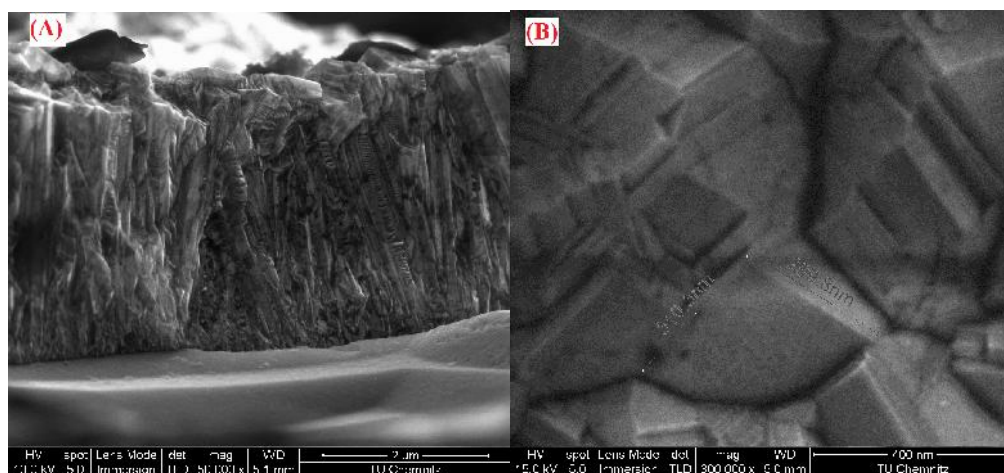


Figure S2 SEM images of cross section (a) and surface morphology (b) of BDD.

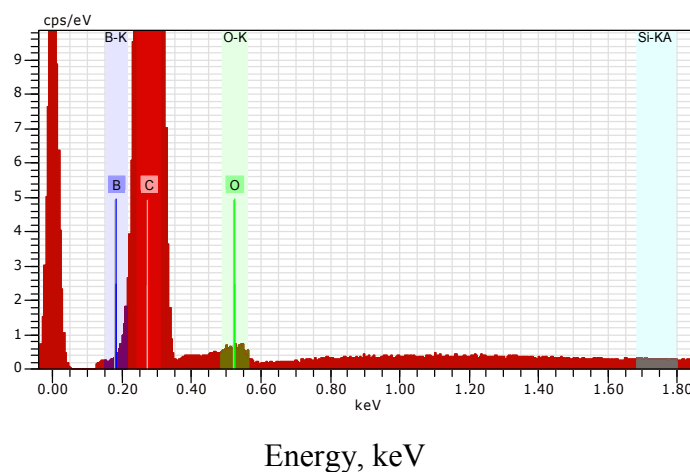


Figure S3 Elemental analysis for BDD electrode. The elemental analysis shows that the main element in layer of BDD consists of 94.75 % carbon (w/w) and the other elements are 0.91 % (w/w) oxygen and 4.33 % (w/w) boron.

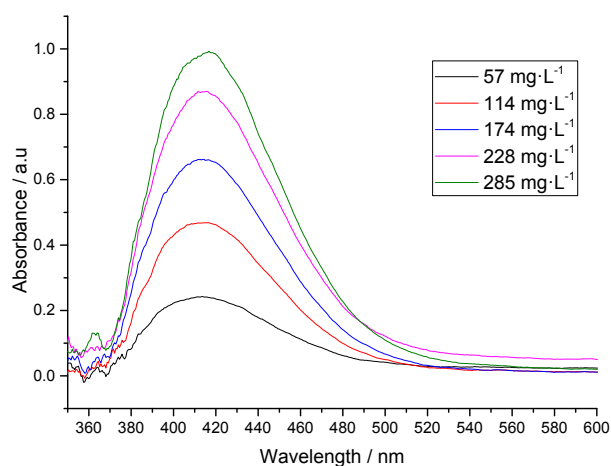


Figure S4 UV-Vis spectrum for the determination of Cartap content in treatment processes of Padan 95 SP.

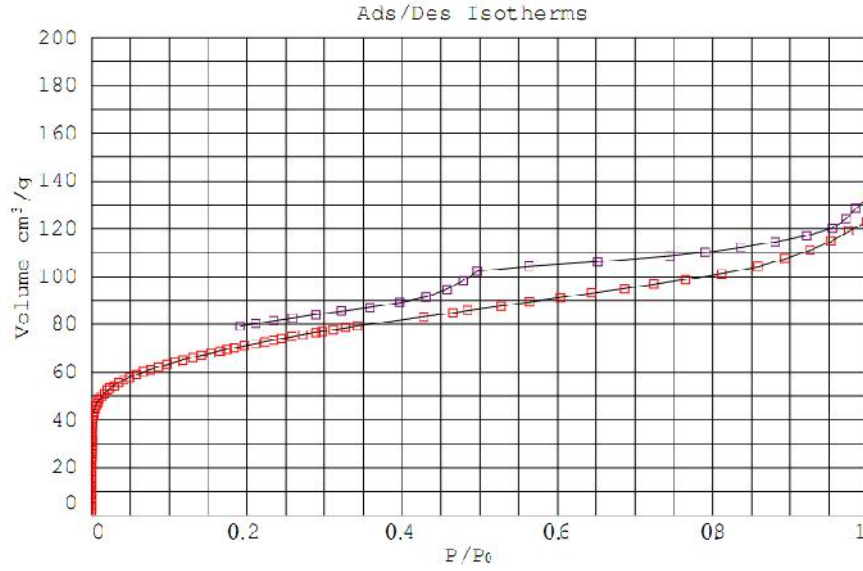


Figure S5 Adsorption/desorption isotherms of nitrogen at 77 K on GC before adsorption.

The Figure S5 shows that the adsorption isotherms is type I of the BET classification (according to the International Union of Pure and Applied Chemistry (IUPAC) classification [157]) with a well-developed sharp “knee” at the low relative pressure (a typical characteristic of micropores) and become almost a plateau at higher relative pressure, and the main porous size of AC in the range of 4 Å–100 Å (more than 80 %) can be also seen in Fig. S7 and Table S1. It is necessary and important to analyze the whole pore size distribution of adsorbent because the difference in the pore size affects the adsorption capacity for molecules of different sizes and shapes, and also this is one of the criteria by which carbon adsorbents are selected for a particular application [158].

The specific surface area (S_{BET}) of GAC is calculated according to BET adsorption isotherm equation (see Eq. S1):

$$\frac{1}{V_a \left(\frac{P_0}{P} - 1 \right)} = \frac{C-1}{V_m C} \times \frac{P}{P_0} + \frac{1}{V_m C} \quad (S1)$$

where P : partial vapour pressure of adsorbate gas in equilibrium with the surface at 77.4 K, Pa.

P_0 : saturated pressure of adsorbate gas, Pa.

V_a : volume of gas adsorbed at standard temperature and pressure, mL.

C : dimensionless constant that is related to the enthalpy of adsorption of the adsorbate gas on the powder sample.

V_m : volume of gas adsorbed at monolayer of sample which can be obtained from Eq. S2, mL.

$$V_m = \frac{1}{A + I} \quad (S2)$$

where A is slop, I is intercept from BET plot.

$$S_{total} = \frac{(V_m N s)}{V} \quad (S3)$$

where N : Avogadro constant ($6.022 \times 10^{23} \text{ mol}^{-1}$).

s : effective cross-sectional area of one adsorbate molecule, (0162 nm^2 for nitrogen), m^2 .

V : the molar volume of the adsorbate gas ($22400 \text{ mL} \cdot \text{mol}^{-1}$).

S_{BET} is obtained from Eq. S4:

$$S_{BET} = \frac{S_{total}}{m} \quad (S4)$$

Where: m is mass of test powder, g.

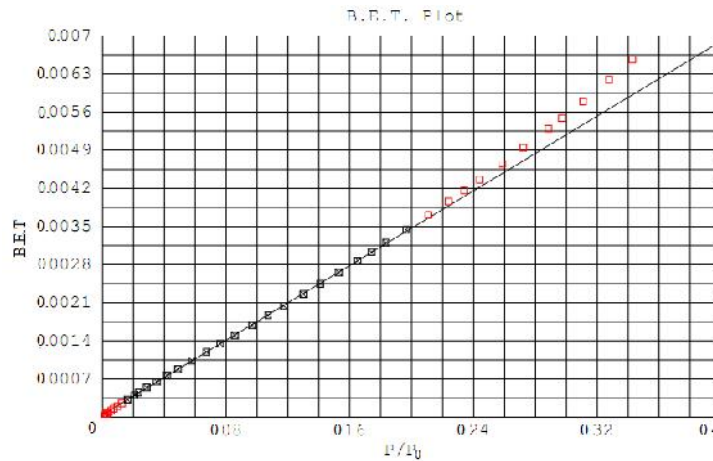


Figure S6 B.E.T plot for GAC.

Depending on the raw material, temperature and carbonization methods the BET surface area may differ. As can be obtained in Fig. S7 S_{BET} of GAC in our study shows the quite low value of $253.3 \text{ m}^2 \cdot \text{g}^{-1}$.

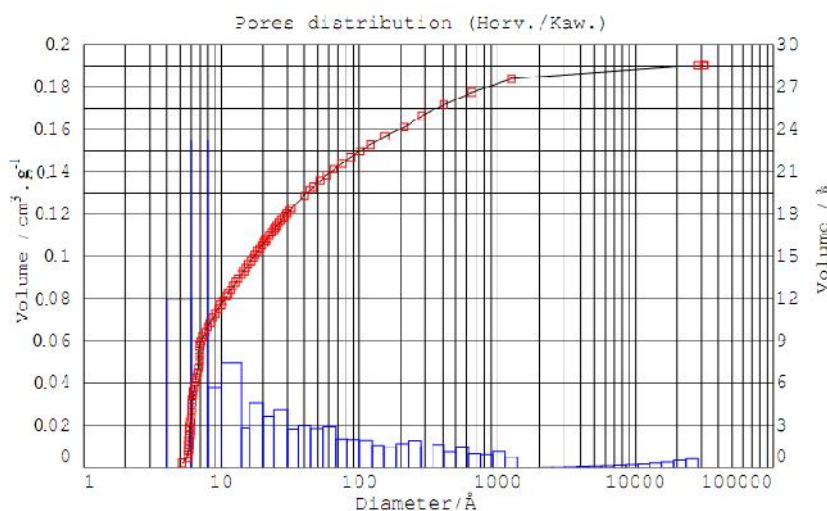


Figure S7 Pore size distribution of GAC. The pore size distribution of sample was evaluated by Horvarth–Kawazoe (Horv./Kaw.) method [159].

Table S1 Porous distribution of AC.

Pore ranges	Relative Vol. %	Cumulative Vol. %	Relative Vol.	Cumulative Vol.
(Å)	(%)	(%)	(cm ³ /g)	(cm ³ /g)
4-6	11.94	11.94	0.022700	0.02270
6-8	23.21	35.15	0.044135	0.06684
8-10	5.66	40.81	0.010758	0.07759
10-14	7.39	48.20	0.014057	0.09165
14-16	2.81	51.01	0.005346	0.09700
16-20	4.63	55.64	0.008796	0.10579
20-24	3.61	59.25	0.006868	0.11266
24-30	4.10	63.34	0.007787	0.12045
30-36	2.71	66.06	0.005159	0.12561
36-44	2.96	69.02	0.005629	0.13123
44-54	2.75	71.77	0.005231	0.13647
54-68	2.87	74.64	0.005452	0.14192
68-82	2.00	76.64	0.003811	0.14573
82-100	1.97	78.61	0.003752	0.14948
100-124	1.92	80.54	0.003657	0.15314
124-150	1.61	82.15	0.003062	0.15620
150-184	1.47	83.61	0.002786	0.15899

184-226	1.68	85.30	0.003201	0.16219
226-276	1.91	87.20	0.003626	0.16581
276-338	1.51	88.71	0.002862	0.16867
338-412	1.65	90.35	0.003128	0.17180
412-504	1.14	91.49	0.002171	0.17397
504-618	1.41	92.91	0.002690	0.17666
618-756	1.00	93.91	0.001901	0.17856
756-924	0.94	94.85	0.001791	0.18035
924-1130	1.15	96.01	0.002196	0.18255
1130-1382	0.74	96.75	0.001411	0.18396
1382-1692	0.04	96.79	0.000071	0.18403
1692-2070	0.05	96.83	0.000086	0.18412
2070-2532	0.06	96.89	0.000106	0.18422
2532-3096	0.07	96.95	0.000129	0.18435
3096-3788	0.08	97.04	0.000158	0.18451
3788-4634	0.10	97.14	0.000193	0.18471
4634-5670	0.12	97.26	0.000237	0.18494
5670-6936	0.15	97.42	0.000289	0.18523
6936-8484	0.19	97.60	0.000354	0.18559
8484-10378	0.23	97.83	0.000433	0.18602
10378-12696	0.28	98.11	0.000530	0.18655
12696-15532	0.34	98.45	0.000648	0.18720
15532-19000	0.42	98.87	0.000793	0.18799
19000-23244	0.51	99.38	0.000970	0.18896
23244	0.62	100.00	0.001186	0.19015

REFERENCES

- [1] World development indicator, <https://blogs.worldbank.org/opendata/chart-globally-70-freshwater-used-agriculture> (accessed August 19, 2018).
- [2] A.J. Llopis, Advanced technologies applied to wastewater treatment plant effluents, (*Doctoral Thesis*) *Universtiat de Barcelona*, 2015.
- [3] D. Bixio, C. Thoeye, J. De Koning, D. Joksimovic, D. Savic, T. Wintgens, Wastewater reuse in Europe, *Desalination* 187 (2006) 89–101.
- [4] Battery Manufacturing Effluent Guidelines, Washington DC: U.S. Environmental Protection Agency (EPA) (2017), <https://www.epa.gov/eg/battery-manufacturing-effluent-guidelines#what-is> (accessed September 19, 2018).
- [5] Development Document for Effluent Limitations Guidelines, New Source Performance Standards and Pretreatment Standards for the Organic Chemicals, Plastics And Synthetic Fibers Point Source Category; Volume I (Report) (1987), EPA 440/1-87/009, https://www.epa.gov/sites/production/files/201510/documents/ocpsf_tdd_1987_vol1.pdf (accessed September 19, 2018).
- [6] Effluent Limitations Guidelines and Standards for the Steam Electric Power Generating Point Source Category, EPA (2015), <https://www.epa.gov/eg/steam-electric-power-generating-effluent-guidelines-2015-final-rule> (accessed October 10, 2018).
- [7] Development Document for Final Effluent Limitations Guidelines and Standards for the Iron and Steel Manufacturing Point Source Category (Report), EPA (2002) 7, https://www.epa.gov/sites/production/files/2015-10/documents/ironsteel_dd_2002.pdf (accessed October 10, 2018).
- [8] Guide for the Application of Effluent Limitations Guidelines for the Petroleum Refining Industry (Report), EPA (1985) 5, https://www.epa.gov/sites/production/files/2015-09/documents/petro-refining_guidance_june-1985.pdf (accessed October 10, 2018).
- [9] Sewage, <https://en.wikipedia.org/wiki/Sewage> (accessed October 2, 2018).
- [10] Cartap (Pesticides residues in food: 1978 evaluation), <http://www.inchem.org/documents/jmpr/jmpmono/v076pr08.htm> (accessed October 2, 2018).
- [11] E. Choi, I.H. Cho, J. Park, The Effect of Operational Parameters on the Photocatalytic Degradation of Pesticide, *J. Environ. Sci. Health B* 39 (2004) 53–61.

- [12] K. Tian, C. Ming, Y. Dai, K.M.H. Ake, Fenton degradation of Cartap hydrochloride: identification of the main intermediates and the degradation pathway, *Water Sci. Technol.* 72 (7) (2015) 1198–1205.
- [13] Arun Mittal, Biological Wastewater Treatment, Water today (2011). <https://www.watertoday.org/Article%20Archive/Aquatech%2012.pdf> (accessed October 2, 2018).
- [14] Woodard and Curran, Industrial Waste Treatment Handbook, Second Edition, 2005.
- [15] Treatment solutions, <https://aosts.com/what-is-sedimentation-in-water-treatment-types-settling-tanks/> (accessed October 2, 2018).
- [16] Different Types of Sedimentation Tanks used in Water Treatment, https://theconstructor.org/environmental-engg/types-of-sedimentation-tank/14711/#Types_of_Sedimentation_Tanks_based_on_Methods_of_Operation (accessed October 2, 2018).
- [17] Th.F. Zabel, Flotation in Water Treatment, https://link.springer.com/chapter/10.1007/978-94-011-2658-8_23 (accessed October 6, 2018).
- [18] J. Rubio, M.L. Souza, R.W. Smith, Overview of flotation as a wastewater treatment technique, *Minerals Eng.* 15(3) (2002) 139–155.
- [19] Adsorption Techniques, <https://emis.vito.be/en/techniekfiche/adsorption-techniques> (accessed October 2, 2018).
- [20] V. Yargeau, Water and wastewater treatment processes, McGill University, Canada, *Woodhead Publishing Limited* (2012) 390–405.
- [21] R. Andreozzi, V. Caprio, A. Insola, R. Marotta, Advanced oxidation processes (AOP) for water purification and recovery, *Catalysis Today* 53 (1999) 51–59.
- [22] J.R. Bolton, K.G. Bircher, W. Tumas, C.A. Tolman, Figures-of-merit for the technical development and application of advanced oxidation processes. *Pure Appl. Chem.* 73(4) (2001) 627–637.
- [23] J.J. Pignatello, Dark and photoassisted Fe^{3+} catalyzed degradation of chlorophenoxy herbicides by hydrogen peroxide, *Environ. Sci. Technol.* 26 (1992) 944–951.
- [24] N.H. Ince, and I.G. Apikyan, Combination of activated carbon adsorption with light-

- enhanced chemical oxidation via hydrogen peroxide, *Water Research* 34(17) (2000) 4169–4176.
- [25] R. Munter, Advanced oxidation processes—current status and prospects. Proceedings of the Estonian Academy of Science Chemistry 50(2) (2001) 59–80.
- [26] D. Liu, Water Treatment by Adsorption and Electrochemical Regeneration Development of a Liquid-Lift Reactor, (*Doctoral Thesis*) *The University of Manchester* (2015).
- [27] L.C. Chiang, J.E. Chang, T.C. Wen, Indirect oxidation effect in electrochemical oxidation treatment of landfill leachate, *Water Research* 29 (1995) 671–678.
- [28] Ch. Comninellis, G. Chen, Electrochemistry for the Environment, *Springer Sci. Business Media, LLC* (2010).
- [29] J. Roeser, N.F.A. Alting, H.P. Permentier, A.P. Bruins, R. Bischoff, Boron-Doped Diamond Electrodes for the Electrochemical Oxidation and Cleavage of Peptides, *Anal. Chem.* 85 (14) (2013) 6626–6632.
- [30] R. L. McCreery, Advanced carbon electrode materials for molecular electrochemistry, *Chem. Rev.* 108 (2008) 2646–2687.
- [31] J.H.T. Luong, K.B. Male, J.B. Glennon, Boron-doped diamond electrode: synthesis, characterization, functionalization and analytical applications, *Analyst* 134 (10) (2009) 1965–1979.
- [32] A. Kraft, Doped Diamond: A Compact Review on a New, Versatile Electrode Material Int., *J. Electrochem. Sci.* 2 (2007) 355–385.
- [33] G. Xu, M.R. Chance, Hydroxyl Radical-Mediated Modification of Proteins as Probes for Structural Proteomics, *Chem. Rev.* 107 (2007) 3514–3543.
- [34] Y. V. Pleskov, Electrochemistry of Diamond: A Review, *Russ. J. Electrochem.* 38 (2002) 1275–1291.
- [35] K. Peckova, J. Musilova, J. Barek, Boron-doped diamond film electrodes - New tool for voltammetric determination of organic substances. *Crit. Rev. Anal. Chem.* 39 (2009) 148–172.
- [36] E. Peralta, G. Roa, J.A. Hernandez-Servin, R. Romero, P. Balderas, R. Natividad, Hydroxyl Radicals quantification by UV spectrophotometry, *Electrochimica Acta.* 129

- (2014) 137–141.
- [37] M. Sato, T. Ohgiyama, J.S. Clements, Formation of Chemical Species and Their Effects on Microorganisms Using a Pulsed High-Voltage Discharge in Water, *IEEE Trans. Ind. Appl.* 32 (1996) 106–112.
- [38] R. Ono, T. Oda, Measurement of hydroxyl radicals in pulsed corona discharge. *J. Electrostat.* 55 (2002) 333–342.
- [39] W. F. L. M. Hoebe, E.M. van Veldhuizen; W.R. Rutgers, G. M.W. Kroesen, Gas Phase Corona Discharges for Oxidation of Phenol in an Aqueous Solution. *J. Phys. D: Appl. Phys.* 32 (1999) 133–137.
- [40] P. Sunka, V. Babicky, M. Clupek, P. Lukes, M. Simek, J. Schmidt, M. Cernak, Generation of Chemically Active Species by Electrical Discharges in Water Plasma Sources, *Sci. Technol.* 8 (1999) 258–265.
- [41] B. Sun, M. Sato, J. D. Clements, Optical Study of Active Species Produced by a Pulsed Streamer Corona Discharge in Water, *J. Electrostat.* 39 (1997) 132–189.
- [42] U. Černigoj, U.L. Štangar, P. Trele, M. Sarakha, Determination of catalytic properties of TiO₂ coatings using aqueous solution of coumarin: Standardization efforts, *J. Photochem. Photobiol. A*: 201 (2009) 142–150.
- [43] L. Luo, A.T. Cooper, M. Fan, Preparation and application of nanoglued binary titania–silica aerogel, *J. Hazard. Mater.* 161 (2009) 175–182.
- [44] K. Bubacz, E. Kusiak-Nejman, B. Tryba, A.W. Morawski, Investigation of •OH radicals formation on the surface of TiO₂/N photocatalyst at the presence of terephthalic acid solution. Estimation of optimal conditions, *J. Photochem. Photobiol. A: Chem.* 261 (2013) 7–11.
- [45] K. Ishibashi, A. Fujishima, T. Watanabe, Detection of active oxidative species in TiO₂ photocatalysis using the fluorescence technique, *Electrochem. Commun.* 2 (2000) 207–210.
- [46] M. Janus, J. Choina, A.W. Morawski, Azo dyes decomposition on new nitrogen-modified anatase TiO₂ with high adsorptivity, *J. Hazard. Mater.* 166 (2009) 1–5.
- [47] Q. Xiao, L. Ouyang, Photocatalytic activity and hydroxyl radical formation of carbon-doped TiO₂ nanocrystalline: Effect of calcination temperature, *Chem. Eng. J.* 148 (2009) 248–253.
- [48] S. Sharma, J.P. Ruparelia and M.L. Patel, A general review on Advanced Oxidation

- Processes for waste water treatment, *Institute of Technology, Nirma University, Ahmedabad* (2011) 382–481.
- [49] A. Wang, J. Qu, J. Ru, H. Liu, J. Ge, Mineralization of an azo dye Acid Red 14 by electro- Fenton's reagent using an activated carbon fiber cathode, *Dyes and Pig.* 65 (2005) 227–233.
- [50] M. P. Titus, V. G. Molina, M. A. Baños, J. Giménez, S. Esplugas, Degradation of chlorophenols by means of advanced oxidation processes: a general review, *App. Cat. B: Env.* 47 (2004) 219–256.
- [51] H. Lin, Removal of organic pollutants from water by indirect electro – oxidation using hydroxyl and sulphate radical species (2006) HAL 1–164.
- [52] O.A. Alafadehan, O.W. Junadu, L. Salami, O.T. Popoola, Treatment of brewery wastewater effluent using activated carbon prepared from coconut shell, *J. Appl. Sci. Technol.* 2 (1) 2012 165–178.
- [53] F. Mazille, D. Spuhler, Adsorption (Activated Carbon), <https://www.sswm.info/sswm-university-course/module-6-disaster-situations-planning-and-preparedness/further-resources-0/adsorption-%28activated-carbon%29> (accessed August 19, 2018).
- [54] Activated carbon, <http://www.sushrutchchemicals.com/activatedCarbon.html> (accessed August 19, 2018)
- [55] D.J. de Ridder, Adsorption of organic micropollutants onto activated carbon and zeolites, *Water Management Academic Press, Printed Gildeprint Drukkerijen BV, (Doctoral Thesis)* 2002.
- [56] J.K. Brennan, T.J. Bandosz, K.T. Thomson, K.E. Gubbins, Review: Water in porous carbons, *Colloids and Surfaces A: Physicochem. Eng. Aspects* 187–188 (2001) 539–68.
- [57] R. Holze, Carbon as electrocatalyst in electrochemical energy conversion - An overview, 4th Int. Carbon Conf. Baden-Baden, 1986, 361–363.
- [58] D. Rajkumar, K. Palanivelu, N. Balasubramanian, Combined electrochemical degradation and activated carbon adsorption treatments for wastewater containing mixed phenolic compounds, *J. Environ. Eng. Sci.* 4 (2005) 1–9.

- [59] L. Guzzellaa, D. Ferettib, S. Monarcab, Advanced oxidation and adsorption technologies for organic micro-pollutant removal from lake water used as drinking-water supply, *Water Research* 36 (2002) 4307–4318.
- [60] M. Santhanam, R. Selvaraj, S. Annamalai, M. Sundaram, Combined electrochemical, sunlight-induced oxidation and biological process for the treatment of chloride containing textile effluent, *Chemosphere* 186 (2017) 1026–1032.
- [61] S.J. Lee, P. Caboni, M. Tomizawa, J. E. Casida, Cartap Hydrolysis Relative to Its Action at the Insect Nicotinic Channel, *J. Agric. Food Chem.* 52 (2004) 95–98.
- [62] Determination of cartap hydrochloride content (spectrophotometric method) copyrighted by Bureau of Indian Standards, IS 14159:1994.
- [63] G.L. Ellman, Tissue sulfhydryl groups, *Arch. Biochem. Biophys.* 82 (1959) 70–77.
- [64] Y. Asani, T. Yoshida, Kinetics of Hydrolysis of Insecticides: Cartap Hydrochloride and Nereistoxin, *Chem. Pharm. Bull.* 25(9) (1977) 2211–2216.
- [65] P.W. Riddles, R.L. Blakeley, B. Zerner, Reassessment of Ellman's reagent. Methods Enzymol. 91 (1983) 49–60.
- [66] E.J. Ruiz, A.H. Ramírez, J.M. Peralta-Hernández, C. Arias, E. Brillas, Application of solar photoelectro-Fenton technology to azo dyes mineralization: effect of current density, Fe^{2+} and dye concentration. *Chem. Eng J.* 171 (2011) 385–392.
- [67] G.M. Eisenberg, Colorimetric determination of hydrogen peroxide. *Ind. Eng. Chem.* 15 (1943) 327–328.
- [68] E.W. Rice: Standard methods for the examination of water and wastewater, American Public Health Association, Washington, DC 2012.
- [69] J. Strähle, E. Schweda: Jander Blasius Einführung in das anorganisch-chemische Praktikum 15. edition, S. Hirzel Verlag. Stuttgart 2005, p. 424.
- [70] E.O. Kraemer, A.J. Stamm, Mohr's Method for the Determination of Silver and Halogens in other than Neutral Solutions, *J. Am. Chem. Soc.* 46 (1924) 2707–2709.
- [71] M.J. Pacheco, V. Santos, L. Ciriaco, A. Lopes, Electrochemical degradation of aromatic amines on BDD electrodes, *J. Hazard. Mater.* 186 (2011) 1033–1041.
- [72] I. Kisacik, A. Stefanova, S. Ernst, H. Baltruschat, Oxidation of carbon monoxide, hydrogen peroxide and water at a boron doped diamond electrode: the competition for

- hydroxyl radicals, *Phys. Chem. Chem. Phys.* 15 (2013) 4616–4624.
- [73] C. Zhang, L. Liu, J. Wang, F. Rong, D. Fu, Electrochemical degradation of ethidium bromide using boron-doped diamond electrode, *Sep. Purif. Technol.* 107 (2013) 91–101.
- [74] A. Fernandes, M.J. Pacheco, L. Ciriaco, A. Lopes, Anodic oxidation of a biologically treated leachate on a boron-doped diamond anode, *J. Hazard. Mater.* 199–200 (2012) 82–87.
- [75] M. Murugananthan, S.S. Latha, G.B. Raju, S. Yoshihara, Role of electrolyte on anodic mineralization of atenolol at boron doped diamond and Pt electrodes, *Sep. Purif. Technol.* 79 (2011) 56–62.
- [76] C. Zhang, L. Yang, F. Rong, D. Fu, Z. Gu, Boron-doped diamond anodic oxidation of ethidium bromide: process optimization by response surface methodology, *Electrochim. Acta* 64 (2012) 100–109.
- [77] N.A. Ghalwa, H.M. Abu-Shawish, H.M. Tamous, H. Al Harazeen, Determination of Electrochemical Degradation of E102 Dye at Lead Dioxide-Doped Carbon Electrodes Using Some Potentiometric and Spectrophotometric Methods, *Chem. J.* 03 (2013) 1–6.
- [78] C. C. de Almeida, P.R.F. da Costa, M.J. de M-Melo, E.V. dos Santos, C.A.M-Huitle, (Review) Application of Electrochemical Technology for Water Treatment of Brazilian Industry Effluents, *J. Mex. Chem. Soc.* 58 (2014) 276–286.
- [79] H. Li, J. Ni, Electrogenation of disinfection by-products at a boron-doped diamond anode with resorcinol as a model substance, *Electrochim. Acta.* 69 (2012) 268–274.
- [80] B. Tryba, M. Toyoda, A.W. Morawski, R. Nonaka, M. Inagaki, Photocatalytic activity and OH radical formation on TiO₂ in the relation to crystallinity, *Appl. Catalysis B* 71 (2007) 163–168.
- [81] Y.L. Jiang, H.L. Liu, Q.H. Wang, Zh.H. Jang, Determination of hydroxyl radicals in TiO₂/Ti photo-electrocatalytic oxidation system using Fe(phen)₃²⁺ spectrophotometry, *J. Environ. Sci.* 18 (2006) 158–161.
- [82] B. Marselli, J. Garcia-Gomez, P.A. Michaud, M.A. Rodrigo, C. Comninellis, Electrogenation of Hydroxyl Radicals on Boron-Doped Diamond Electrodes, *J. Electrochem. Soc.* 150(3) (2003) 78–83.
- [83] T.S. Chen, R.W. Tsai, Y.S. Chen, K.L. Huang, Electrochemical Degradation of Tetracycline on BDD in Aqueous Solutions, *Int. J. Electrochem. Sci.* 9 (2014) 8422–8434.

- [84] K. Okamoto, Y. Yamamoto, H. Tanaka, A. Itaya, Heterogeneous Photocatalytic Decomposition of Phenol over TiO₂ Powder, *Bull. Chem. Soc. Jpn.* 58 (1985) 2015–2022.
- [85] S. Goldstein, G. Czapski, J. Rabani, Oxidation of Phenol by Radiolytically Generated •OH and Chemically Generated SO₄•⁻. A Distinction between •OH Transfer and Hole Oxidation in the Photolysis of TiO₂ Colloid Solution, *J. Phys. Chem.* 98 (1994) 6586–6591.
- [86] J. Peral, J. Casado, J. Domenech, Light-induced Oxidation of Phenol over ZnO Powder *J. Photochem. Photobiol. A: Chem.* 44 (1988) 209–217.
- [87] H. Hayashi, S. Akamine, R. Ichiki, S. Kanazawa, Comparison of •OH Radical Concentration Generated by Underwater Discharge Using Two Methods, *Inter. J. of Plasma Environ. Sci. Technol.* 10 (2016) 24–28.
- [88] Y. Nakabayashi, Y. Nosaka, The pH dependence of OH radical formation in photo-electrochemical water oxidation with rutile TiO₂ single crystals, *Phys. Chem. Chem. Phys.* 17 (2015) 30570–30576.
- [89] U. Cernigoj, M. Kete, U.L. Štangar, Development of a fluorescence-based method for evaluating of self-cleaning properties of photocatalytic layers, *Catalysis Today* 151 (2010) 46–52.
- [90] G.L. Newton, J.R. Milligan, Fluorescence detection of hydroxyl radicals, *Radiat. Phys. Chem.* 75 (2006) 473–478.
- [91] X. Quanjun, J. Yu, K.W. Po, Quantitative characterization of hydroxyl radicals produced by various photocatalysts, *J. Coll. Interf. Sci.* 357 (2011) 163–167.
- [92] Y. Asahi, T. Yoshida, Kinetics of hydrolyses of insecticides: cartap hydrochloride and nereistoxin, *Chem. Pharm. Bull* 25 (9) (1977) 2211–2216.
- [93] Yutaka Asahi and Toshiko Yoshida, Kinetics of hydrolyses of insecticides: cartap hydrochloride and nereistoxin, *Chem. Pharm. Bull* 25 (9) 2211–2216(1977)
- [94] Y. Yavuz, R. Shahbazi, Anodic oxidation of Reactive Black 5 dye using boron-doped diamond anodes in a bipolar trickle tower reactor, *Sep. Purif. Technol.* 85 (2012) 130–136.
- [95] J. Joonseon, K. Choonsoo, Y. Jeyong, The effect of electrode material on the generation of oxidants and microbial inactivation in the electrochemical disinfection processes, *Water Res.* 43 (2009) 895–901.

- [96] N. Rabaaoui, Y. Moussaoui, M.S. Allagui, B. Ahmed, E. Elaloui, Anodic oxidation of nitrobenzene on BDD electrode: Variable effects and mechanisms of degradation, *Sep. Purif. Technol.* 107 (2013) 318–323.
- [97] E. Petrucci, D. Montanaro, Anodic oxidation of a simulated effluent containing Reactive Blue 19 on a boron-doped diamond electrode, *Chem. Eng. J.* 174 (2011) 612–618.
- [98] M. Panizza, G. Cerisola, Direct and mediated anodic oxidation of organic pollutants, *Chem. Rev.* 109 (2009) 6541–6569.
- [99] C. Walling, Fenton's reagent revisited, *Acc. Chem. Res.* 8 (1975) 125–131.
- [100] M.El Haddad, A. Regti, M.R. Laamari, R. Mamouni, N. Saffaj, Use of Fenton reagent as advanced oxidative process for removing textile dyes from aqueous solutions, *J. Mater. Environ. Sci.* 5 (2014) 667–674.
- [101] K.H. Chan, W. Chu, The dose and ratio effects of Fe(II) and H₂O₂ in Fenton's process on the removal of atrazine, *Environ. Technol.* 24 (2003) 703–710.
- [102] S. Sundarapandiyam, R. Chandrasekar, B. Ramanaiah, S. Krishnan, P. Saravanan, Electrochemical oxidation and reuse of tannery saline wastewater, *J. Hazard. Mater.* 180 (2010) 197–203.
- [103] J. Bacardit, J. Stötzner, E. Chamarro, S. Esplugas, Effect of Salinity on the Photo-Fenton Process, *Ind. Eng. Chem. Res.* 46 (2007) 7615–7619.
- [104] J.D. Laat, T.G. Le, B. Legube, A comparative study of the effluents of chloride, sulphate and nitrate ions on the rates of decomposition of H₂O₂ and organic compounds by Fe(II)/H₂O₂ and Fe- (III)/H₂O₂. *Chemosphere.* 55 (2004) 715–723.
- [105] M. Lu, Y. Chang, I. Chen, Y. Huang, Effect of chloride ions on the oxidation of aniline by Fenton's reagent, *J. Environ. Manag.* 75 (2005) 177–182.
- [106] J. Gaca, M. Kowalska, M. Mróz, The Effect of Chloride Ions on Alkylbenzene sulfonate Degradation in the Fenton Reagent, *Polish J. Environ. Studies* 14 (2005) 23–27.
- [107] P.K. Malik, S.K. Saha, Oxidation of direct dyes with hydrogen peroxide using ferrous ion as catalyst, *Sep. Purif. Technol.* 31 (2003) 241–250.
- [108] E. Brillas, M.A. Banos, S. Camps, C. Arias, P.L. Cabot, J.A. Garrido, R.M. Rodríguez, Catalytic effect of Fe²⁺, Cu²⁺ and UVA light on the electrochemical degradation of nitrobenzene using an oxygen-diffusion cathode, *New J. Chem.* 28 (2004) 314–322.

- [109] I. Sirés, J.A. Garrido, R.M. Rodríguez, P.L. Cabot, F. Centellas, C. Arias, E. Brillas, Electrochemical degradation of paracetamol from water by catalytic action of Fe^{2+} , Cu^{2+} and UVA light on electrogenerated hydrogen peroxide, *J. Electrochem. Soc.* 153 (2006) D1–D9.
- [110] H. Gallard, J. De Laat, B. Legube, Comparative study of the rate of decomposition of H_2O_2 and of atrazine by $\text{Fe(III)/H}_2\text{O}_2$, $\text{Cu(II)/H}_2\text{O}_2$, $\text{Fe(III)/Cu(II)/H}_2\text{O}_2$, *Rev. Sci. Eau* 12 (1999) 715–728.
- [111] C. Flox, S. Ammar, C. Arias, E. Brillas, A.V. Vargas-Zavala, R. Abdelhedi, Electro-Fenton and photoelectro-Fenton degradation of indigo carmine in acidic aqueous medium, *Applied catalysis B : Environ.* 67 (2006) 93–104.
- [112] D. Mansour, F. Fourcade, N. Bellakhal, M. Dachraoui, D. Hauchard, A. Amrane, Biodegradability Improvement of Sulfamethazine Solutions by Means of an Electro-Fenton Process, *Water, Air and Soil Pollution*, 223 (2012) 2023–2034.
- [113] A. K. Abdessalem, N. Bellakhal, N. Oturan, M. Dachraoui, M. A. Oturan, Treatment of a Mixture of Three Pesticides by Photo and Electro-Fenton Processes, *Desalination* 250 (2010) 450–455.
- [114] M. A. Oturan, M. C. Edelahi, N. Oturan, K. El Kacemi, J. Aaron, Kinetics of Oxidative Degradation/Mineralization Pathways of the Phenylurea Herbicides Diuron, Monuron and Fenuron in Water during Application of the Electro-Fenton Process, *Appl. Catal. B: Environ.* 97 (2010) 82–89.
- [115] S. Hammami, N. Oturan, N. Bellakhal, M. Dachraoui, M. A. Oturan, Oxidative Degradation of Direct Orange 61 by Electro-Fenton Process Using a Carbon Felt Electrode: Application of the Experimental Design Methodology, *J. Electroanalytical Chem.* 610 (2007) 75–84.
- [116] M. Karatas, Y.A. Argun, M.E. Argun, Decolorization of anthraquinonic dye, Reactive Blue 114 from synthetic wastewater by Fenton process: Kinetics and thermodynamics, *J. Ind. Eng. Chem.* 18 (2012) 1058–1062.
- [117] X.Y. Tang, X.S. Shuang, L.Z. Hua, Degradation of polyvinyl-alcohol wastewater by Fenton's reagent: Condition optimization and enhanced biodegradability, *J. Cent. South Univ. Technol.* 18 (2011) 96–100.

- [118] C. Wang, S. Zhang, Z. Zhang, M. Zeng, S. Yuji, Optimization and Interpretation of Fenton and UV/Fenton Processes for Degradation of Syringyl Lignin, *J. Environ. Anal. Chem.* 1 (2) (2014) 115–119.
- [119] W.G. Kuo, Decolorizing dye wastewater with Fenton's reagent, *Water Res.* 26 (1992) 881–886.
- [120] I. Gulkaya, G. A. Surucu, F.B. Dilek, Importance of $\text{H}_2\text{O}_2/\text{Fe}^{2+}$ ratio in Fenton's treatment of a carpet dyeing wastewater, *J. Hazard. Mater.* B136 (2006) 763–769.
- [121] B.G. Kwon, D.S. Lee, N. Kang, J. Yoon, Characteristics of p-chlorophenol oxidation by Fenton's reagent, *Water Res.* 33 (1999) 2110–2118.
- [122] J.P. Schriman, S.Y. Delavarenne, Hydrogen Peroxide in Organic Chemistry, *Edition et documentation industrielle, Paris* (1979).
- [123] C.Flox, S. Ammar, C. Arias, E. Brillas, A. Viridiana Vargas-Zavala, R. Abdelhedi, Electro-Fenton and photoelectro-Fenton degradation of indigo carmine in acidic aqueous medium, *Appl. catalysis B: Environ.* 67 (2006) 93–104.
- [124] A. El-Ghenymy, J.A. Garrido, F. Centellas, C. Arias, P.L. Cabot, R.M. Rodríguez, E. Brillas, Electro-Fenton and Photoelectro-Fenton Degradation of Sulfanilic Acid Using a Boron-Doped Diamond Anode and an Air Diffusion Cathode, *J. Phys. Chem. A* 116 (2012) 3404–3412.
- [125] E. Brillas, C. Arias, P.L. Cabot, F. Centellas, J.A. Garrido, Rodríguez, Degradation of Organic Contaminants by Advanced Electrochemical Oxidation Methods, *Portugalia Electrochimica. Acta.* 24 (2006) 159–189.
- [126] C. Fan, L. Tsui, M.C. Liao, Parathion degradation and its intermediate formation by Fenton process in neutral environment, *Chemosphere* 82 (2011) 229–236.
- [127] S. Kaneco, N. Li, K.K. Itoh, H. Katsumata, T. Suzuki, K. Ohta, Titanium dioxide mediated solar photocatalytic degradation of thiram in aqueous solution: kinetics and mineralization, *Chem. Eng. J.* 148 (2009) 50–56.
- [128] E. Brillas, E. Mur, R. Sauleda, L. Sanchez, J. Peral, X. Domènech, J. Casado, Aniline mineralization by AOPs: anodic oxidation, photocatalysis, electro-Fenton and photoelectro-Fenton processes. *Appl. Catal. B: Environ.* 16 (1998) 31–42.

- [129] V.A. Sakkas, T.A. Albanis, Photocatalyzed degradation of the biocides chlorothalonil and dichlofluanid over aqueous TiO₂ suspensions. *Appl. Catal. B: Environ.* 46 (1) (2003) 175–188.
- [130] E. Brillas, A review on the degradation of Organic Pollutants in Waters by UV Photoelectro-Fenton and Solar Photoelectro-Fenton, *J. Braz. Chem. Soc.* 25(3) (2014) 393–417.
- [131] P. Maletzky, R. Bauer, The photo-Fenton method degradation of nitrogen containing organic compounds. *Chemosphere.* 37 (1998) 899–909.
- [132] K. Tanaka, K. Padermole, T. Hisanaga, Photocatalytic degradation of commercial azo dyes. *Water Res.* 34 (2000) 327–333.
- [133] X.Duan , Y. Zhao, W. Liu , L.Chang, Investigation on electro-catalytic oxidation properties of carbon nanotube-Ce-modified PbO₂ electrode and its application for degradation of m-nitrophenol, *Arab.J.Chem.* xxx (2014) xxx-xxx.
- [134] J. Joseph, H. Destailats, H. Hung, M. Hoffman, The sonochemical degradation of azobenzene and related azo dyes: rates enhancements via Fenton's reactions, *J. Phys. Chem A* 104 (2000) 301–307.
- [135] E. Guivarch, S. Trevin, C. Lahitte, M.A. Oturan, Degradation of azo dyes in water by Electro-Fenton process, *Environ. Chem. Lett.* 1 (1) (2003) 38–44.
- [136] Chapter 3: activated carbon column plant design, <http://bibing.us.es/proyectos/abreproy/20087/fichero/CHAPTER+3.pdf> (accessed September 19, 2018).
- [137] K. Wilaingam, S. Tanaka. P. Chularueanksorn, Y. Suzuki, R. Ono, S. Fujii, Effect of Anions on Perfluorohexanoic Acid adsorption onto Anion Exchange Polymers, Non-ion Exchange Polymers and Granular Activated Carbon, *J. Jap. Soc. Civil Eng. G (Environ. Research)* 70 (2014) 65–72.
- [138] M. Galamos, M. Dano, E. Viglasova, L. Krivosudsky, O. Roskopfova, I. Novak, D. Berek, P. Rajec, affect of competing anions on pertechnetate adsorption by activated carbon, *J. Radio. Nucl. Chem.* 304 (2015) 1219–1224.
- [139] H. Ohtaki, T. Radnai, Structure and dynamics of hydrated ions, *Chem. Rev.* 93 (1993) 1157-1204.

- [140] J. Barret, Inorganic chemistry in aqueous solution, *Royal Society of Chemistry. Education*, Cambridge (2003) 184.
- [141] J. Kieland, Individual activity coefficients of ions in aqueous solutions, *J. Am. Chem. Soc.* 59 (1937) 1675–1678.
- [142] T.S. Chen, R.W. Tsai, Y.S. Chen, K.L. Huang, Electrochemical Degradation of Tetracycline on BDD in Aqueous solutions, *Int. J. Electrochem. Sci.* 9 (2014) 8422–8434.
- [143] C. Zhang, L. Liu, J. Wang, F. Rong, D. Fu, Electrochemical degradation of ethidium bromide using boron-doped diamond electrode, *Sep. Purif. Technol.* 107 (2013) 91–101.
- [144] National Research Council (US) Safe Drinking Water Committee, Washing DC, Drinking Water and Health (Volume 2), *National Academies Press (US)*, 1980.
- [145] K. Ratnani, A. Leduy, R.S. Ramalho, Activated Carbon Adsorption Treatment of Spent Pickle Brine, *The Canadian J. of Chem. Eng.* 58 (1980) 329–331.
- [146] S. Gur-Reznik, I. Katz, C.G. Dosoretz, Removal of dissolved organic matter by granular-activated carbon adsorption as a pretreatment to reverse osmosis of membrane bioreactor effluents, *Water Res.* 42 (2008) 1595–1605.
- [147] D. Leea, S.H. Honga, K.H. Paekb, W.T. Ju, Adsorbability enhancement of activated carbon by dielectric barrier discharge plasma treatment, *Surface & Coatings Tech.* 200 (2005) 2277–2282.
- [148] G. Socrates, Infrared and Raman Characteristic Group Frequencies: Tables and Charts, 3rd ed., *John Wiley & Sons Ltd., West Sussex*, 2001.
- [149] G. Liu, X. Li, L. C. Campos, Role of the functional groups in the adsorption of bisphenol A onto activated carbon: thermal modification and mechanism, *J. of Water Supply: Research and Tech.* 66 (2017) 105–115.
- [150] S.G. Mohammad, S.M. Ahmed, Preparation of environmentally friendly activated carbon for removal of pesticide from aqueous media, *Inter. J. of Indust. Chem.* 8 (2017) 121–132.
- [151] Z. Al-Qodah, R. Shawabkah, Production and characterization of granular activated carbon from activated sludge, *Braz. J. Chem. Eng.* 26 (2009) 127–136.
- [152] K. Yang, B. Xing, Adsorption of organic compounds by carbon nanomaterials in aqueous phase: Polanyi theory and its application, *Chem. Rev.* 110 (2010) 5989–6008.

- [153] E. Mousset, Integrated processes for removal of persistent organic pollutants: soil washing and electrochemical advanced oxidation processes combined to a possible biological post-treatment, (*Doctoral Thesis*) Université Paris-Est, 2014.
- [154] H. Nagasaka, Y. Teranishi, Y. Kondo, Growth Rate and Electrochemical Properties of Boron-Doped Diamond Films Prepared by Hot-Filament Chemical Vapor Deposition Methods, *e-J. Surf. Sci. Nanotech.* 14 (2016) 53–58.
- [155] V.V.S.S. Srikanth, P.S. Kumar, V.B. Kumar, A Brief Review on the In Situ Synthesis of Boron-Doped Diamond Thin Films, *Inter. J. of Electrochem.* 2012.
- [156] E. Brillas, C. A.M. Huitle, Synthetic Diamond Films: Preparation, Electrochemistry, *Characterization and Applications*, John Wiley & Sons, Hoboken, NJ, USA, 2011.
- [157] F. Rouquerol, J. Rouquerol, K. Sing, Adsorption by Powders and Porous Solids, Principles, *Methodology and Applications*; Academic Press: London, UK, 1999.
- [158] M. Saadial, O. Nazha, A. Abdlemjid, B. Ahmed, C. M'hamed, Preparation and Characterization of Activated Carbon from Residues of Oregano, *J. Surface Sci. Technol.* 28 (3-4) (2012) 91–100.
- [159] E.A. Ustinov, D.D. Do, Adsorption in slit-like pores of activated carbons: improvement of the Horvath and Kawazoe method, *Langmuir* 18 (2002) 4637–4647.

Selbständigkeitserklärung

Hiermit erkläre ich an Eides statt, die vorliegende Arbeit selbständig und ohne unerlaubte Hilfsmittel durchgeführt zu haben.



Chemnitz, den 29.07.2019

Nguyen Tien Hoang

Curriculum Vita

Name	Nguyen Tien Hoang
Date of birth	12.03.1987
Place of birth	Quangnam province, Vietnam
Nationality	Vietnamese
Marriage Status	Married-2016

School Education

1994-1999	Tamquang primay school
1999-2003	Tamquang secondary school
2003-2005	Nuithanh high school

University Education

2005-2006	Danang University of Technology
2006-2010	B.Sc, Kazan National Research Technological University, Russia
2010-2012	M.Sc, Kazan National Research Technological University, Russia

Experience and Skills

2012-2015	Lecturer at Danang University of Education Some drawing software: Plant 3D, Autocad 2D, 3D Simulation calculation software: Hysys Aspen
Since August 2015	Working as research follow under the supervision of Prof. Dr. Rudolf Holze, TU Chemnitz, Germany

Publications

1. Перспективы добычи и переработки нефти в Социалистической Республике Вьетнама, author: Nguyen Tien Hoang and Phakhruchinob PZ, Вестник Казанского Технологического Университета, **2011**, 18, 187–190.
2. Размещение мощностей и выбор направления переработки нефти в Социалистической Республике Вьетнам, Nguyen Tien Hoang and Phakhruchinob PZ, Вестник Казанского Технологического Университета, **2012**.
3. Testing and increasing capacity of Dung Quat Refinery in Quang Ngai Province -Vietnam using Aspen Hysys7.1 software, Nguyen Tien Hoang and Ngo Minh Duc, University of Hue, **2014**.